NASA TECHNICAL NOTE

NASA TN D-4454

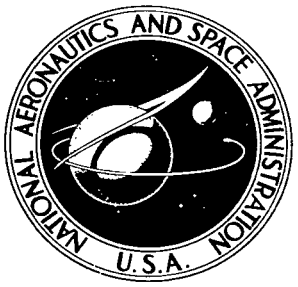

NASA TN D-4454

RESPONSE CHARACTERISTICS OF IMPACTING PENETROMETERS APPROPRIATE TO LUNAR AND PLANETARY MISSIONS

by John Locke McCarty and Huey D. Carden

Langley Research Center
Langley Station, Hampton, Va.

NATIONAL AERONAUTICS AND SPACE ADMINISTRATION • WASHINGTON, D. C. • APRIL 1968

RESPONSE CHARACTERISTICS OF IMPACTING PENETROMETERS APPROPRIATE TO LUNAR AND PLANETARY MISSIONS

By John Locke McCarty and Huey D. Carden

Langley Research Center
Langley Station, Hampton, Va.

NATIONAL AERONAUTICS AND SPACE ADMINISTRATION

For sale by the Clearinghouse for Federal Scientific and Technical Information
Springfield, Virginia 22151 – CFSTI price $3.00

CONTENTS

RESPONSE CHARACTERISTICS OF IMPACTING PENETROMETERS APPROPRIATE TO LUNAR AND PLANETARY MISSIONS

By John Locke McCarty and Huey D. Carden
Langley Research Center

SUMMARY

A study was made of the impact characteristics of penetrometers designed for potential use in the Apollo mission and having possible application to the exploration of other extraterrestrial bodies. The objectives were to evaluate the capability of such penetrometers to identify structural characteristics which potentially might exist for materials on the surface of the moon and planets and to study the effects of variations in both the penetrometer design and the conditions at impact. The effects on penetrometer impact characteristics – primarily acceleration time histories – of such variables as impact velocity and angle, penetrometer size and mass, environmental pressure, and target structure and penetration resistance were examined. The target materials included a rigid nonyielding plate, a cobble-pebble agglomerate, two grades of quartz and basalt sands, fine silica powder, and a low-density open-cell foam.

The results of this investigation demonstrated that suitably designed penetrometers perform satisfactorily over a wide range of impact conditions on a rigid surface and have ample sensitivity to permit the detection of low-density materials having a bearing strength considerably below that required to support manned landings. Several structural characteristics of the target materials are identifiable from characteristics of the impact acceleration time history. The shape of the signature defines whether the impacted material has a rigid nonyielding surface or has a compressive or collapsible failure mode during penetration, and the magnitude of the accelerations and characteristic times establishes the strength of the target material. Penetrometer impacts on impenetrable surfaces generate signatures of short duration with a high peak acceleration, which describe the crushing of the impact limiter designed to protect the internal penetrometer instrument sphere. The strength of materials having a collapsible failure mode can be calculated from derived simplified expressions which relate characteristics of the impact acceleration time history to the size and mass of the penetrometer and the crushing strength of the target. Sufficient differences exist in the characteristics of the impact acceleration signatures for the particulate materials which fail in compression to provide penetrometers with the capability of distinguishing between targets of different bearing strengths. An increase in the bearing strength of such materials, whether due to packing, environmental

pressure (when effective), or use of a different material, produces an increase in the peak acceleration and a decrease in the characteristic times of a penetrometer impact acceleration signature.

INTRODUCTION

One objective contemplated for future lunar and planetary missions is to perform a remote exploration of the structural properties of the surface of those bodies for scientific knowledge or to provide information in support of subsequent manned or unmanned landings. A system employing impacting penetrometers is one attractive means of providing this information. In its general operation, this system consists of the deployment of penetrometers – projectiles equipped with an acceleration sensor and transmitting equipment – to impact the surface and the simultaneous transmission of the impact acceleration signals to a receiver for analysis and interpretation.

The application of penetrometers to payloads of various lunar and planetary spacecraft was considered in reference 1 on the basis of results from impact studies conducted on various terrestrial materials as reported in reference 2 and supported later by the data of reference 3. As indicated in reference 1, penetrometer designs are based upon the objectives of the intended mission within constraints imposed by mission operations. The penetrometer designs of references 2 and 3 were not oriented toward any specific mission but were essentially research instruments designed to evaluate the feasibility of the penetrometer technique.

In view of the initial concern over the capability of the moon's surface to support manned landings, studies were undertaken to devise a penetrometer system for possible use in the Apollo mission. A system was developed which provides general design information and research data appropriate to both lunar and planetary missions. The purpose of this paper is to summarize and discuss the results of the impact research performed as part of the overall development effort. These results may have general use for other possible penetrometer applications. The research was performed for NASA by the Aeronutronic Division of the Philco Corporation. Detailed objectives of this effort are given in reference 4 and the results of the associated instrumentation development and a portion of the penetrometer impact research data are presented in reference 5.

The impact research discussed herein extends penetrometer knowledge to include designs and test conditions of a penetrometer system which may be applicable to the exploration of extraterrestrial surfaces. Earlier penetrometer research (refs. 2 and 3), performed with penetrometers of simple rugged construction, was limited to impacts normal to the target surface at velocities generally less than 10 m/sec. This report

presents the results of impact tests performed with penetrometers designed for possible use in the Apollo mission. Impact data were obtained at impact velocities up to approximately 76 m/sec and at impact angles extending to 60^{o} from the normal. Tests were conducted in both atmospheric and vacuum environments on targets having a range of hardness or penetrability compatible with potential lunar and planetary surfaces. Considerable information, including photographs, has been extracted from reference 5 particularly in the description and use of the test apparatus.

SYMBOLS

a_{max}	peak acceleration, g units (1g = 9.8 meters per second^2)
D	penetrometer diameter, meters
m	penetrometer mass, kilograms
t_r	rise time for peak acceleration in acceleration time history, milliseconds
t_t	total time for acceleration time history, milliseconds
$\bar{t}_t$	effective total pulse time required for acceleration to decrease from peak to 5 percent a_{max}, measured from onset of acceleration, milliseconds
V	penetrometer impact velocity, meters per second
y	penetration depth, meters
β	penetrometer impact angle measured with respect to normal to target surface, degrees
ρ_{lim}	density of impact limiter material, kilograms per meter^3
ρ_{tar}	bulk density of target material, kilograms per meter^3
σ	bearing strength, loading per unit area of 6.35-centimeter probe required to affect a penetration of 10 centimeters into target material, kilonewtons per meter^2

PENETROMETER MISSION CONCEPT AND DESIGN CONSIDERATIONS

One concept of a penetrometer system suggested for the Apollo mission and appropriate to other space applications is depicted in figure 1. The basic components of the system include an orbiting spacecraft which delivers a probe to the vicinity of the surface and the probe package which carries the penetrometers and deploys them from above the surface. The penetrometers impact the surface and the acceleration signatures are transmitted to the orbiting spacecraft through a data relay system contained in the probe package. Impact of the probe is delayed until after the acceleration data from all impacting penetrometers has been relayed.

Considerations of data communication requirements and penetrometer structural demands for shock loads from a potential lunar or planetary surface suggested a nominal penetrometer impact velocity of approximately 46 m/sec for this and other similar mission concepts. In addition, an upper shock limit of 10 000 g (earth) was prescribed for preservation of the penetrometer instrumentation systems to insure satisfactory performance throughout the impact process. Finally, penetrometers designed for such a mission would be required to have the capability to sense the impact accelerations and transmit them to a receiver regardless of the penetrometer orientation during impact. Penetrometers having these omnidirectional characteristics would avoid the difficulties involved in providing the penetrometers with attitude stability and control and would also eliminate the need for elaborate deployment systems within the probes. In order to satisfy these requirements, the selected penetrometer design consisted of a spherical configuration equipped with an outer layer of crushable impact limiter material. In addition to affording protection to the penetrometer instrumentation during impacts with impenetrable surfaces, the impact limiter would also serve to increase the sensitivity of penetrometers to impacts on very weak low-density surfaces since a limiter increases the size while lowering the overall density of the penetrometer. Although such a penetrometer design is incapable of uniquely defining target surfaces harder than the limiter material, an accurate discrimination between such materials was considered unnecessary since such surfaces are credited with sufficient strength to support a manned landing.

A research program was devised to examine the impact characteristics of penetrometers based upon this design under test conditions corresponding to the operations of a penetrometer system adapted to the Apollo mission. This program included a range of test parameters which could possibly extend the application of the results to other extraterrestrial missions. The objectives of this program were to evaluate the capability of such penetrometers to identify structural characteristics which potentially might exist for materials on the surface of the moon or planets and to study the effects of variations in both the penetrometer design and the conditions at impact.

APPARATUS

Penetrometers

The penetrometers used in this investigation are given in table I in order of increasing diameter. The table also includes the mass and materials employed in the construction of each configuration. The penetrometers were of two basic types of construction – limiter-equipped configurations and rigidly constructed configurations. Figure 2(a) presents a sectional sketch of a configuration equipped with an impact limiter. This configuration consisted of an aluminum sphere (which housed the electronics) encapsulated within a balsa impact limiter covered by a thin fiber-glass outer shell. Balsa wood was selected as the limiter material because it yields at a substantially constant stress level throughout a crushing stroke of approximately 80 percent of its initial thickness, because it absorbs more energy per unit mass than any other readily available material, and because it is transparent to radio frequencies. (See ref. 6, for example.) The figure also includes a photograph showing one of the limiter hemispheres before installation of the aluminum sphere and one of the 20 tetrahedral segments used in the limiter fabrication. A large number of segments are necessary to provide essentially radial orientation of the balsa wood grain which is required for uniform crushing strength and hence omnidirectional sensitivity. Details of the impact limiter fabrication are given in reference 5. The nominal penetrometer design, employing this construction, is designated in the table as configuration 7. The physical characteristics of configuration 7 were based upon estimated mass and volume of the electronics package and the thickness and density of the impact limiter, which were computed to satisfy penetrometer design requirements for the Apollo mission. Configuration 5 was similar to the nominal configuration but employed a somewhat lower density balsa impact limiter.

The fabrication of the rigidly constructed configurations depended upon the size of the penetrometers. The smallest diameter penetrometers consisted of two rigidly connected hemispherical metallic shells (fig. 2(b)) and the larger penetrometers consisted of a metal impact base with a stiff fiber-glass shell filled with urethane foam (fig. 2(c)). The mass of these penetrometers was controlled by varying the material or thickness of the upper hemisphere in the small penetrometers and by adjusting the volume of the impact base in the large penetrometers. The mass and diameter of the seven rigid penetrometer configurations, also included in table I, were selected to span a range of values which included those of the nominal penetrometer to provide for design contingencies. The effect of diameter changes on the characteristics of the impact acceleration time histories was studied with configurations 3 and 9 and the effect of mass changes was studied with configurations 4 and 8. Configuration 6 represented the rigidly constructed counterpart to the nominal design and configurations 1 and 2 were included to corroborate the parametric study.

The impact characteristics of the limiter-equipped configurations were evaluated on the firm target materials where projectile deformation occurred. However, in view of the time and expense required to design and construct penetrometers equipped with impact limiters, the impact characteristics of penetrometers upon weaker penetrable target materials were generally evaluated with the rigid penetrometers. Impact data obtained with these rigid penetrometers would be applicable to the limiter-equipped penetrometers on materials offering low penetration resistance where the energy at impact would be absorbed in penetrating the target and not in crushing or deforming the projectile. Both configurations 5 and 7 were used in limited testing on several of the penetrable target materials and in some tests slight projectile deformation occurred; however, the impact characteristics, when compared with those from rigid penetrometers, showed negligible differences. Tests on the more dense penetrable materials, particularly at high impact velocities where projectile deformation may be substantial, could possibly produce significant differences between the impact characteristics of the rigid and the limiter-equipped penetrometers.

Launching Mechanisms

Pneumatic accelerators were used as launching mechanisms to propel the penetrometers to the desired impact test velocities. Photographs of an accelerator mounted for vertical impact tests are presented as figures 3 and 4. Each accelerator consists of a piston within an air cylinder and a rod which extends externally from the piston. The end of the rod is equipped with a penetrometer adapter as shown in figure 3. A quick-opening valve releases high pressure nitrogen from an accumulator into the cylinder; thus, the piston and rod are accelerated. The chamber beneath the piston serves as a snubbing cushion to decelerate the piston after the penetrometer has reached the desired velocity. Penetrometer velocity is controlled by varying the accumulator pressure.

Target Materials and Preparation

A wide variety of surface materials was selected as targets for this investigation to evaluate the capability of penetrometers to identify structural characteristics which potentially might exist for materials on the surface of the moon and planets. The targets included a reinforced steel plate as a smooth impenetrable surface, an agglomerate of basalt cobbles and pebbles which served as an essentially nonyielding mixture of random size particles, and materials which were representative of two general classes of penetrable targets. One class, having a compressive failure mode where penetration resistance increases with penetration, included two grades of round quartz sand (Nevada 60 and Nevada 120), two grades of angular basalt sand, and fine silica powder; the other class, having a collapsible failure mode where penetration resistance is invariant with penetration, was simulated by an open-cell urethane foam of low density. These materials

are given in table II which also includes the compositions, preparation techniques, and various appropriate physical characteristics. For the granular and dust-like materials, the physical characteristics include the shape and size range of the grains, the angle of repose and nominal densities as measured in situ prior to testing. A more complete description of all the test materials is given in reference 5.

Because a number of impact tests were required on a given target material to accomplish the parametric studies, it was necessary to insure repeatable target characteristics from test to test. Materials subject to packing and density changes during handling required special preparation techniques to assure repeatability in both density and bearing strength. These materials, namely the sands and powdered silica, were conditioned prior to each test by an aerification process similar to that employed in reference 3. The densely packed state of Nevada 120 sand was obtained by inserting a vibrator, of a type used to settle concrete, into the material at several locations for a short time period following the general aerification process. An intermediate or light packing state was also attained in the Nevada 120 sand by baking a reservoir of the material to remove extraneous moisture and then aerification of the material prior to initiating the tests.

In addition to the characteristics given in table II, all target materials except the steel plate and the agglomerate were examined for their resistance to quasi-static loadings or bearing strength. The apparatus employed for this examination is shown in figure 5. Spherical and disk probes having dimensions corresponding to those of various test penetrometers were forced into the materials to a depth of approximately 50 cm at a constant penetration rate of 1.27 cm/sec – a rate found to yield essentially the same results as slower more time-consuming penetration rates. Loads incurred during penetration and the probe displacement were monitored and recorded directly on an x-y plotter. Figure 6 presents typical results of probe tests in these targets where the loading divided by the maximum projected area of the probe is presented as a function of the probe penetration depth. Also included in this figure are the results from a 6.35-cm-diameter spherical probe which served as a standard to assure target consistency with respect to previous tests. The curves of figure 6 illustrate load-penetration relationships and trends which are significant in describing the quasi-static bearing strength of the target materials. The urethane foam was in the form of molded units approximately 25 cm thick and showed some variation between pieces; hence, the curves of figure 6(h) are appropriate to only that particular combination of stacked units.

Instrumentation

The penetrometers were equipped with three piezoelectric accelerometers mounted orthogonally within a housing block (fig. 2) to provide the penetrometers with an omnidirectional acceleration-measuring capability. The signals generated during impact were routed through low-noise coaxial cables to charge amplifiers and then in parallel to a

galvanometer driver amplifier and to a tape recorder. The galvanometers were used to provide a quick-look display on direct read oscillograph paper. The tape recorded data were rerecorded onto a continuous loop tape and played into an analog computer for processing. The data processing consisted of computing the resultant impact accelerations (achieved by taking the square root of the sum of the squares of the outputs of the three accelerometers) and performing a single and double integration of this resultant to verify the measured impact velocity and penetration depth, respectively. A sample of a computer output is presented in figure 7. Note that to verify the penetration depth it was necessary to introduce the measured impact velocity as an initial condition into the computer.

Penetrometer impact velocity was measured by means of an electronic counter which recorded the time required for the penetrometer to traverse the velocity trap shown in figures 3 and 4. The velocity trap was mounted near the target surface and consisted of two light beams spaced a known distance apart along the projectile path. The electronic counter was triggered by the penetrometer as it interrupted the first beam and stopped when the penetrometer interrupted the second. Maximum timing error based upon the trap-spacing accuracy, switching sensitivity, and the counter resolution was computed to be less than ±0.6 m/sec at 60 m/sec.

TEST PROCEDURE

The testing technique consisted of impacting the penetrometers onto the various target materials at velocities ranging from approximately 6 to 76 m/sec and recording the measured impact characteristics. The rigid penetrometer nominal configuration (configuration 6) was impacted upon all penetrable targets over this velocity range, which included the mission nominal velocity of 45.7 m/sec, whereas the other penetrometer configurations were tested at selected impact velocities within this range which were dependent upon the target material and the specific test objective. Except for the 6.1 m/sec impacts which were obtained by the gravity-drop principle, the desired impact velocity was obtained with the accelerators described in the section entitled "Launching Mechanisms."

Prior to each impact on the particulate materials, the target was prepared by the aerification technique and generally tested for its bearing strength and consistency with respect to previous tests. Following each impact, a measurement was taken of the penetrometer penetration depth and the recorded acceleration time history was processed in the analog computer.

All impact tests were conducted in an atmospheric environment except for limited testing in a vacuum. The vacuum tests were performed in a cylinder 2.44 m in diameter, 8.23 m long at pressures which extended to 1×10^{-5} torr (1 torr = 133.3 N/m^2). In addition, several impact tests were conducted wherein the penetrometer trajectory was

inclined either 30^{o} or 60^{o} from the normal to the target surface. To accomplish these angular tests, the prepared targets were tilted the desired amount with no change in the accelerator position (either vertical or horizontal, depending upon the mechanism employed).

PRESENTATION OF DATA

Acceleration time histories recorded during the impact of accelerometer-equipped projectiles with target materials have been shown (refs. 2 and 3, for example) to have certain characteristics which are of significance in defining the impacted material. These characteristics include the magnitude of the peak acceleration a_{max}, the rise time required to reach that acceleration t_r, the total duration of the pulse t_t, and the overall shape of the acceleration time history. The acceleration time histories of figure 8 show variations in these characteristics during the impact of the nominal penetrometer design with the various target materials. Variations in the characteristics range from the short duration and high peak acceleration associated with the crushing of the balsa impact limiter against a steel plate to the long duration and lower peak accelerations which characterize impacts upon particulate materials. The response of the penetrometer to impacts with targets which offer a constant resistance with penetration is typified by the acceleration time history produced by impacts with urethane foam (fig. 8(i)).

Characteristics of the acceleration time histories from all impact tests are included in table III. This table gives the diameter D and mass m of the penetrometer and the impact variables, velocity V and angle β measured with respect to the normal to the target surface. Physical characteristics of the firm targets are obvious; however, the penetrable targets are defined by their bulk density ρ_{tar} and bearing strength σ as measured in situ prior to each test. The target bearing strength for these tests was arbitrarily defined as the pressure necessary to force a 6.35-cm-diameter spherical probe under essentially static loading to a depth of 10 cm in the target material. Values for the bearing strength were obtained from curves similar to those of figure 6. The relative differences between the bearing strengths of the various target materials are dependent upon the penetration depth at which the bearing strength is defined since, as shown by figure 6, differences exist in the shape of the load-penetration curves for the target materials. Hence, caution must be exercised in comparing the relative strength of the target materials. For example, at 10 cm penetration the densely packed Nevada 120 sand (fig. 6(b)) has approximately twice the bearing strength of that material when loosely packed (fig. 6(d)), whereas at 30 cm penetration the ratio of their bearing strengths is approximately 3.5 to 1. The bearing strengths given in the table for powdered silica under vacuum are based upon measurements taken with the 10.16-cm-diameter spherical

probe since the sensitivity of the force gage was insufficient to accurately measure the low target resistance to the smaller probe.

In delineating the characteristics of the acceleration time histories, measurements of the total pulse time were complicated in many cases by the lack of a well-defined impact pulse conclusion time. Several of the acceleration time histories of figure 8 illustrate the difficulty involved in determining a distinct time at which the low level acceleration returns to zero following the peak acceleration. For such time histories, an effective total pulse time $\bar{t}_t$ was recorded where $\bar{t}_t$ was arbitrarily defined as the time required for the acceleration level to decrease from the peak to 5 percent of the peak value measured from onset of the impact acceleration.

Table III also includes the penetration depth of the penetrometer into the different penetrable target materials. Listed are both the penetration depths measured subsequent to each test and, when possible, the penetrations obtained through a double integration of the acceleration time histories.

DISCUSSION OF RESULTS

Effectiveness of Nominal Penetrometer Design Configuration

The primary objective of this investigation was to establish the capability of penetrometers designed for lunar application to distinguish between surfaces having different structural characteristics under appropriate impact conditions. The acceleration time histories of figure 8 typify impacts of one such penetrometer (21.59 cm in diameter and 2.27 kg in mass) with the test target materials. Except for the basalt agglomerate, the impact velocities for these time histories were approximately the same for all targets. A comparison of the shapes as well as the magnitude of the characteristics of these acceleration time histories reveals much information about the nature of the impacted material. Impacts with a rigid surface such as a steel plate (fig. 8(a)) are identifiable from the pulse shape associated with the crushing of the balsa impact limiter. The acceleration during limiter crush increases as the imprint area of the balsa sphere gets larger and decreases rapidly during the brief relaxation period. These impacts are of short duration and generate high acceleration levels. The response to impacts on particulate materials is typified by a peak acceleration which occurs during the entry phase of the impact followed by a long duration of low level accelerations. The peak acceleration which occurs almost immediately in these materials is believed to be associated with the rapid compression of the target ahead of the partially embedded penetrometer and which, upon expansion, is responsible for the crater-forming ejecta. The subsequent low level acceleration is attributed to drag forces. Penetrometer response to targets whose penetration resistance is depth independent is illustrated by the acceleration time history of an impact

upon urethane foam (fig. 8(i)). The signature shows that the acceleration becomes effectively constant once the penetrometer reaches a depth equal to its radius. In figure 8(i) two 25-cm-thick foam units were used and the signature shows that the penetrometer has completely penetrated the first and stopped in the second unit of somewhat higher crushing strength.

The acceleration signatures generated during the impacts of the nominal penetrometer design with powdered silica (figs. 8(j) and 8(k)) illustrate the capability of the design to respond to very weak targets. Powdered silica has a bearing strength on the order of light, dry snow, which is considerably less than that required to support manned landings. The acceleration time histories reproduced from the powdered silica impacts show that the penetrometer completely penetrated the powdered silica and impacted the bottom of the container. The acceleration signatures from both the urethane foam units and powdered silica illustrate the capability of the penetrometer to distinguish layered configurations and emphasize the importance of obtaining the complete impact acceleration time history for best target definition. It is significant to note that, at an impact velocity of approximately 46 m/sec, the peak acceleration generated by the nominal penetrometer design impacting on a rigid surface was less than 100 times greater than that generated during impact on a surface having an insignificant load-supporting capability. Thus, the range of sensitivity response required of the penetrometer instrumentation is not severe.

It has been shown that the shape of the impact acceleration time history indicates the structural nature of the impacted material; that is, whether it is a rigid nonyielding material or has a compressive or collapsible failure mode during penetration. For penetrometer applications under consideration, an accurate discrimination between rigid materials was considered unnecessary as pointed out in the section entitled "Penetrometer Mission Concept and Design Considerations." Furthermore, the strength of materials having a collapsible failure mode can be calculated with reasonable accuracy from elementary expressions (discussed in section "Collapsible target structures") which relate characteristics of the impact acceleration time history to the size and mass of the penetrometer and the crushing strength of the target material. Penetrable target materials which fail in compression do not, however, lend themselves to analytical treatment. Hence, it was important to experimentally evaluate the capability of penetrometers to differentiate between the penetration resistance or bearing strength of such materials.

Figure 9 summarizes the impact characteristics of the nominal penetrometer design configuration on all examined particulate materials at the nominal impact velocity of 46 m/sec. The target materials are identified on the figure at their respective test bearing strength range. Figure 9(a) shows that the peak acceleration increases with increasing target bearing strength, particularly in the low bearing-strength region where the rate of increase with bearing strength is rapid. Figures 9(b) and 9(c) show that over the range of bearing strengths associated with the weak dust-like targets, the rise times

and the effective total pulse times decrease rapidly with increasing bearing strength and decrease slightly over the range associated with the higher bearing strength granular targets. The trends of the data of these figures for the nominal penetrometer configuration are realized by all penetrometer configurations with differences occurring only in the magnitude of the characteristics. Figure 9 shows that the characteristics of the impact acceleration time histories exhibit variations with bearing strength which appear to be sufficiently adequate to provide a penetrometer with the capability to distinguish between particulate materials of different bearing strength. Although these variations are slight in the higher bearing-strength regime, the penetrometer is shown to have its maximum sensitivity to bearing strength in the region which would pose the greatest potential hazard to a manned landing mission.

The effectiveness of the nominal penetrometer design in defining structural properties of the impacted material has been demonstrated for specific impact conditions. The following paragraphs discuss the results of impact tests performed to evaluate the effects upon the impact characteristics of a wide range of penetrometer and impact variables and of variations in the more significant test conditions.

Effect of Penetrometer and Impact Variables

Firm targets.- Impacts onto impenetrable targets were limited to the nominal penetrometer configuration. Impacts of this penetrometer onto a firm nonyielding material such as the reinforced steel plate was considered a severe test of the protective capability of the impact limiter since it had to absorb all the system energy. The acceleration time history of figure 8(a) typifies the impact response of these balsa spheres and closely resembles in shape those of reference 2 for hemispherical-nose projectiles impacting a flat balsa target surface. The data of table III show that, at impact velocities of approximately 47 (nominal) and 60 m/sec, the peak accelerations (5000g and 5100g, respectively) are well within the upper limit design goal of 10 000g. A penetrometer of the same diameter but designed to accommodate an instrument sphere of lower mass with the same g-limitation resulted in a penetrometer with an impact limiter having a density, and hence crushing strength, lower than that of the nominal design. The impact characteristics of this penetrometer, also given in the table, were quite similar to those of the nominal design configuration.

The nominal penetrometer design was also impacted onto another hard surface comprised of an agglomerate of olivine basalt, which ranged in particle size from 0.2 to 21.6 cm, at 63.4 m/sec. On the basis of this one test, presented in table III, the steel plate target appeared to be a more severe test of the nominal design since the peak acceleration recorded during the agglomerate test was somewhat less than that recorded during impact with the steel plate. Punctures of the balsa limiter by the sharp agglomerate particles did not noticeably deteriorate the energy-absorbing qualities of the limiter.

Particulate targets.- The impact characteristics of penetrometers with the particulate targets are presented in figures 10 to 13. In figure 10 the peak accelerations sensed by various penetrometer configurations during impact with the different sands and powdered silica are shown as a function of parameters empirically developed for each target. The parameters were evolved by separately examining the variation of peak acceleration with the test variables: impact velocity, penetrometer mass, and penetrometer diameter. Expressions containing these parameters which best fit the test data are also included in the figure and indicate the influence of the test variables on the peak accelerations. The peak accelerations are shown to increase with the square of the impact velocity for impacts in all examined particulate materials regardless of the degree of compaction or particle size and shape. The parameters of figure 10 also show that the peak acceleration varies directly with the penetrometer diameter in quartz sands, varies with $D^{3/2}$ in the basalt sands, and varies with D^2 in powdered silica. The parameters further show that peak impact accelerations vary inversely with penetrometer mass for the powdered silica target and inversely with $m^{0.7}$ for all granular targets. The parameters developed for the peak acceleration of the various penetrometer-target combinations presented here are not significantly different from those developed in reference 3 from low velocity impact tests of somewhat smaller penetrometers on similar targets. Indeed, the parameter for powdered silica, which is composed of minute spheres having a fluid-like behavior (negligible shear strength), is essentially the same as that for the water and light dust targets of reference 3.

The effects of the test variables on the rise and effective total pulse times of the acceleration time histories for the particulate target materials are illustrated in figures 11 and 12, respectively. Data, again taken from table III, are presented which show separately the influence of penetrometer diameter, mass, and impact velocity on these characteristic times. The figures show that in general both the rise and effective total pulse times decrease with increasing penetrometer diameter and impact velocity and increase with increasing penetrometer mass. The exceptions to these trends are the rise times in the weak low-density basalt silt and powdered silica targets where the rise times are shown to vary directly with penetrometer diameter, which suggests a target collapsing failure mode. No effective total pulse times are presented for powdered silica in figure 12 because, with the exception of several low velocity impact tests, the penetrometers completely penetrated the target and struck the bottom of the container.

Figure 13 presents the penetration data from penetrometer impacts into the particulate materials showing the effect of the test variables. Data are presented for penetration depths measured at the test site subsequent to each impact and for penetrations obtained through a double integration of each resulting acceleration time history. Acceleration time histories in some tests were either not obtained or were of insufficient quality to permit integration; however, physical penetration measurements were always

available. Hence, the quantity of measured penetration data exceeds the integrated data in figure 13. With the exception of the data for the loosely and lightly packed Nevada 120 sand, the agreement between the measured and available integrated penetrations is reasonably good. Curves are drawn to fair the data and to better illustrate the effects of the test variables on the penetration depths. For the loosely and lightly packed Nevada 120 sand, these curves are faired only through the measured penetrations. The figure shows that, as expected, an increase in penetration depth results from decreasing the diameter or increasing the mass of the impacting penetrometer. The figure further shows that the penetration depth of the smaller lightweight penetrometers increases with increasing impact velocity; likewise, penetrations of the larger and heavier nominal penetrometer design increase with velocity until reaching a depth of approximately a penetrometer radius. No significantly deeper penetrations of the nominal design were measured at higher impact velocities except in the basalt silt where penetrations extended to approximately 1 penetrometer diameter. It is apparent from the data of figure 13 that the penetration depth of penetrometers of the size and mass tested at velocities ranging between approximately 6 and 76 m/sec cannot be described by an expression similar to that developed for penetrations in references 2, 3, and 6.

Collapsible target structures.- As evidenced by the static loading curves of figure 6(h), the penetration resistance afforded by the urethane foam units is essentially independent of the depth of the probe. Target materials having this collapsible failure mode readily lend themselves to analyses which provide straightforward expressions for the impact characteristics in terms of the test variables and the crushing strength (bearing strength) of the target. An expression for the peak acceleration sensed by a spherical penetrometer during impact with such a target is readily derived with the application of Newton's second law. This expression is

$$a_{max} = \frac{\pi D^2}{4} \frac{\sigma}{m} \tag{1}$$

where D and m are the diameter and mass of the penetrometer, respectively, and σ is the bearing strength of the target material. Since the force exerted upon the penetrometer by the target is a function of the projected area of the immersed penetrometer, the sensed acceleration increases with penetration until the penetrometer reaches a depth equal to its radius and the acceleration remains at that level during any further penetration. With the simplifying assumption that the penetrometer undergoes a negligible change in velocity while penetrating to a depth equal to its radius, the time to peak acceleration or rise time may be approximated by an expression in terms of the diameter of the penetrometer and its impact velocity or

$$t_r = \frac{D}{2V} \tag{2}$$

From impulse and momentum considerations, the duration of the acceleration, or total pulse time, may be approximated by

$$t_t = \frac{4}{\pi D^2} \frac{mV}{\sigma} \tag{3}$$

and, on the basis of energy considerations, approximate penetration depths can be calculated from the expression

$$y = \frac{2}{\pi D^2} \frac{mV^2}{\sigma} \tag{4}$$

where, in both expressions, the target resistance force is assumed to remain constant throughout the impact.

Because of the very low density of the target, these expressions neglect any mass contributions of the target material (apparent mass) accrued by the penetrating penetrometer. It should also be emphasized that the expressions for these characteristics are applicable only to impacts in which the penetrometer has penetrated to a depth of at least a radius. Calculations of the impact characteristics at shallower depths require a penetration time history to define the projected area of the immersed penetrometer and the corresponding target force. Furthermore, the assumptions for equations (2) and (4) are consistent only at deep penetrations.

Figure 14 relates the impact characteristics obtained experimentally to those calculated by these expressions. Data from the two test conditions in which the measured penetrations were less than the penetrometer radius are not included in this figure since the analytical expressions are not applicable. Figure 14(a) shows that the analytical expression for acceleration describes the peak acceleration as measured experimentally during penetrometer impacts on urethane foam.

The experimental rise times are related to the calculated rise times in figure 14(b). The figure shows that the calculated times are generally shorter than the experimental; this implies a decreasing penetrometer velocity during the entry phase of the impact. The rise times associated with the angular impacts in foam are longer than the rise times for the vertical impacts since, commencing with the initial penetration, a longer time is required for the projected penetrometer immersed area to reach a maximum – the greater the impact angle, the longer the rise time.

The expressions for the total pulse time and the penetration depth of penetrometers impacting targets which have essentially constant bearing strength with depth yield only approximate values since, in the derivation, the force exerted on the spherical penetrometers by the target is assumed to be constant throughout the penetration process. However, the target force actually varies from the onset of impact until the target has been

penetrated to a depth of a penetrometer radius (rise time). Therefore, the analyses overestimate the energy absorbed by the target during the initial impact stage and thus the calculated total pulse times and penetration depths would be expected to be less than those measured experimentally. Figure 14(c) shows that the experimental total pulse time does exceed the calculated total pulse time and that the relative difference between the two becomes less at the longer times since the rise time becomes a smaller percentage of the total pulse duration. However, figure 14(d) which relates the experimental and calculated penetration depths shows that the line of perfect agreement is a good fairing of the data; some calculated penetrations are less than the experimental whereas others are greater. Variations in the relationship between experimental and calculated values of penetration depth and other impact characteristics may be attributed to slight variations in the foam units and to data resolution accuracies.

Effect of Test Conditions

The investigation included an evaluation of the effects on the impact characteristics attributed to certain variables associated with the test conditions: the penetrometer impact angle, the target packing state or density, and the test pressure environment of the target material. These effects are discussed separately in the paragraphs which follow.

Penetrometer impact angle.- In the application of penetrometers, it may not necessarily be possible to insure that the penetrometers have a trajectory that would result in a normal impact with the target surface. Thus, the objectives of one phase of this investigation were to evaluate characteristics of acceleration time histories resulting from impacts where the penetrometer flight path was inclined to the normal and to compare them with those from normal impacts on the same target. From an examination of normal impact data the conclusion can be made that targets having penetration resistance invariant with depth (collapsible failure mode) will yield peak acceleration values independent of the impact angle provided sufficient penetration occurs to immerse the penetrometer cross-sectional area. Furthermore, characteristic times from angular impacts in such targets should increase with the angle of impact since a longer time from onset of impact is required for the target resistance force to reach a maximum. The data from the angular tests in the cellular urethane foam (fig. 14), which has such a collapsible failure mode, verify these contentions. The total pulse time for the 60° impact test is shorter than that for $\beta = 30^{\circ}$ (fig. 14(c)) because the penetrometer stopped in a unit of somewhat higher bearing strength than that of other tests.

Different effects can be anticipated from angular impacts with a rigid target or with a penetrable target whose strength is depth dependent (compressive failure mode). For impacts upon a rigid surface, the energy dissipated by a body depends upon the impact angle – the greater the angle, the less energy dissipated during the impact process and,

hence, the lower the shock loading. Similarly, for impacts with targets having a compressive failure mode, the shock loading becomes less severe with increased impact angle since, as the angle becomes greater, more of the body impact energy is dissipated in the weaker upper layers of the target material. In an effort to evaluate effects due to angular impacts on targets having these failure modes, a limited number of angular tests were conducted with the nominal penetrometer design on a rigid steel plate and on Nevada 60 and Nevada 120 sands. The steel plate was impacted at a 60^{o} angle and the sands were impacted at an angle of 30^{o}. The test technique of tilting the target material container prohibited tests on the sands at higher impact angles because of the angle of repose (36^{o}) for these materials. The data from these tests are presented in figure 15 where the peak acceleration divided by the peak acceleration measured during a normal impact on the same material is plotted as a function of the impact angle. The curve which expresses this ratio as a cosine function of the impact angle is also included in the figure. The figure shows that, on the basis of the limited data, the peak accelerations from impacts on a rigid surface and on a granular material tend to vary with the cosine of the impact angle. The data of table III show that the characteristic times, in general, increase with increasing angles of impact with these targets. It is realized that some variations in the sand data may possibly be influenced by the proximity of the impact angle with the material angle of repose.

Target packing.- The effects of target packing on characteristics of acceleration time histories are shown in figure 16. Data are presented for two penetrometer configurations at different velocities impacting Nevada 120 sand in various states of packing. Since variations in the packing state of a target result in changes to both the material bulk density and penetration resistance or bearing strength, the impact characteristics are presented as a function of target density and the corresponding bearing strengths are identified with the data. Furthermore, since the data of this figure were obtained from only one target material, effects attributed to variations in factors such as size, shape, and density of individual particles are eliminated. As also observed in reference 3, an increase in the bulk density of a particulate material and, hence, an increase in the bearing strength results in increased peak accelerations and decreased characteristic times of impact acceleration time histories. Similar effects are noted from the impact data for powdered silica under two states of packing at atmospheric conditions as shown in figures 10(g) and 11(g).

Test pressure environment.- The application of the penetrometer technique to evaluate characteristics of the lunar surface or the surface of most planets requires that consideration be given to the effects of a reduced pressure environment on the impact characteristics of anticipated penetrometer-target combinations. The results of earlier impact tests (ref. 7) indicate that penetration depths, and hence possibly other impact characteristics, have some degree of dependency upon the environmental pressure for

some particulate materials of small grain size. The air entrapped in the voids of these target materials may become compressed during penetrometer immersion and upon expansion may influence the behavior of the material particles and hence affect the penetrometer impact characteristics. In the course of this investigation, a limited number of impact tests were conducted on several of the target materials within a chamber at pressures ranging from 1×10^{-5} torr to approximately 4×10^{-5} torr. For these tests, pressures measured within the target material approximately 70 cm below the surface ranged between 0.4 and 0.7 torr after considerable soaking time. The effects of vacuum or pore air pressure on the impact characteristics of the nominal penetrometer design with lightly packed Nevada 120 sand, urethane foam, and loose powdered silica are included in table III and are noted on the respective figures. The vacuum test data on Nevada 120 sand and the urethane foam indicate that pore air effects are essentially negligible in these targets since characteristics of the acceleration time histories are either in close agreement or fall within the scatter of the data obtained from atmospheric tests on these target materials. The bearing strength of the Nevada 120 sand measured in the vacuum environment is slightly higher than that measured during the atmospheric tests which may account for the higher peak acceleration generated in the vacuum test. An integrated penetration depth was not obtained from the vacuum test on Nevada 120 sand; however, the measured penetration (fig. 13(c)) agrees reasonably well with the integrated penetrations from the atmospheric pressure tests.

The data of table III show that the bulk density of loose powdered silica in a vacuum environment is consistently higher than that under atmospheric pressure and that the bearing strength is increased by a factor of between approximately 6 and 7. Figure 10(g) shows that the peak accelerations measured in the vacuum tests are approximately twice those measured in the atmospheric tests; and figure 11(g) shows, that for vacuum tests, the rise times are slightly lower than those measured in the atmospheric tests. Thus, on the basis of vacuum tests conducted on the different target materials, it appears that a reduced pressure environment, when effective, increases the bearing strength of the target material with the corresponding effects to the impact acceleration time-history characteristics.

CONCLUSIONS

A study was made of the impact characteristics of penetrometers designed for potential use in the Apollo mission and having possible application to the exploration of other extraterrestrial bodies. The objectives were to evaluate the capability of such penetrometers to identify structural characteristics which potentially might exist for materials on the surface of the moon and planets and to study the effects of variations in both the penetrometer design and the conditions at impact. The results of this research suggest the following conclusions:

1. Penetrometers designed for application to the Apollo mission are capable of identifying structural characteristics of impacted surfaces under conditions corresponding to the operation of a penetrometer system adapted to such missions. The shape of the impact acceleration time history identifies the nature of the impacted material (rigid surface or materials having compressive or collapsible failure modes) and the magnitude of the accelerations and characteristics times defines the strength of the target material. Penetrometer impacts with impenetrable surfaces generate signatures of short duration with a high peak acceleration which describe the crushing of the penetrometer impact limiter. The strength of materials having a collapsible failure mode can be calculated from simplified expressions which relate characteristics of the impact acceleration time history to the size and mass of the penetrometer and the crushing strength of the target. Characteristics of the impact acceleration signatures for particulate materials which fail in compression show variations between materials of different bearing strength thereby providing penetrometers with the capability to distinguish between materials of different load-supporting ability.

2. The balsa impact limiter for the penetrometer satisfactorily restricts maximum anticipated shock loads well within the tolerable limits specified for the instrumentation at impact velocities somewhat greater than that contemplated for a penetrometer mission. Tests indicated that this design performed satisfactorily during impacts with a rigid surface and had sufficient sensitivity to detect low density targets which have a bearing strength considerably below that required to support manned landings.

3. Parameters were developed which relate the peak acceleration in particulate target materials to the various penetrometer and impact variables. These parameters are similar to those developed in earlier investigations for lower velocity impacts of smaller penetrometers on similar targets. In general, characteristic times of acceleration time histories generated during penetrometer impacts in particulate materials decrease with increasing velocity and penetrometer diameter and increase with increasing penetrometer mass. Penetration depth increases with a decrease in the diameter or an increase in the mass of the penetrometer; however, the effects of impact velocity on the penetration depth appears to be dependent upon the penetrometer configuration. In general, penetrations obtained through a double integration of the impact acceleration time histories were in good agreement with those penetrations measured subsequent to each test.

4. On the basis of limited data, peak accelerations generated during impacts on a rigid surface or on a target having a compressive failure mode vary with the cosine of the impact angle measured with respect to the normal to the target surface. Peak accelerations are independent of the impact angle on materials which fail in a collapsible mode. Generally, acceleration rise times and total pulse times increase with increasing impact angle.

5. An increase in the bearing strength of a particulate target whether due to packing, environmental pressure (when effective) or use of a different material increases the peak acceleration and decreases the characteristic times of penetrometer impact acceleration time histories, particularly in the low bearing strength region where the rate of change of these characteristics is high. The variations in these characteristics with bearing strength appear to be sufficiently adequate to provide penetrometers with the capability to distinguish between particulate materials of different bearing strength. Although these variations are slight in the region of high bearing strength, the penetrometers have maximum sensitivity to bearing strength in the region of low bearing strength which would pose the greatest potential hazard to a manned landing mission.

Langley Research Center,
National Aeronautics and Space Administration,
Langley Station, Hampton, Va., August 10, 1967,
124-08-05-15-23.

REFERENCES

1. McCarty, John Locke; Beswick, Alfred G.; and Brooks, George W.: Application of Penetrometers to the Study of Physical Properties of Lunar and Planetary Surfaces. NASA TN D-2413, 1964.

2. McCarty, John Locke; and Carden, Huey D.: Impact Characteristics of Various Materials Obtained by an Acceleration-Time-History Technique Applicable to Evaluating Remote Targets. NASA TN D-1269, 1962.

3. Hanks, Brantley R.; and McCarty, John Locke: Investigation of the Use of Penetrometers To Determine the Capability of Dust Materials To Support Bearing Loads. NASA TN D-3200, 1966.

4. Beswick, Alfred G.; and McCarty, John Locke: Penetrometer Research and Development for Lunar Surface Evaluation. Conference on Langley Research Related to Apollo Mission, NASA SP-101, 1965, pp. 61-68.

5. Anon.: Final Report – Research, Development, and Preliminary Design for the Lunar Penetrometer System Applicable to the Apollo Program. Publ. No. U-3556 (Contract No. NAS1-4923), Aeronutronic Div., Philco Corp., Apr. 27, 1966.

6. Daigle, D. L.; and Lonborg, J. O.: Evaluation of Certain Crushable Materials. Tech. Rept. No. 32-120 (Contract No. NASw-6), Jet Propulsion Lab., California Inst. Technol., Jan. 13, 1961.

7. Clark, Leonard V.; and McCarty, John Locke: The Effect of Vacuum on the Penetration Characteristics of Projectiles Into Fine Particles. NASA TN D-1519, 1963.

TABLE I.- DESCRIPTION OF PENETROMETERS

[Nominal values]

Configuration	Diameter, D, cm	Mass, m, kg	Construction material
1	10.16	1.00	Aluminum
2	10.16	1.81	Aluminum and steel
3	10.16	2.27	Aluminum and steel
4	21.59	1.00	Fiber-glass shell with magnesium base
5	21.59	1.81	Aluminum sphere (8.9 cm in diam.) with balsa limiter (ρ_{lim} = 112 kg/m^3)
6	21.59	2.27	Fiber-glass shell with magnesium base
7	21.59	2.27	Aluminum sphere (9.6 cm in diam.) with balsa limiter (ρ_{lim} = 176 kg/m^3)
8	21.59	3.63	Fiber-glass shell with magnesium base
9	30.48	2.27	Fiber-glass shell with magnesium base

TABLE II.- DESCRIPTION OF TARGET MATERIALS

[Nominal values]

Material	Composition	Grain size range			Bulk test densities, kg/m^3	Angle of repose, deg	Particle shape	Preparation
		Max.	Mean	Min.				
Reinforced steel plate	Steel plate backed by concrete							
Basalt agglomerate	Olivine basalt	21.6 cm	0.37 cm	0.2 cm	1875		Extremely angular	Hand sorting, mechanical crushing, and sieving
Nevada 60 sand, loosely packed	Quartz	420μ	160μ	105μ	1555 to 1559	36	Rounded	Mechanical sieving
Nevada 120 sand, densely packed	Quartz	120μ	70μ	53μ	1506 and 1618	36	Rounded	Mechanical sieving
Nevada 120 sand, lightly packed	Quartz	120μ	70μ	53μ	1392 to 1426	36	Rounded	Mechanical sieving
Nevada 120 sand, loosely packed	Quartz	120μ	70μ	53μ	1378	36	Rounded	Mechanical sieving
Basalt sand	Olivine basalt	500μ	340μ	63μ	1442	46	Angular	Mechanical crushing and sieving
Basalt silt	Olivine basalt	325μ	32μ	20μ	1297	51	Angular	Mechanical crushing and sieving
Powdered silica	Silica	0.015μ			76 to 83	[a]48	Spheres	Hydrolysis of $SiCl_4$
Urethane foam	Urethane				32			Sawed units

[a]Measured in same state as when impact tested.

TABLE III.- SUMMARY OF PENETROMETER IMPACT TESTS

Configuration	Penetrometer variables		Impact variables		Target characteristics		Acceleration time history			Penetration, cm	
	D, cm	m, kg	V, m/sec	β, deg	ρ_{tar}, kg/m^3	σ, kN/m^2	a_{max}, g units	t_r, msec	$\bar{t}_t$, msec	Measured	Integrated
Reinforced steel plate											
5	22.13	1.79	43.6	0	-----	---	4 800	1.09	2.0	[a]3.3	[a]3.6
7	22.16	2.34	46.6	0	-----	---	5 000	1.08	1.9	[a]2.5	[a]3.8
	21.50	2.35	59.7	0	-----	---	5 100	1.07	2.6	[a]4.3	[a]5.3
	21.64	2.29	45.7	60	-----	---	2 500	.84	2.2	[a]3.8	----
Olivine basalt agglomerate											
7	21.59	2.39	63.4	0	1875	---	4 300	0.95	4.7	[a]3.0	----
Nevada 60 sand, loosely packed											
1	10.16	1.00	45.4	0	1555	70	3 140	0.29	6.8	23.4	23.0
	10.16	1.00	45.7	0	1555	70	3 070	.30	6.6	25.4	23.9
2	10.16	1.81	6.1	0	1555	70	28	2.10	53.4	12.2	14.1
	10.16	1.81	6.1	0	1555	70	37	1.91	52.4	12.2	12.7
	10.16	1.81	6.1	0	1555	70	34	1.87	53.1	11.7	12.2
	10.16	1.81	46	0	1555	70	1 800	.39	12.6	43.2	----
	10.16	1.81	46.6	0	1555	70	1 800	.39	14.1	41.9	----
3	10.16	2.27	45.4	0	1559	73	1 540	0.39	15.0	47.0	50.8
	10.16	2.27	45.4	0	1559	73	1 550	.47	13.7	48.8	48.3
	10.16	2.27	45.7	0	1559	73	1 540	.43	14.9	46.2	44.5
4	21.59	1.05	46.6	0	1559	73	6 900	0.26	2.3	10.9	----
	21.59	1.04	46.6	0	1559	73	6 240	----	2.5	8.9	----
	21.59	1.04	46.6	0	1559	73	6 400	----	3.1	8.9	----
6	21.59	2.27	6.1	0	1557	74	93	1.74	30.9	7.1	6.2
	21.59	2.27	6.1	0	1557	74	93	1.82	32.6	7.1	6.5
	21.59	2.27	45.7	0	1559	73	3 300	----	5.6	8.9	----
	21.59	2.27	46	0	1559	73	3 300	.34	----	14.7	14.5
	21.59	2.27	46.3	0	1559	73	3 500	.32	5.6	10.2	----
	21.59	2.27	48.5	0	1559	73	3 250	.35	5.6	10.2	----
	21.59	2.27	71.3	0	1559	73	11 000	.28	4.1	11.4	----
	20.96	2.26	46	30	1559	59	2 600	.69	5.0	----	----
8	21.59	3.63	44.8	0	1559	73	2 790	0.47	5.5	20.1	19.3
9	29.98	2.25	46.6	0	1559	73	5 900	0.24	3.3	11.4	10.0
Nevada 120 sand, densely packed											
1	10.16	1.00	45.7	0	1506	91	3 306	0.32	5.3	18.8	17.3
	10.16	1.00	45.4	0	[b]1618	517	6 280	.31	1.8	5.1	5.0
3	10.16	2.27	46.6	0	1506	93	1 750	0.35	10.9	33.0	27.9
4	21.59	1.04	44.8	0	1506	91	6 250	0.24	2.7	7.6	8.1
6	21.59	2.32	6.1	0	1506	110	95	1.42	23.9	3.8	4.3
	21.59	2.32	6.1	0	[b]1618	517	294	1.11	6.1	1.0	1.2
	21.59	2.32	46	0	1506	91	3 800	.28	5.7	11.7	10.9
	21.59	2.32	72.2	0	1506	91	9 600	.24	3.7	12.2	11.9
	20.96	2.26	46.3	30	1506	93	3 000	----	6.9	----	----
8	21.59	3.63	45.1	0	1506	91	2 880	0.36	6.2	15.8	13.6
9	30.48	2.29	46.6	0	1506	93	5 400	0.24	4.5	8.9	6.9

[a]Impact limiter crushed.
[b]Extreme packing, no aerification.

TABLE III.- SUMMARY OF PENETROMETER IMPACT TESTS – Continued

Configuration	Penetrometer variables		Impact variables		Target characteristics		Acceleration time history			Penetration, cm	
	D, cm	m, kg	V, m/sec	β, deg	ρ_{tar}, kg/m^3	σ, kN/m^2	a_{max}, g units	t_r, msec	$\bar{t}_t$, msec	Measured	Integrated
Nevada 120 sand, lightly packed											
1	10.16	1.00	45.7	0	1392	63	2590	0.34	7.1	27.9	28.5
	10.16	1.00	46	0	1392	63	----	-----	----	27.4	----
2	10.16	1.81	6.1	0	1392	63	33	1.87	60	15.7	15.0
	10.16	1.81	6.1	0	1392	63	31	1.66	58.2	15.5	14.7
	10.16	1.81	6.1	0	1392	63	37	1.70	48.3	14.7	----
	10.16	1.81	44.8	0	1392	63	1740	.35	13.5	39.4	----
	10.16	1.81	45.1	0	1392	63	1760	.39	10.9	40.6	----
3	10.16	2.27	46.3	0	1392	63	1380	0.39	14.6	48.3	50.8
	10.16	2.27	46.6	0	1392	63	1400	.43	15.1	50.8	41.9
4	21.59	1.04	46	0	1392	60	5400	-----	2.7	5.6	----
	20.96	1.01	46.6	0	1410	58	5350	-----	2.1	7.6	10.2
	21.59	1.04	46.9	0	1392	60	5200	-----	2.2	6.6	----
5	21.59	1.82	21.8	0	1416	66	1410	0.85	4.5	9.7	6.6
	22.10	1.82	25.9	0	1416	66	2300	.79	5.1	9.7	6.5
	21.59	1.82	38.4	0	1416	66	2625	[a].40	3.9	9.1	7.1
6	21.59	2.27	6.1	0	1410	65	72	1.88	48.9	8.1	8.8
	21.59	2.27	6.1	0	1410	65	74	1.72	48.5	7.9	7.9
	21.59	2.27	6.1	0	1410	65	77	1.81	48.2	7.4	7.4
	20.96	2.32	6.1	0	1410	58	61	1.81	56.5	12.2	10.0
	21.59	2.27	42.4	0	1392	63	2700	.39	----	8.9	----
	20.96	2.32	45.7	0	1410	58	2650	.53	5.9	9.7	23.9
	21.59	2.27	46.3	0	1392	60	3000	.27	5.2	8.1	----
	21.59	2.27	47.2	0	1392	60	3040	.35	4.6	8.1	----
	21.59	2.27	71.3	0	1392	60	7200	.22	----	7.6	----
	21.59	2.32	74.1	0	1410	58	7000	.40	3.2	11.4	29.7
	20.96	2.26	46	30	1416	66	2700	.55	4.8	----	----
	21.59	2.25	46.9	0	[c]1426	70	3700	.32	5.0	21.1	----
7	21.59	2.27	15.7	0	1426	65	394	1.11	----	9.7	18.3
	21.59	2.27	26.4	0	1426	65	1200	.44	8.7	11.4	18.8
	21.59	2.27	31.1	0	1426	65	1700	.40	5.7	11.4	20.3
	21.59	2.27	38.7	0	1426	65	2500	.36	4.1	10.2	22.9
	21.59	2.27	46.3	0	1426	65	3350	[a].40	3.4	10.9	23.6
8	21.11	3.63	44.5	0	1410	58	2140	0.47	5.7	12.4	22.4
9	30.48	2.32	45.7	0	1410	58	5000	0.24	3.1	8.1	10.9
Nevada 120 sand, loosely packed											
6	21.59	2.26	6.1	0	1378	50	59	2.05	62.9	8.9	10.2
7	21.59	2.39	15.8	0	1378	50	375	0.91	17.9	10.9	18.0
	21.59	2.39	32.8	0	1378	50	1280	.67	5.7	12.2	25.2
	21.59	2.39	45.1	0	1378	50	2690	.55	5.4	10.9	28.5
8	21.59	3.63	44.2	0	1378	50	2000	0.61	7.3	18.5	27.9

[a]Impact limiter crushed.
[c]Test performed in vacuum.

TABLE III.- SUMMARY OF PENETROMETER IMPACT TESTS – Concluded

Configuration	Penetrometer variables		Impact variables		Target characteristics		Acceleration time history			Penetration, cm	
	D, cm	m, kg	V, m/sec	β, deg	ρ_{tar}, kg/m^3	σ, kN/m^2	a_{max}, g units	t_r, msec	$\bar{t}_t$, msec	Measured	Integrated
Basalt sand											
1	10.16	1.00	46.3	0	1442	19	1880	0.63	9.3	55.4	47.0
	10.16	1.00	46.6	0	1442	19	1890	.47	9.6	55.4	41.1
3	10.16	2.27	45.1	0	1442	19	920	0.55	18.7	76.2	61.0
	10.16	2.27	45.4	0	1442	19	980	.59	-----	(d)	----
6	21.59	2.27	6.1	0	1442	19	39	2.55	110.7	14.0	21.3
	21.59	2.27	6.1	0	1442	19	44	2.95	100.5	14.0	21.6
	21.59	2.27	44.5	0	1442	19	2480	.39	5.9	14.0	18.3
	21.59	2.27	44.8	0	1442	19	2440	.55	6.0	17.3	16.0
	21.59	2.27	71.3	0	1442	19	6100	.40	3.7	15.8	14.7
Basalt silt											
1	10.16	1.00	45.1	0	1297	12.5	1360	0.55	14.8	63.3	41.3
	10.16	1.00	45.7	0	1297	12.5	1280	.62	14.2	48.3	48.0
2	10.16	1.81	46.9	0	1297	12.5	880	0.59	17.4	(d)	----
3	10.16	2.27	45.7	0	1297	7.5	720	0.71	20.9	(d)	----
	10.16	2.27	46.0	0	1297	7.5	715	.63	24.4	69.9	49.9
5	21.59	1.81	44.2	0	1297	12.5	2520	0.79	4.9	10.7	----
	21.59	1.81	45.1	0	1297	12.5	2560	.67	6.2	10.7	----
6	21.59	2.27	6.1	0	1297	7.5	29	3.26	84.7	17.3	12.7
	21.59	2.27	45.4	0	1297	7.5	2050	.78	7.8	21.6	23.9
	21.59	2.27	46.0	0	1297	7.5	2350	.78	6.7	24.6	20.3
	21.59	2.27	71.6	0	1297	7.5	4600	.40	4.3	20.8	22.8
8	21.59	3.64	44.2	0	1297	12.5	----	----	-----	58.4	----
	21.59	3.64	46.6	0	1297	12.5	1600	----	10.5	47.7	----
Powdered silica											
1	10.16	1.00	47.1	0	[c]77	[f]1.75	176	1.19	-----	(d)	----
3	10.16	2.27	46.3	0	[c]77	[f]1.75	66	1.30	-----	(d)	----
4	21.59	1.00	46.3	0	[c]77	[f]1.86	610	1.30	-----	(d)	----
6	21.59	2.32	6.1	0	83	1.4	3.2	2.57	147.5	50.3	55.9
	21.59	2.32	46.3	0	83	1.4	218	1.38	[e]19.7	----	----
	20.96	2.32	6.1	0	76	[f].25	2.4	6.12	-----	(d)	----
	21.59	2.32	46.0	0	76	[f].25	145	1.74	[e]22.1	----	----
	21.59	2.25	8.0	0	[c]77	[f]1.70	11	5.32	142	57.2	54.6
	21.59	2.25	22.7	0	[c]77	[f]1.45	72	3.35	-----	(d)	----
	21.59	2.32	45.1	0	[c]78	[f]1.54	275	1.62	-----	(d)	----
	20.96	2.26	46.3	0	[c]77	[f]1.81	278	1.66	-----	(d)	----
8	21.59	3.63	45.7	0	[c]77	[f]1.75	177	2.05	-----	(d)	----
9	30.48	2.22	47.6	0	[c]77	[f]1.75	480	1.74	-----	(d)	----
Urethane foam											
1	10.16	1.00	45.7	0	32	169	162	1.36	38	72.4	69.8
	10.16	1.00	45.7	0	32	197	160	1.41	36.1	70.6	69.8
3	10.16	2.27	45.7	0	32	236	80	1.73	-----	(d)	----
4	21.59	1.01	46.6	0	32	171	580	2.05	16.3	9.7	8.9
5	21.59	1.81	41.8	0	32	154	400	2.30	24.8	27.9	----
	21.59	1.81	44.5	0	32	208	390	1.99	21.5	25.4	----
	21.59	1.81	44.8	0	32	154	350	2.26	24.2	29.2	----
6	20.96	2.26	6.1	0	32	131	71	8.52	16.4	2.5	4.2
	20.96	2.26	46.0	0	32	225	372	3.54	27.2	27.9	38.1
	20.96	2.26	71.9	0	32	239	380	2.13	33.8	81.8	82.0
	20.96	2.26	46.0	30	32	210	320	5.30	31.4	----	----
	20.96	2.26	46.3	60	32	239	304	7.50	27.2	----	----
	21.59	2.26	46.0	0	[c]32	225	330	2.69	28.5	----	----
8	21.34	3.63	44.8	0	32	139	152	3.36	39.3	66.3	67.3
	21.59	3.64	45.7	0	32	182	198	2.12	38.0	63.5	54.6
9	30.22	2.26	48.2	0	32	190	600	3.03	21.2	26.7	22.9

[c]Test performed in vacuum.
[d]Struck bottom of container.
[e]Time at striking bottom.
[f]10.2-cm-diameter probe.

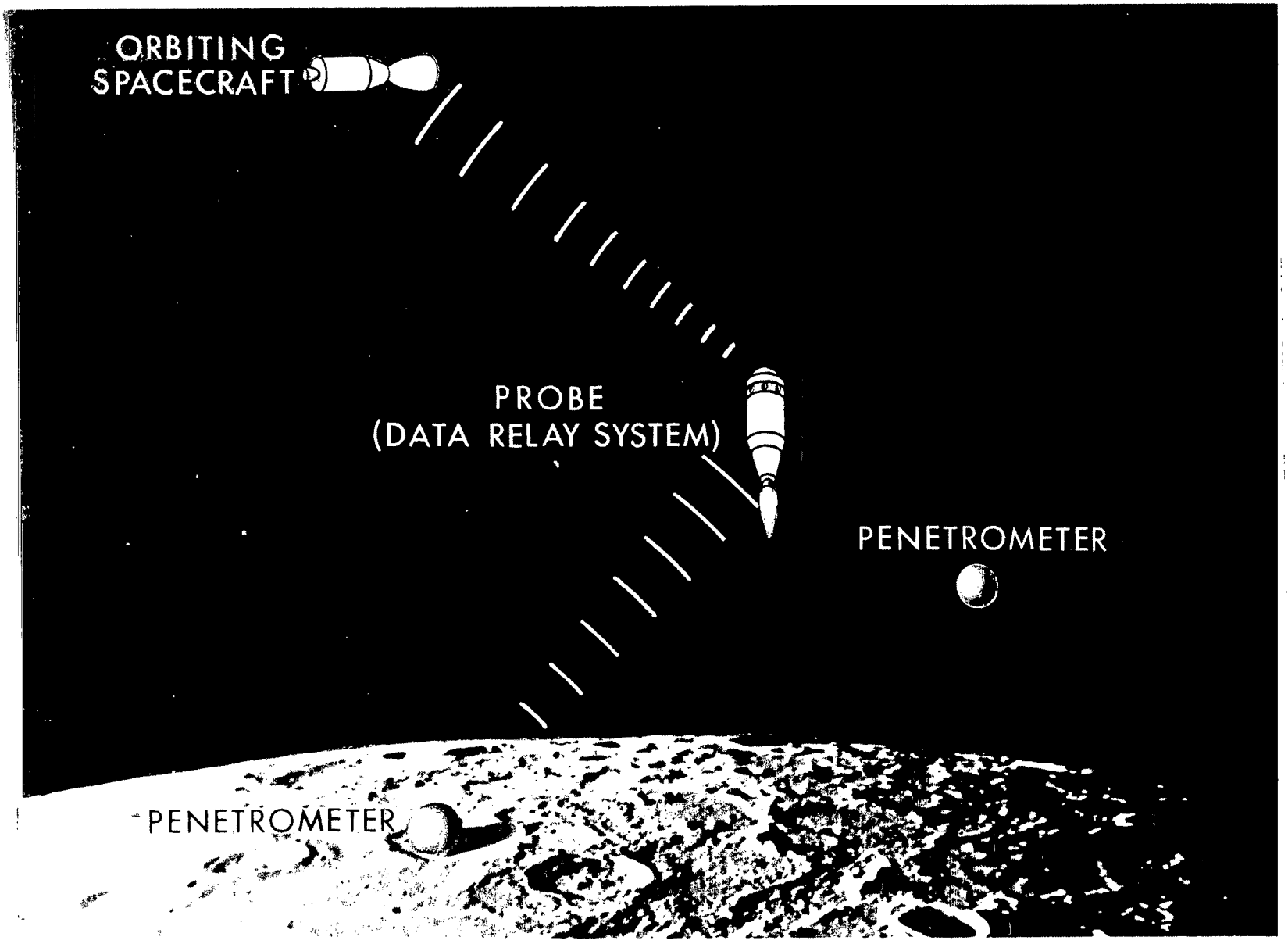

Figure 1.- Penetrometer system proposed for space applications.

L-67-6615

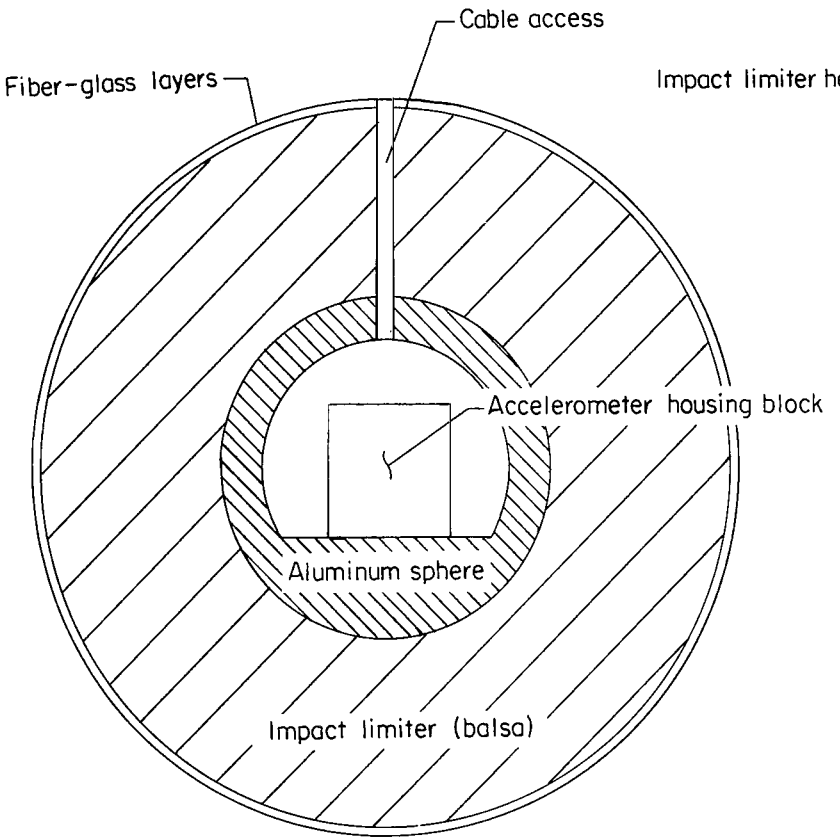

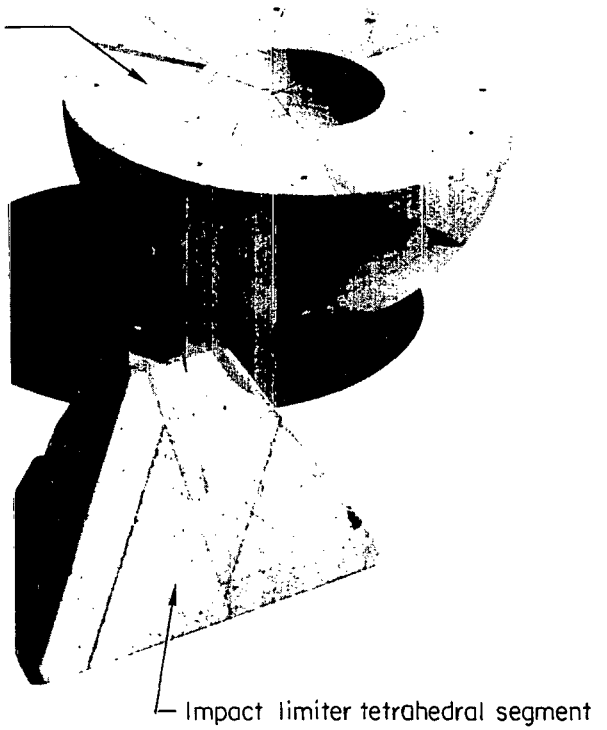

(a) Limiter-equipped configuration and impact limiter sections. L-67-6614

Figure 2.- Penetrometer test configurations and components.

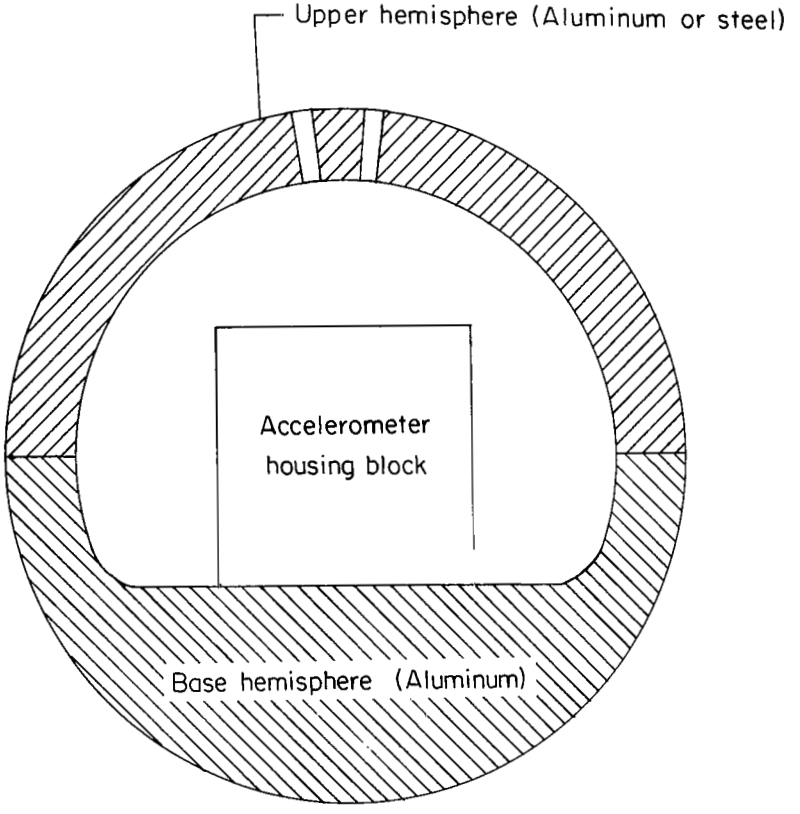

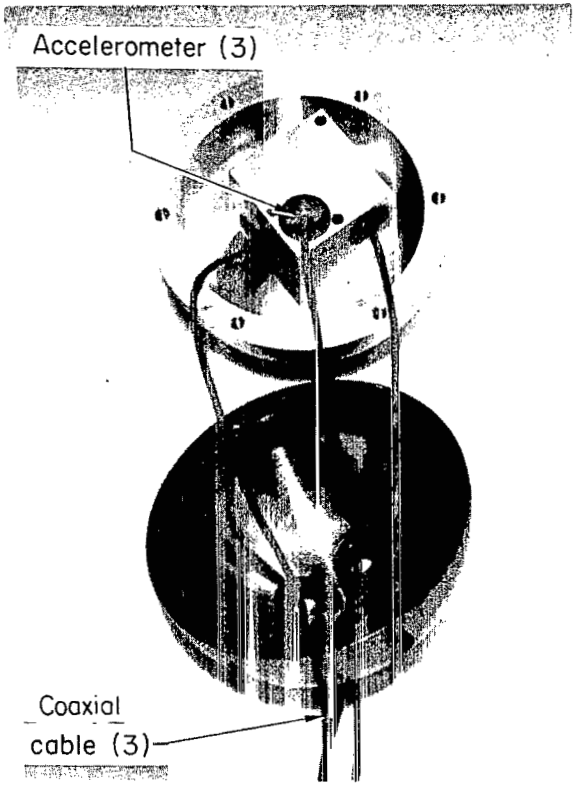

(b) Rigid configuration – all metal construction. L-67-6613

Figure 2.- Continued.

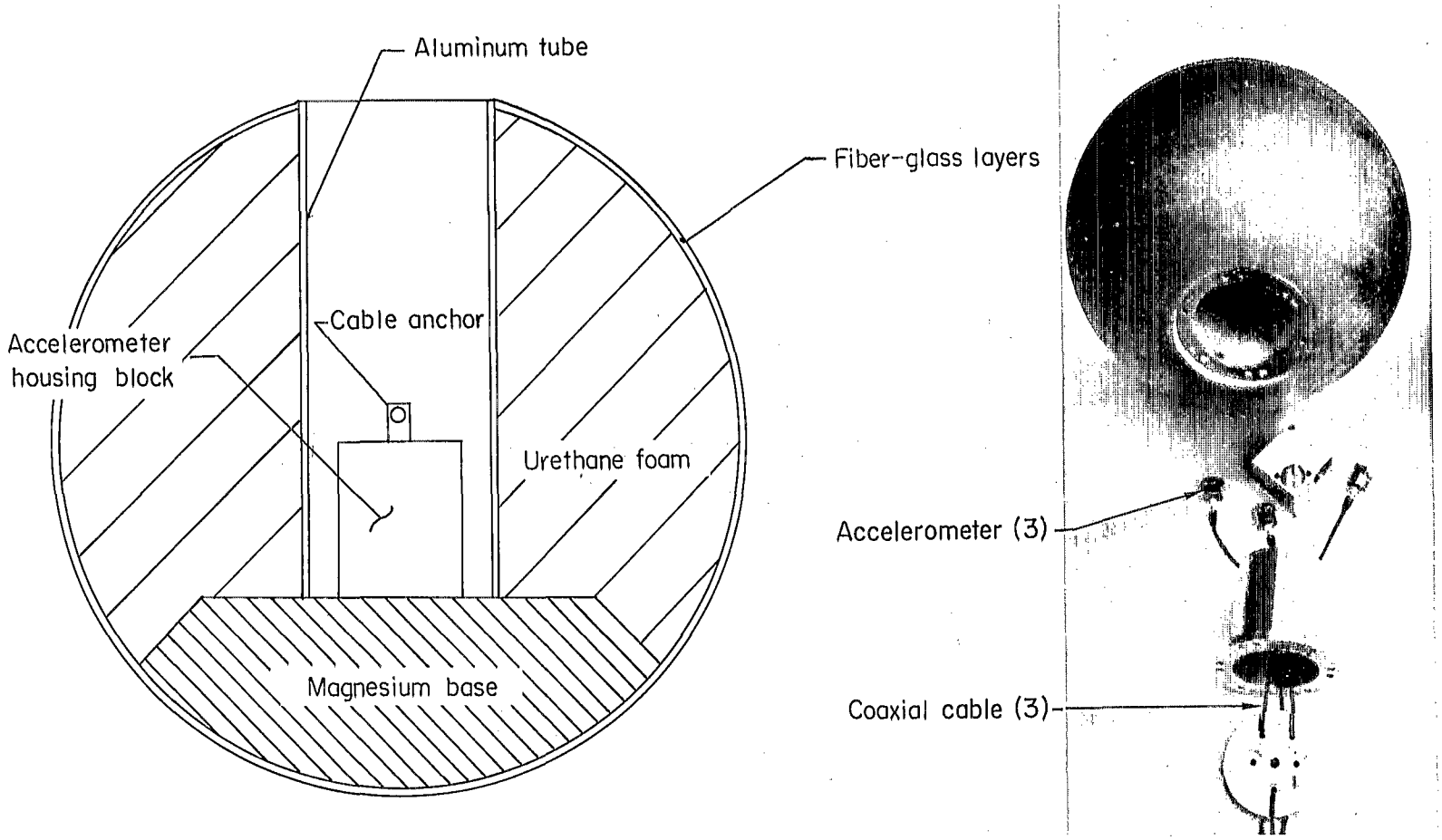

(c) Rigid configuration – metal impact base and fiber-glass shell construction. L-67-6612

Figure 2.- Concluded.

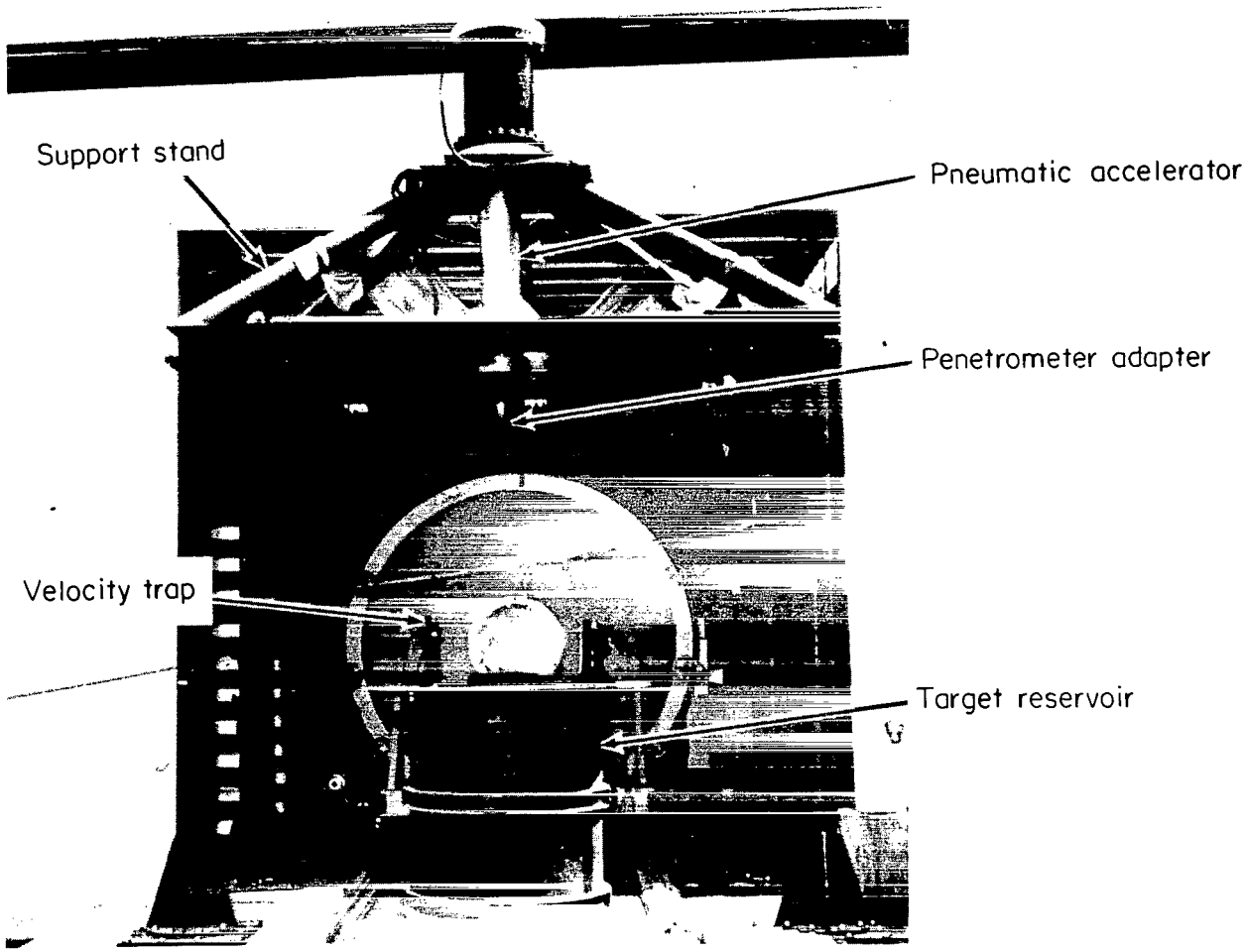

Figure 3.- Apparatus for penetrometer impact tests. L-67-6617

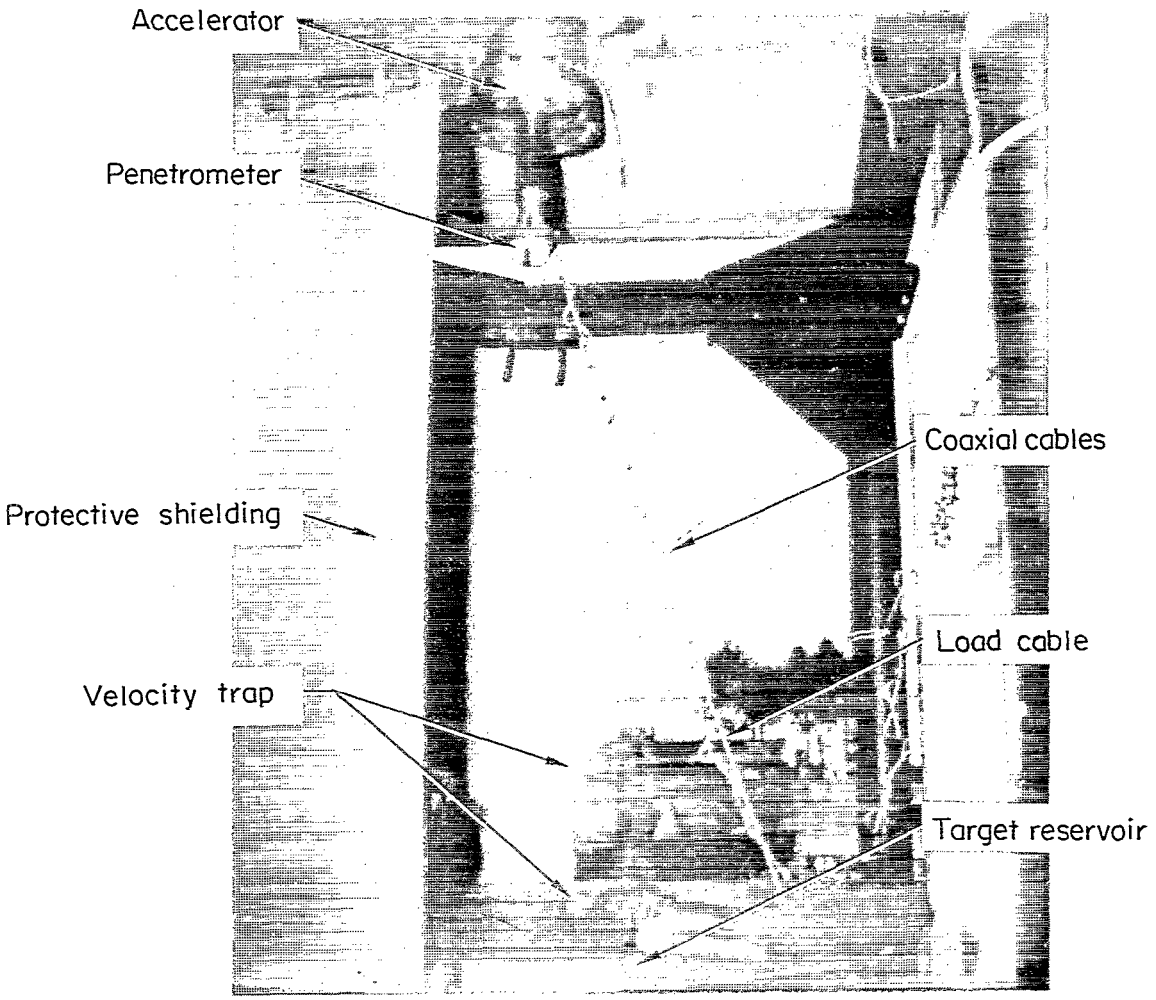

Figure 4.- Setup for penetrometer impact test.

L-67-6616

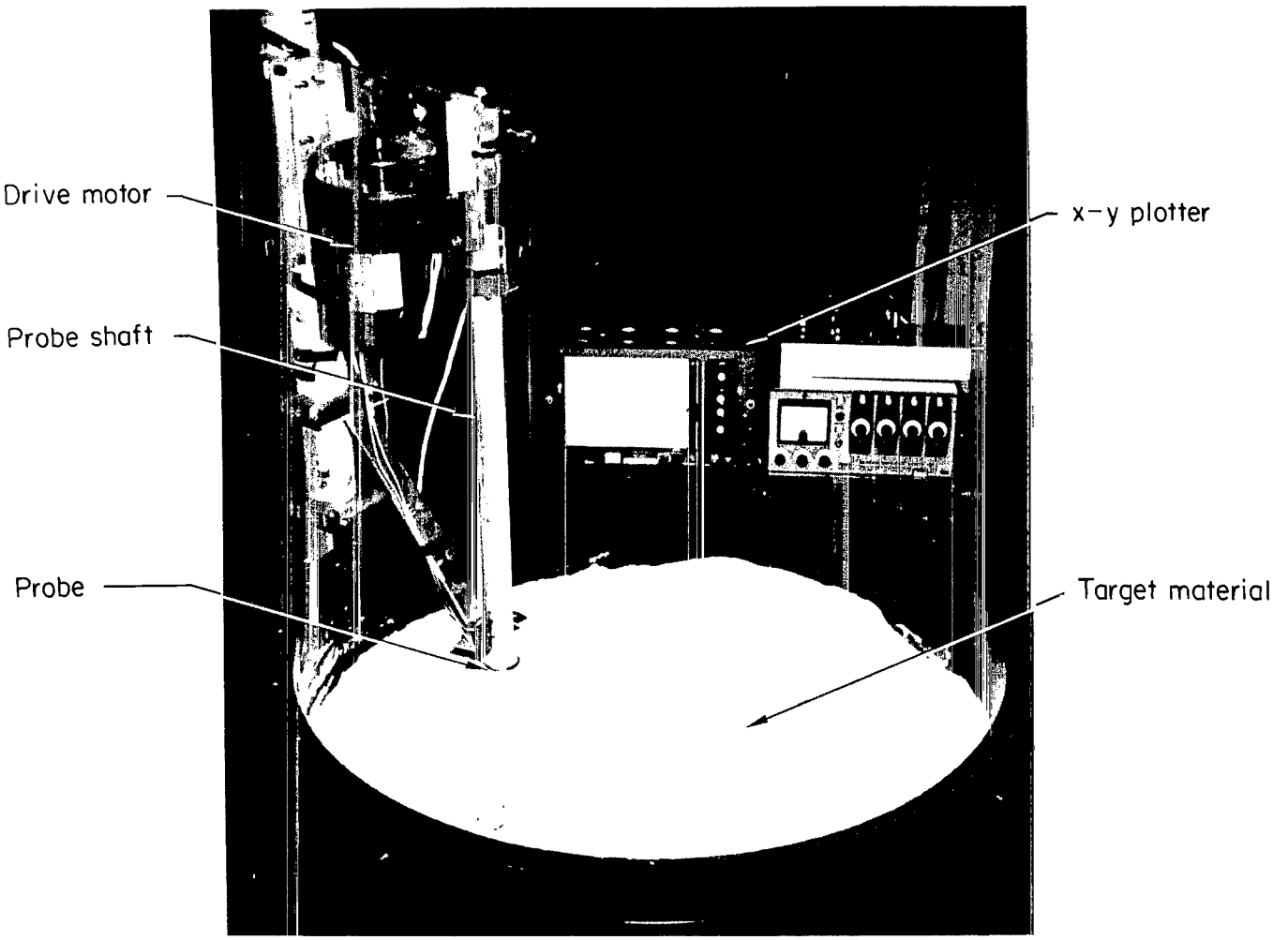

Figure 5.- Apparatus for measuring target material bearing strength. L-67-6618

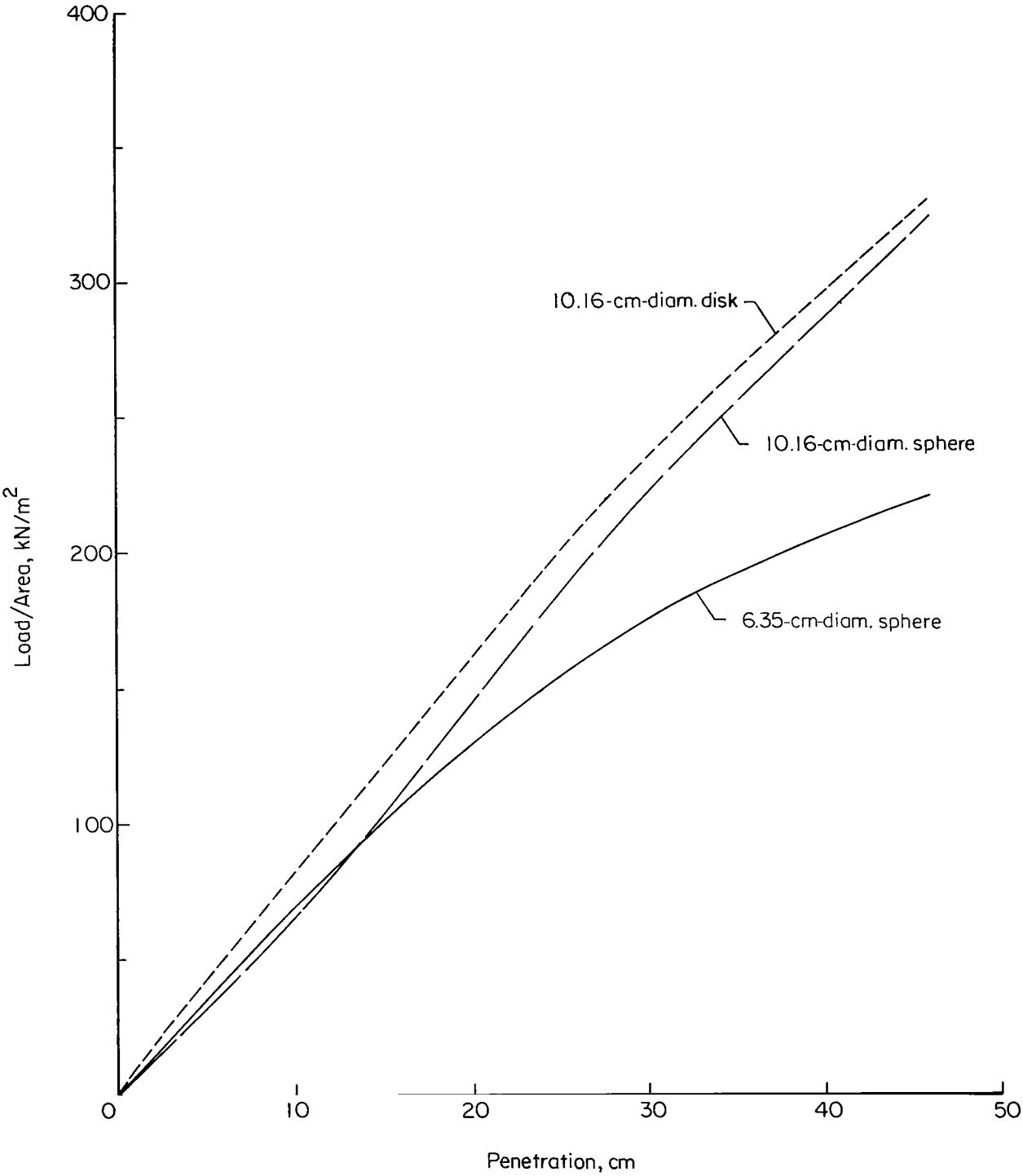

(a) Nevada 60 sand, loosely packed $\left(\rho_{tar} = 1555\ kg/m^3\right)$.

Figure 6.- Results from quasi-static loading tests performed on penetrable target materials.

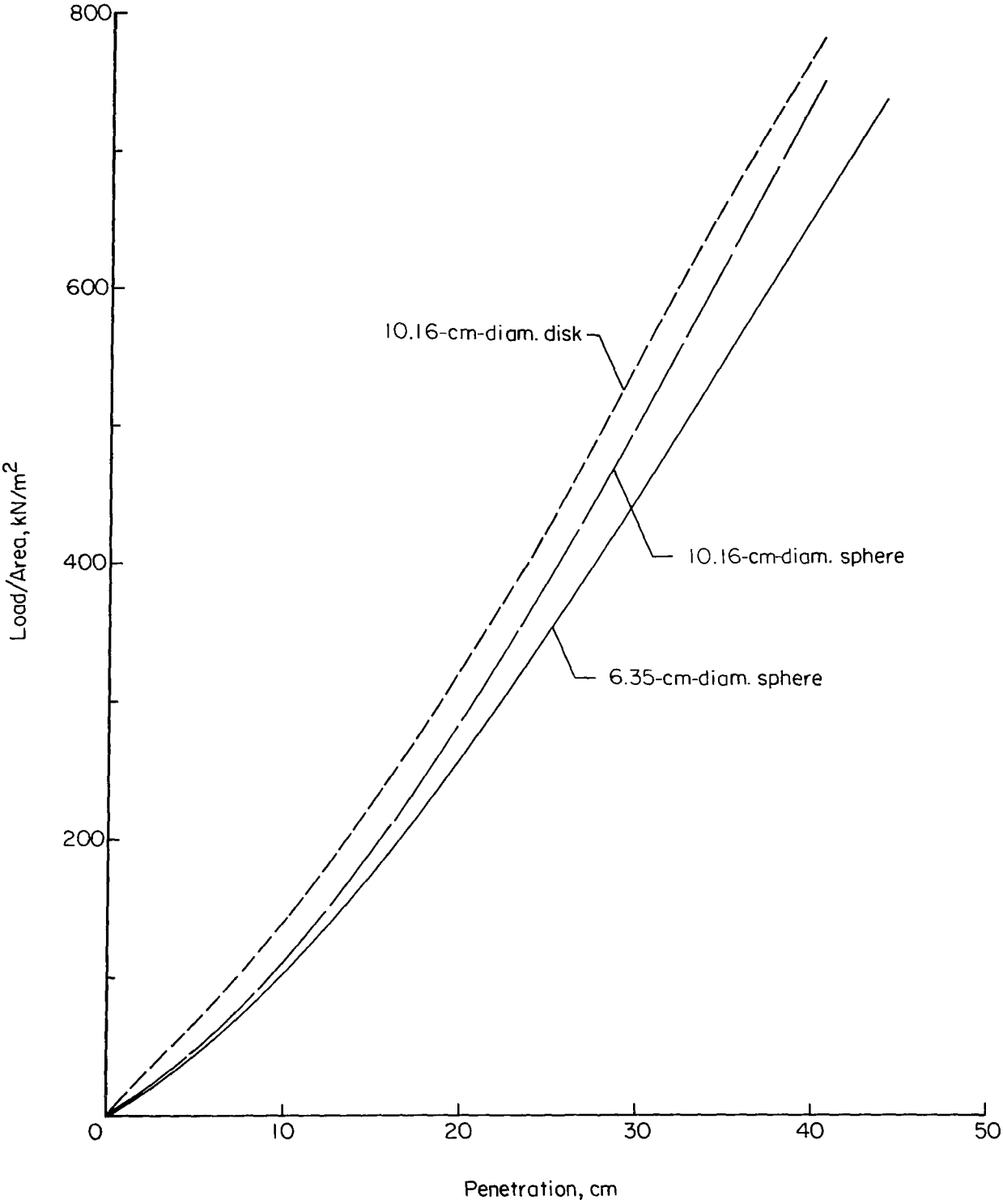

(b) Nevada 120 sand, densely packed (ρ_{tar} = 1506 kg/m^3).

Figure 6.- Continued.

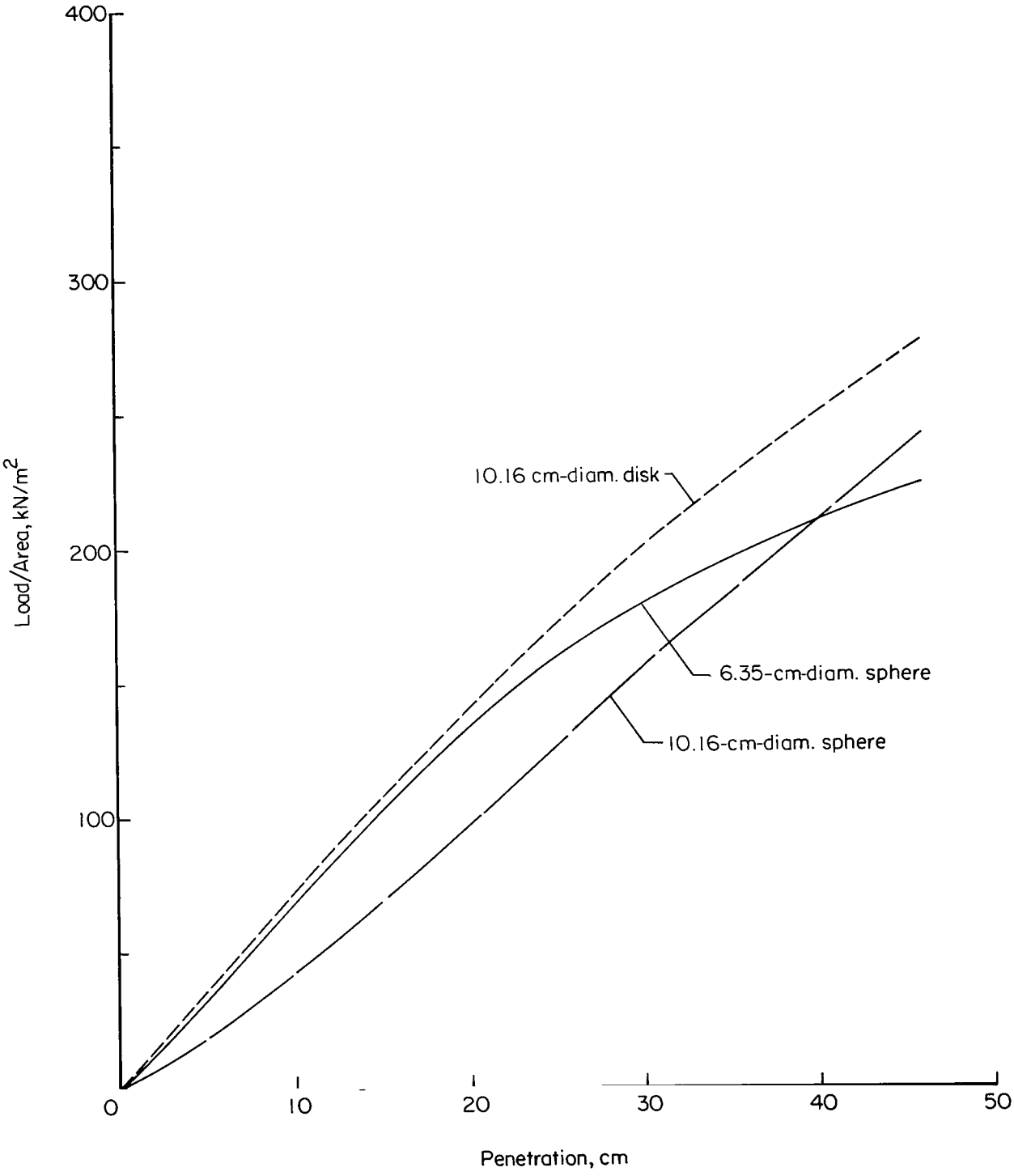

(c) Nevada 120 sand, lightly packed (ρ_{tar} = 1410 kg/m^3).

Figure 6.- Continued.

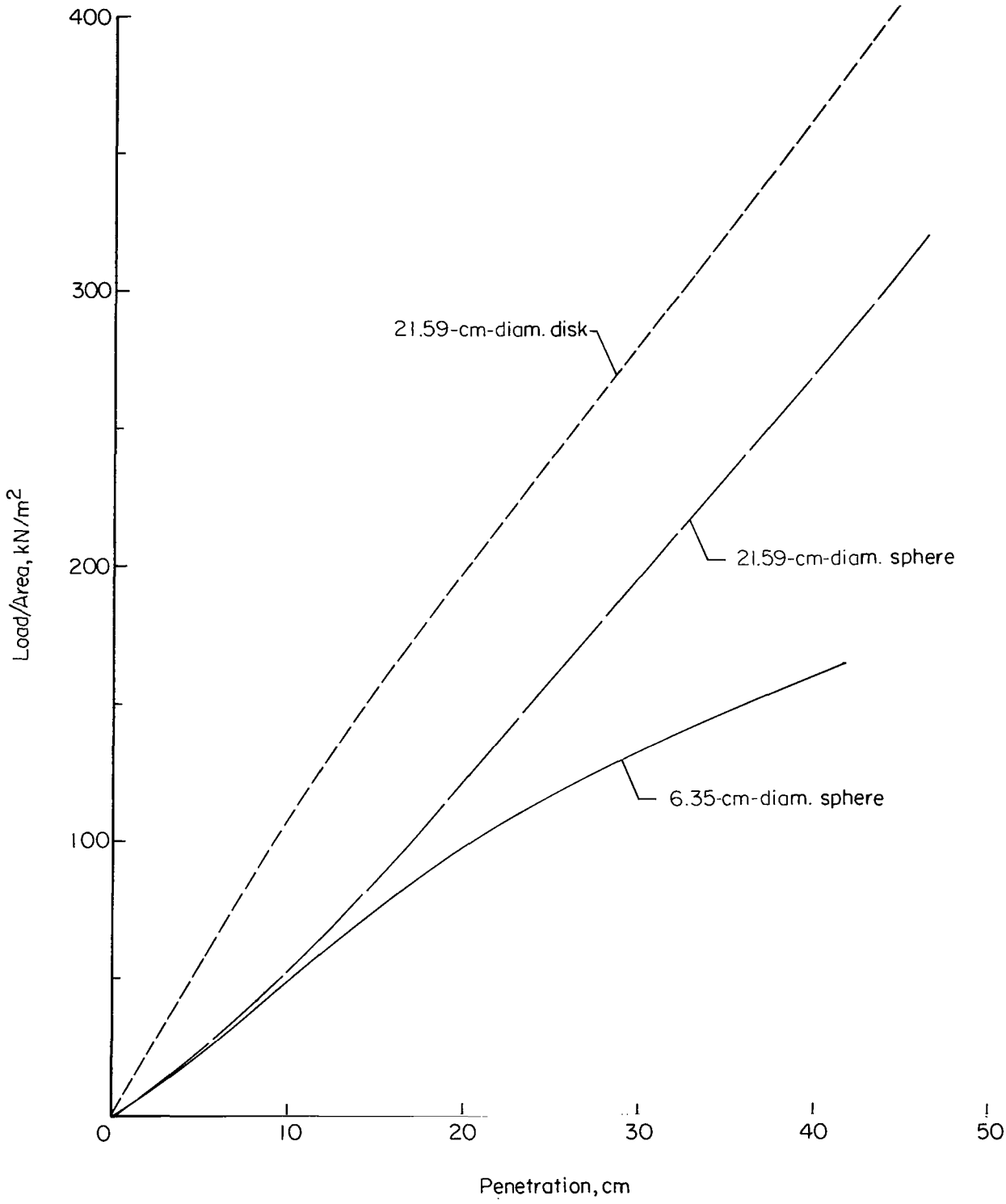

(d) Nevada 120 sand, loosely packed $\left(\rho_{tar} = 1378\ kg/m^3\right)$.

Figure 6.- Continued.

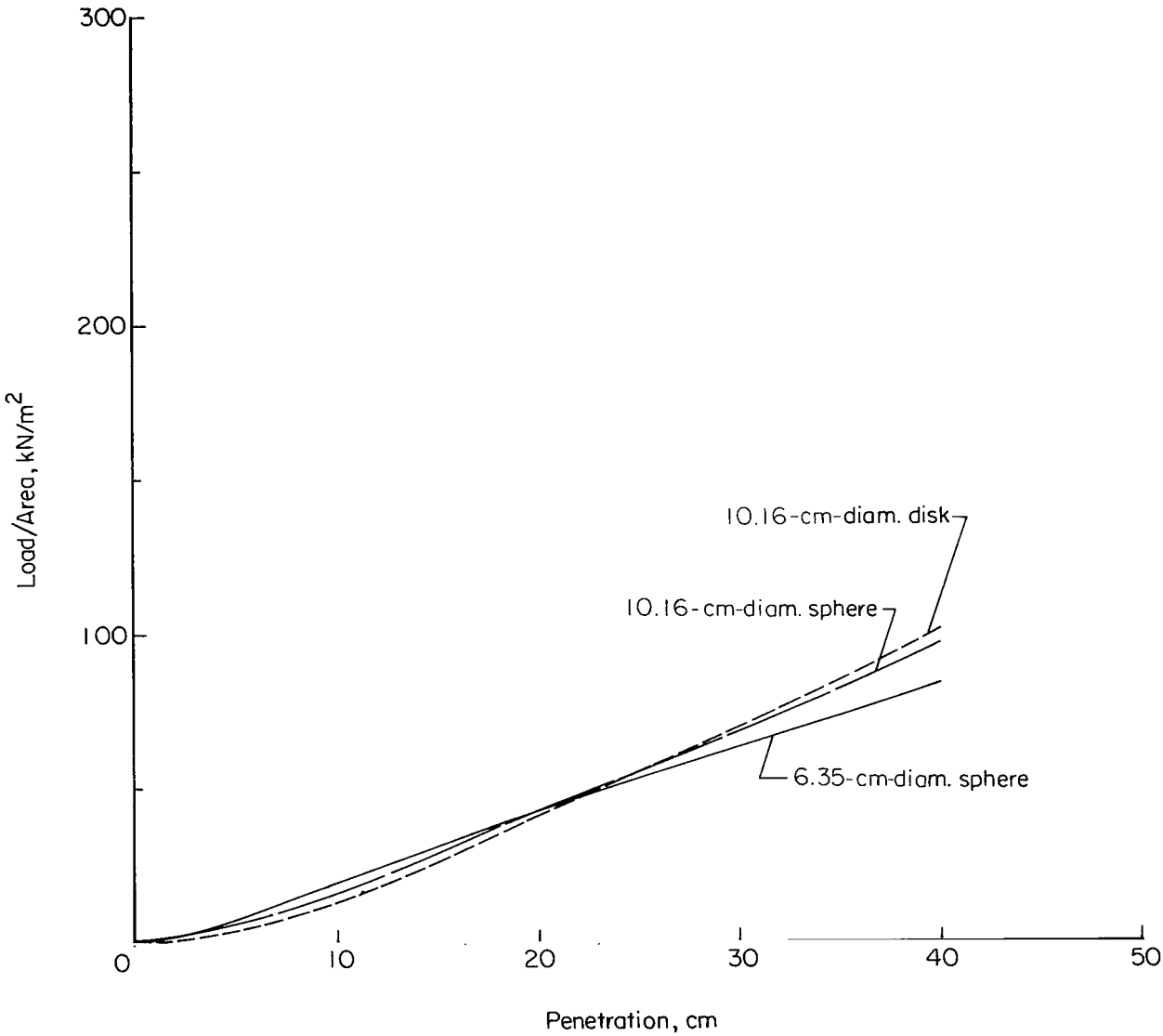

(e) Basalt sand $\left(\rho_{tar} = 1442\ kg/m^3\right)$.

Figure 6.- Continued.

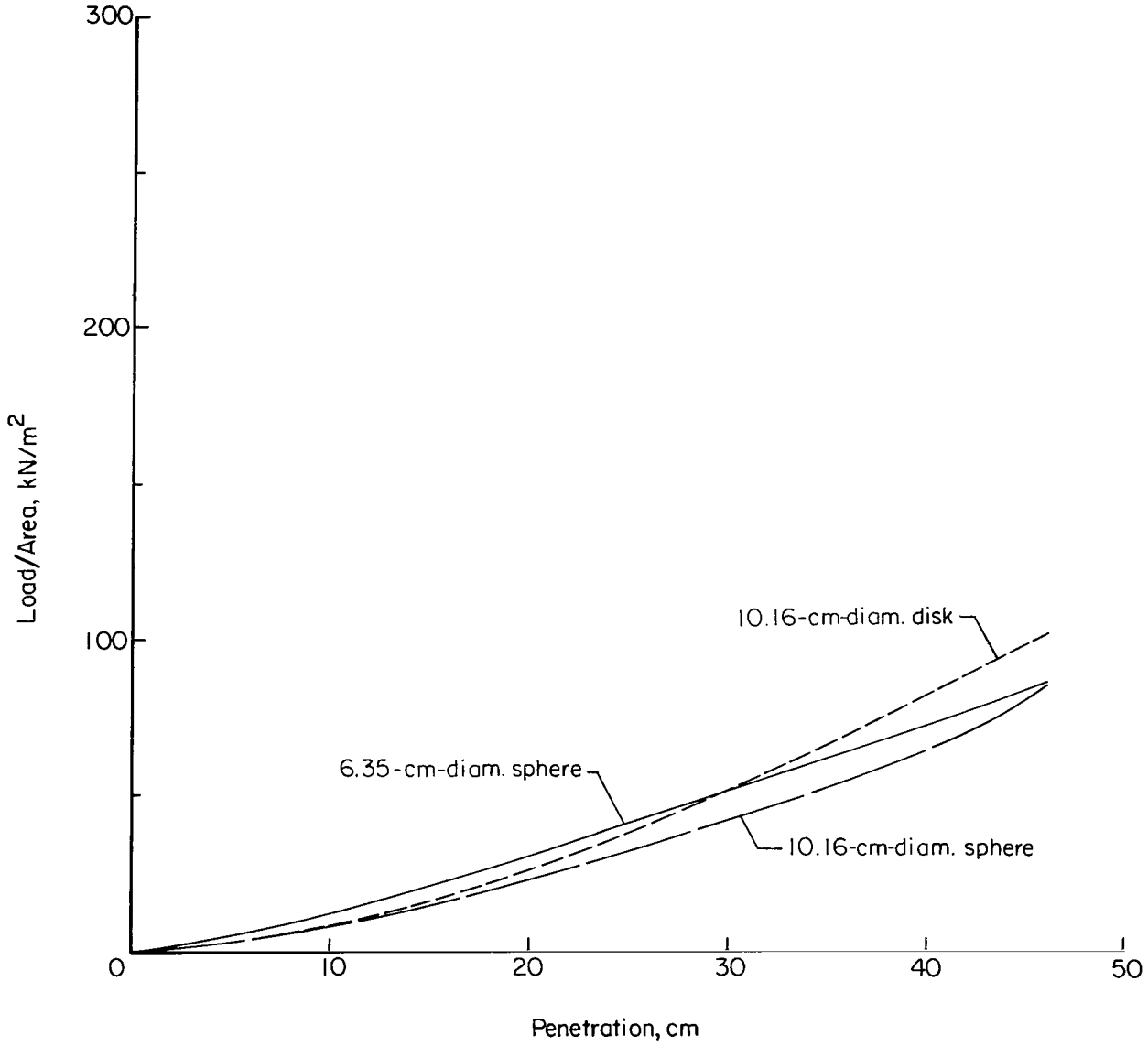

(f) Basalt silt $\left(\rho_{tar} = 1297\ kg/m^3\right)$.

Figure 6.- Continued.

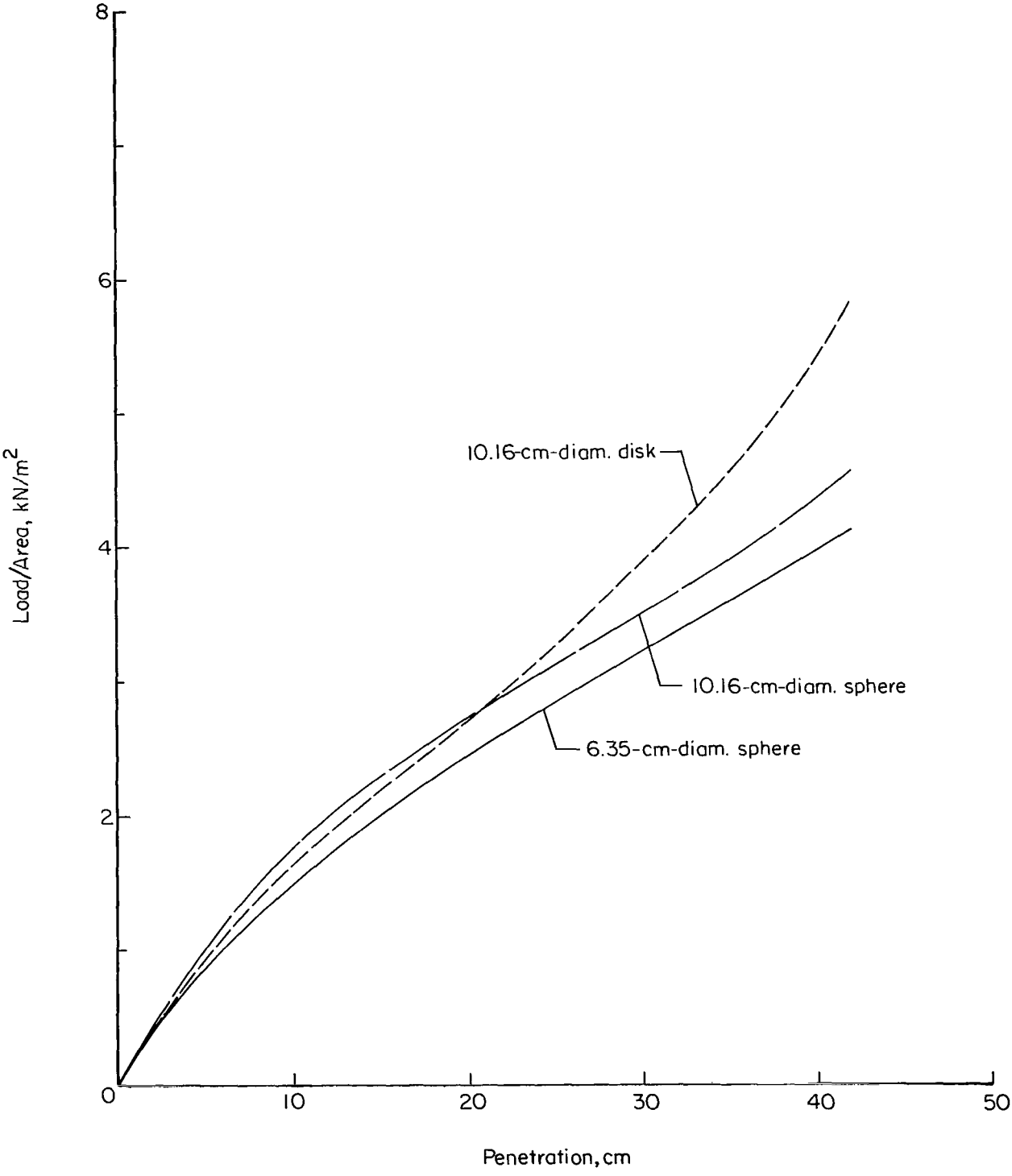

(g) Powdered silica under vacuum (ρ_{tar} = 77 kg/m^3).

Figure 6.- Continued.

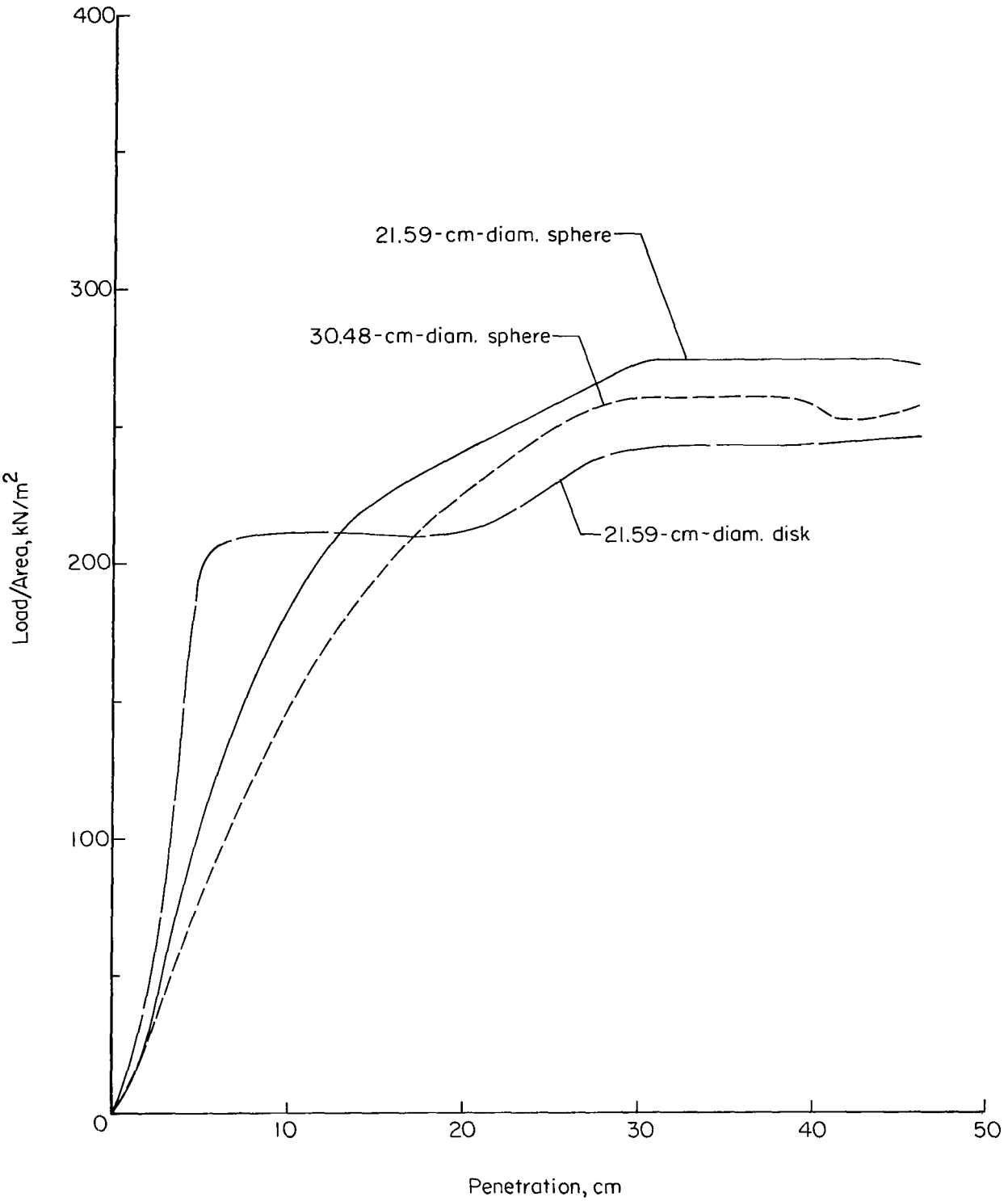

(h) Urethane foam $\left(\rho_{tar} = 32\ kg/m^3\right)$.

Figure 6.- Concluded.

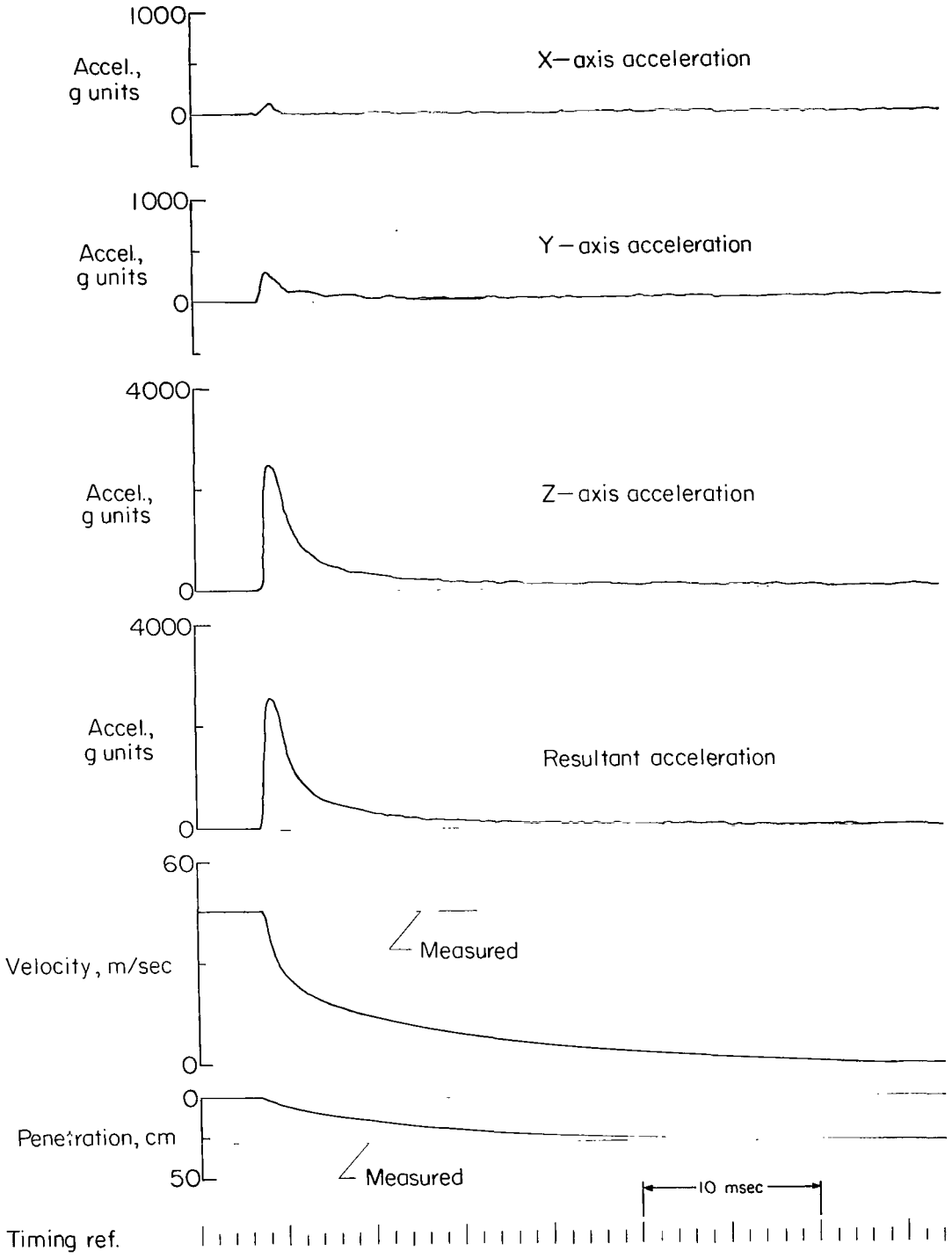

Figure 7.- Typical data output from computer. Penetrometer configuration 1; target material, lightly packed Nevada 120 sand; impact velocity, 45.7 m/sec.

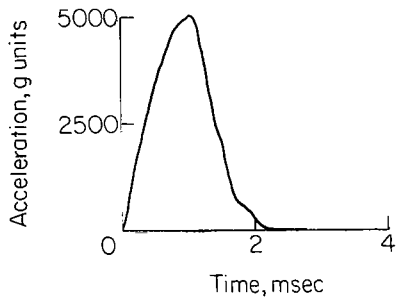

(a) Steel plate. Configuration 7; V = 46.6 m/sec.

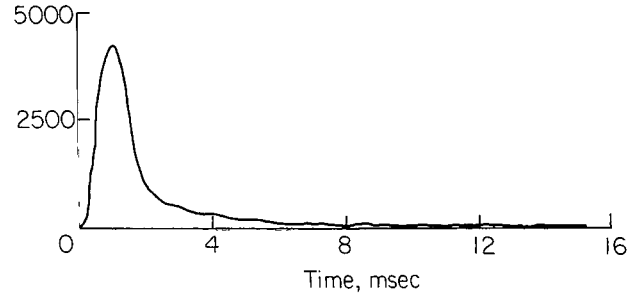

(b) Basalt agglomerate. Configuration 7; V = 63.4 m/sec.

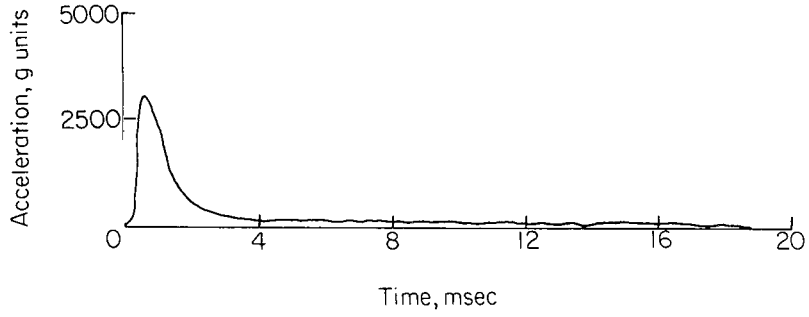

(c) Nevada 60 sand, loosely packed. Configuration 6; V = 46 m/sec.

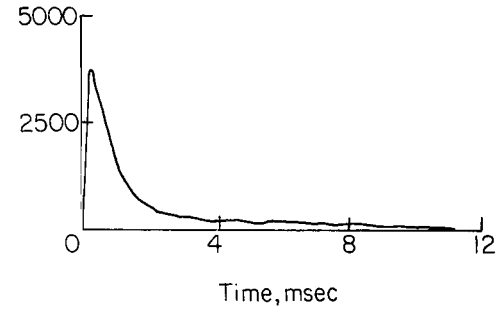

(d) Nevada 120 sand, densely packed. Configuration 6; V = 46 m/sec.

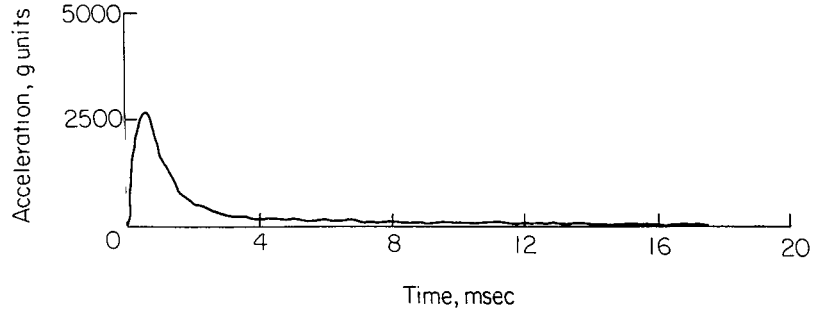

(e) Nevada 120 sand, lightly packed. Configuration 6; V = 45.7 m/sec.

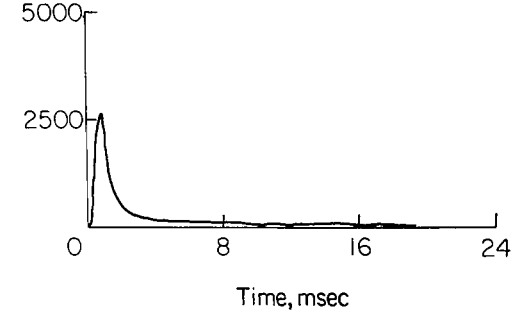

(f) Nevada 120 sand, loosely packed. Configuration 6; V = 45.1 m/sec.

Figure 8.- Reproductions of typical resultant acceleration time histories.

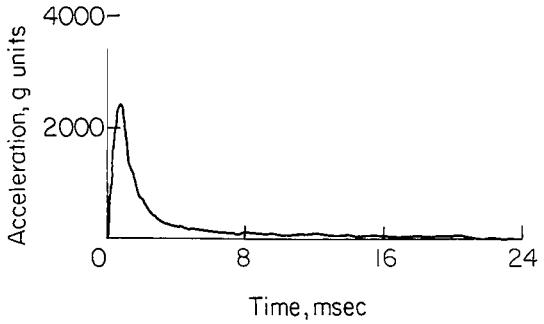

(g) Basalt sand. Configuration 6; V = 44.8 m/sec.

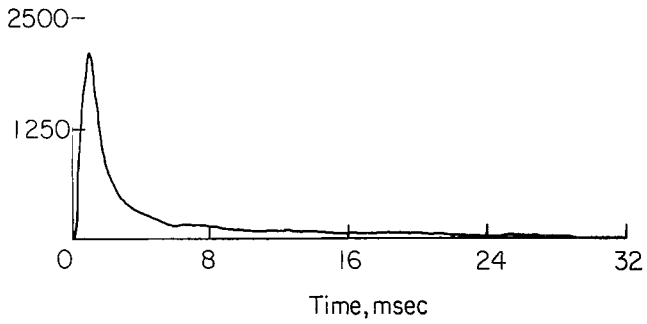

(h) Basalt silt. Configuration 6; V = 45.4 m/sec.

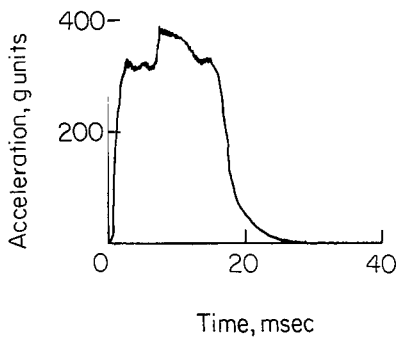

(i) Urethane foam. Configuration 6; V = 46 m/sec.

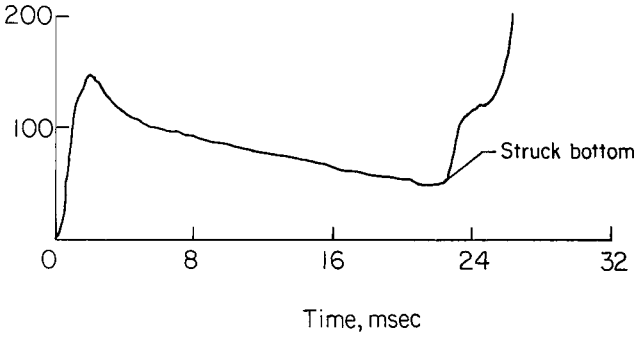

(j) Powdered silica in atmosphere. Configuration 6; V = 46 m/sec.

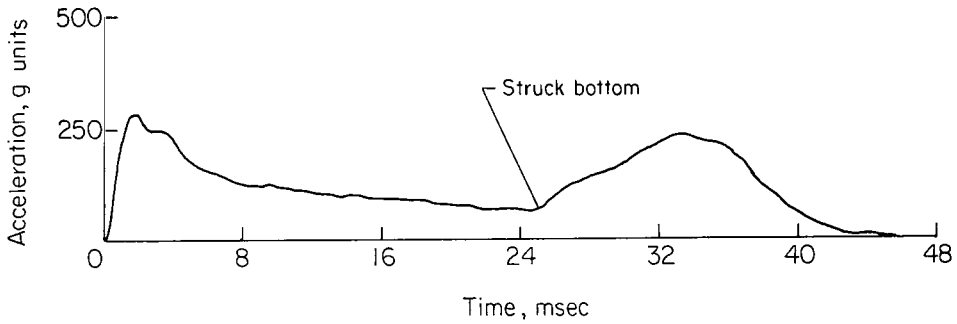

(k) Powdered silica in vacuum. Configuration 6; V = 46.3 m/sec.

Figure 8.- Concluded.

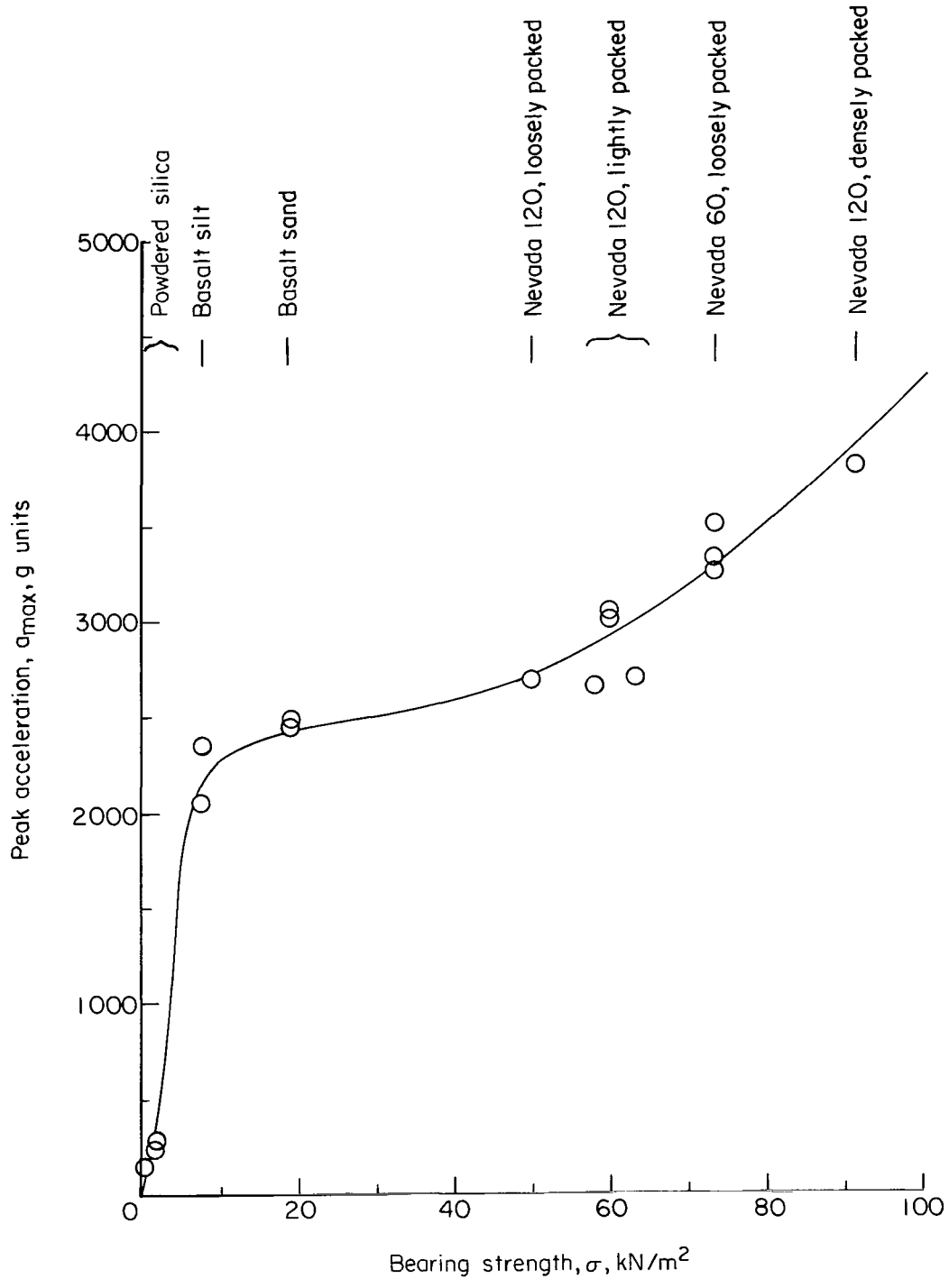

(a) Peak acceleration.

Figure 9.- Variation of nominal penetrometer impact characteristics with the bearing strength of particulate target materials. V ≈ 46 m/sec.

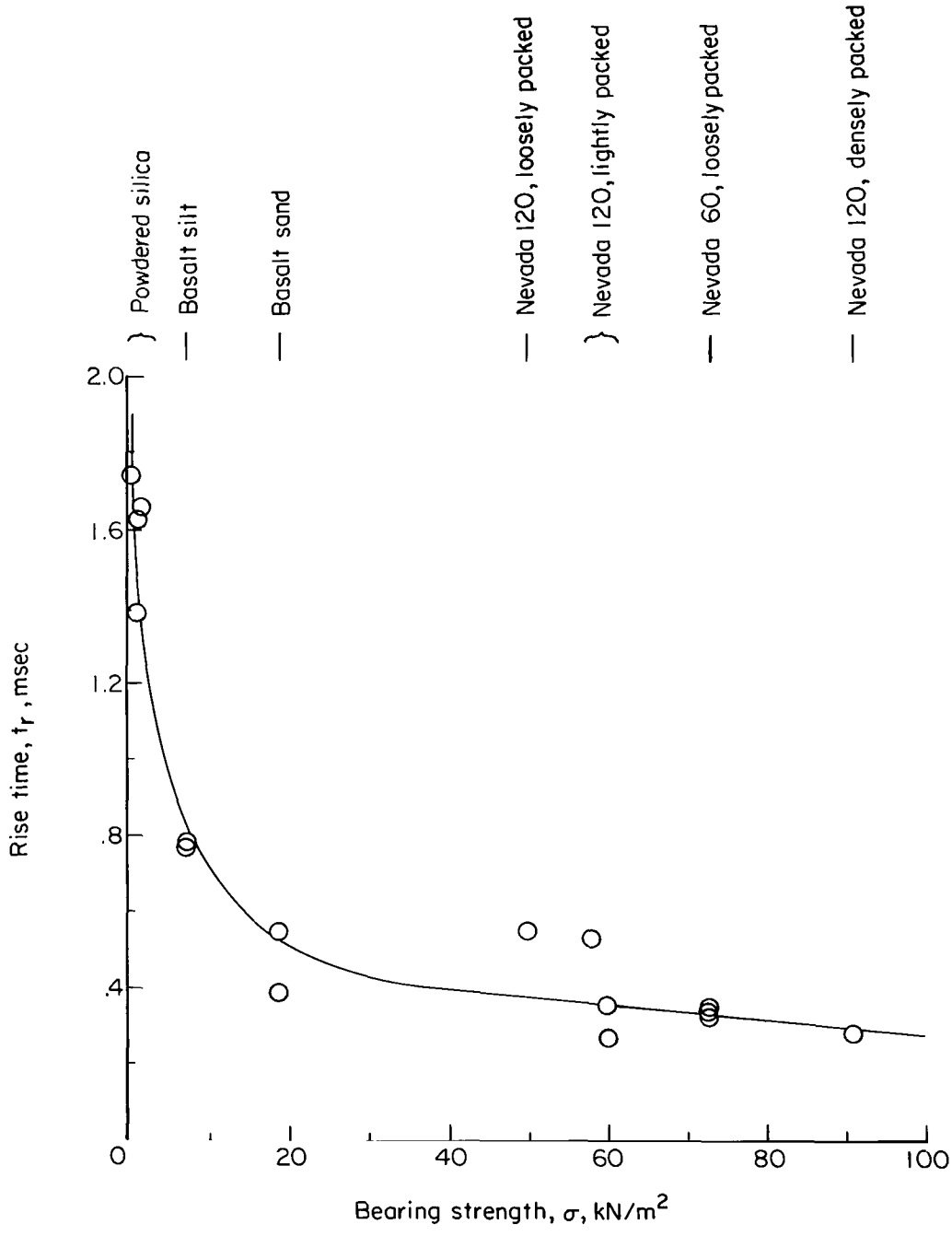

(b) Rise time.

Figure 9.- Continued.

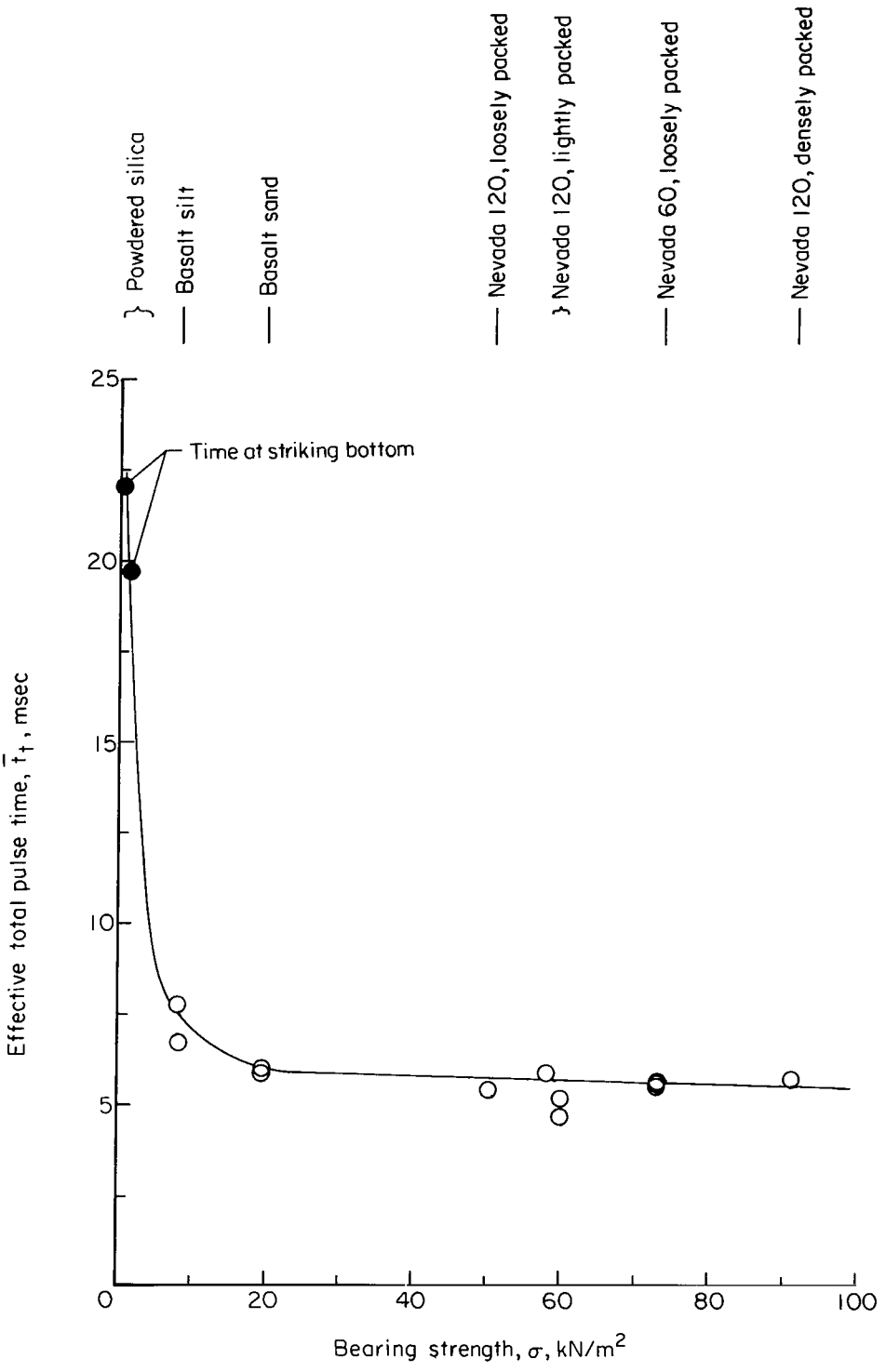

(c) Effective total pulse time.

Figure 9.- Concluded.

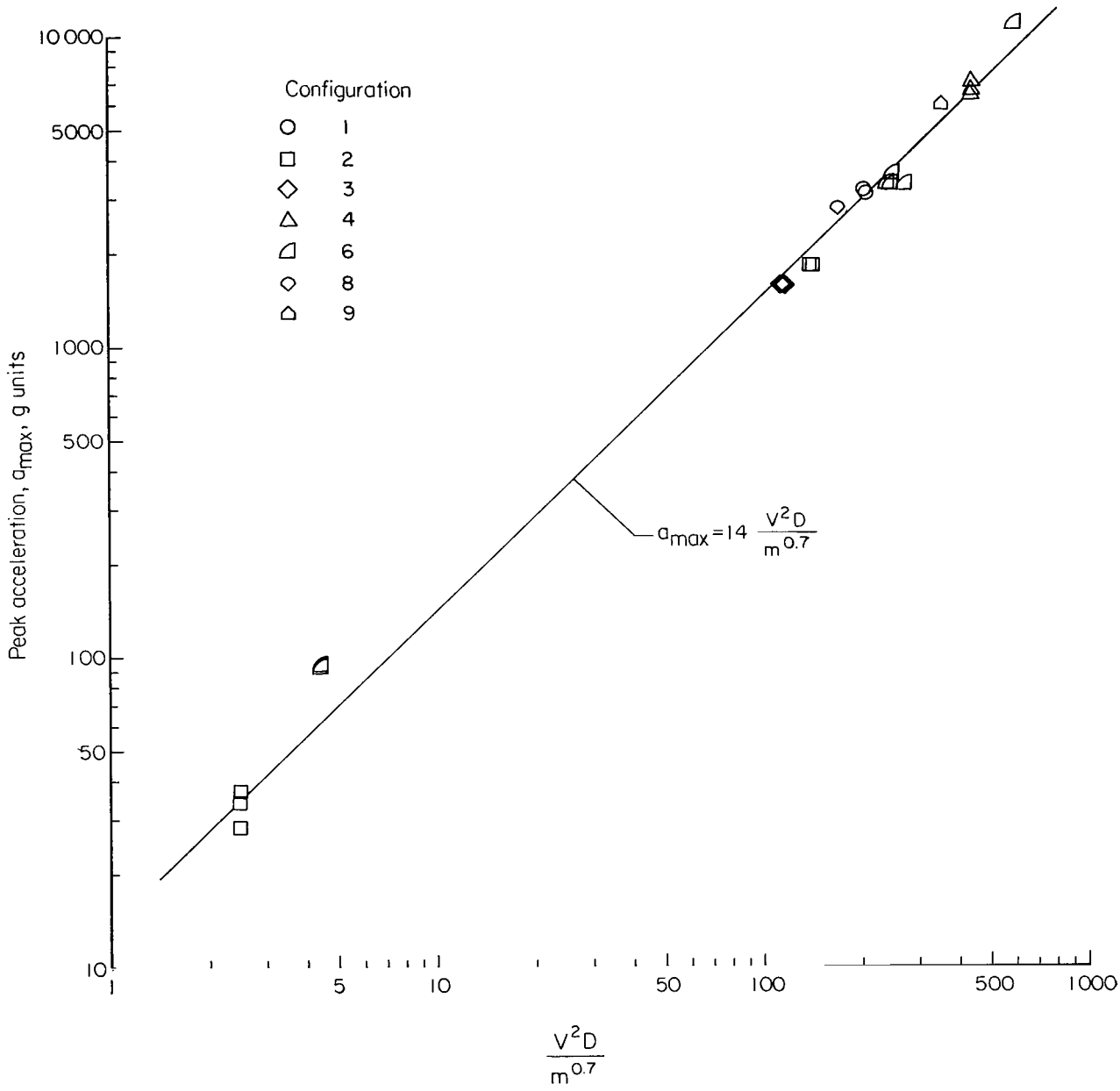

(a) Nevada 60 sand, loosely packed.

Figure 10.- Summary of peak acceleration data from penetrometer impact tests.

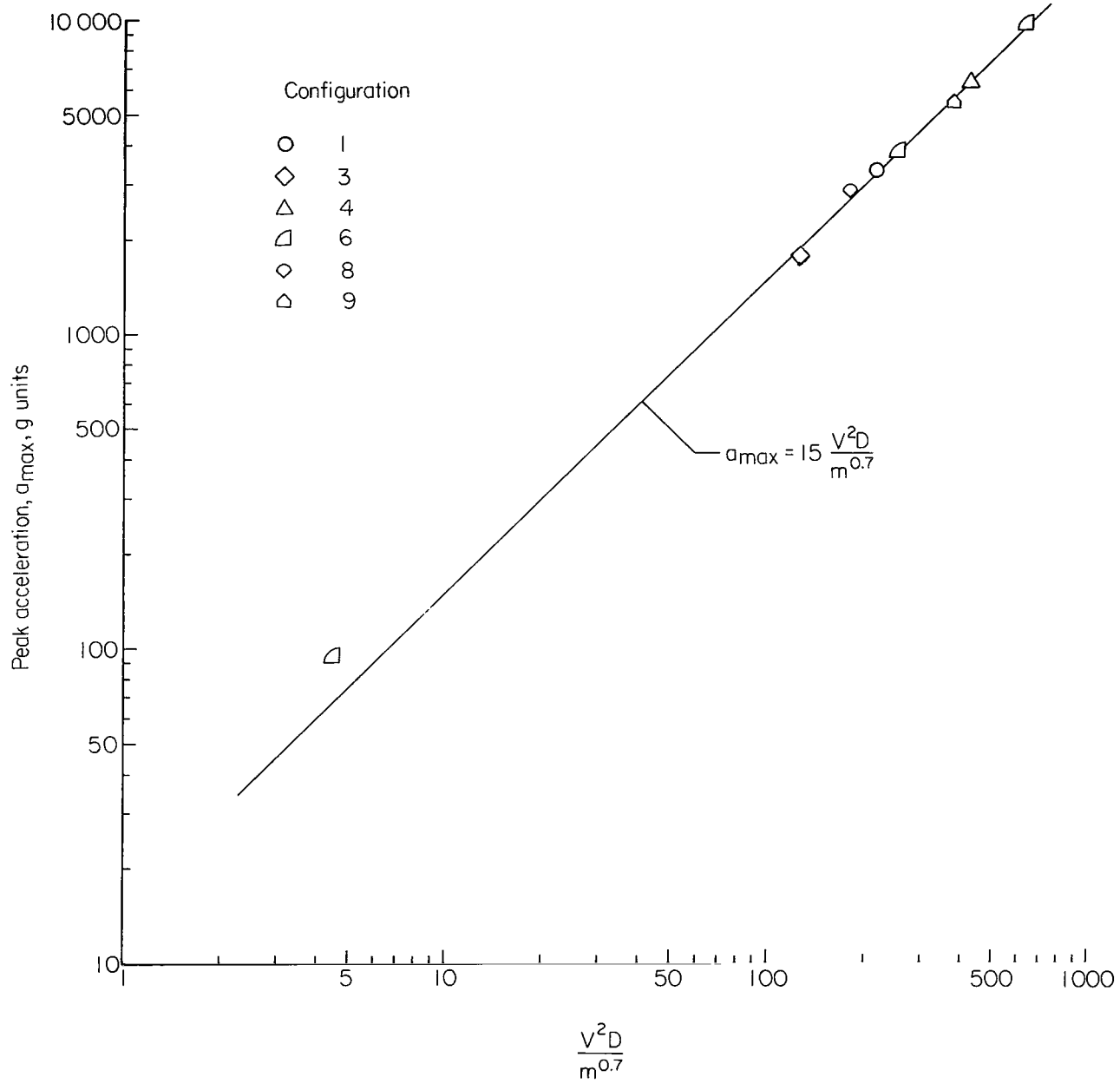

(b) Nevada 120 sand, densely packed.

Figure 10.- Continued.

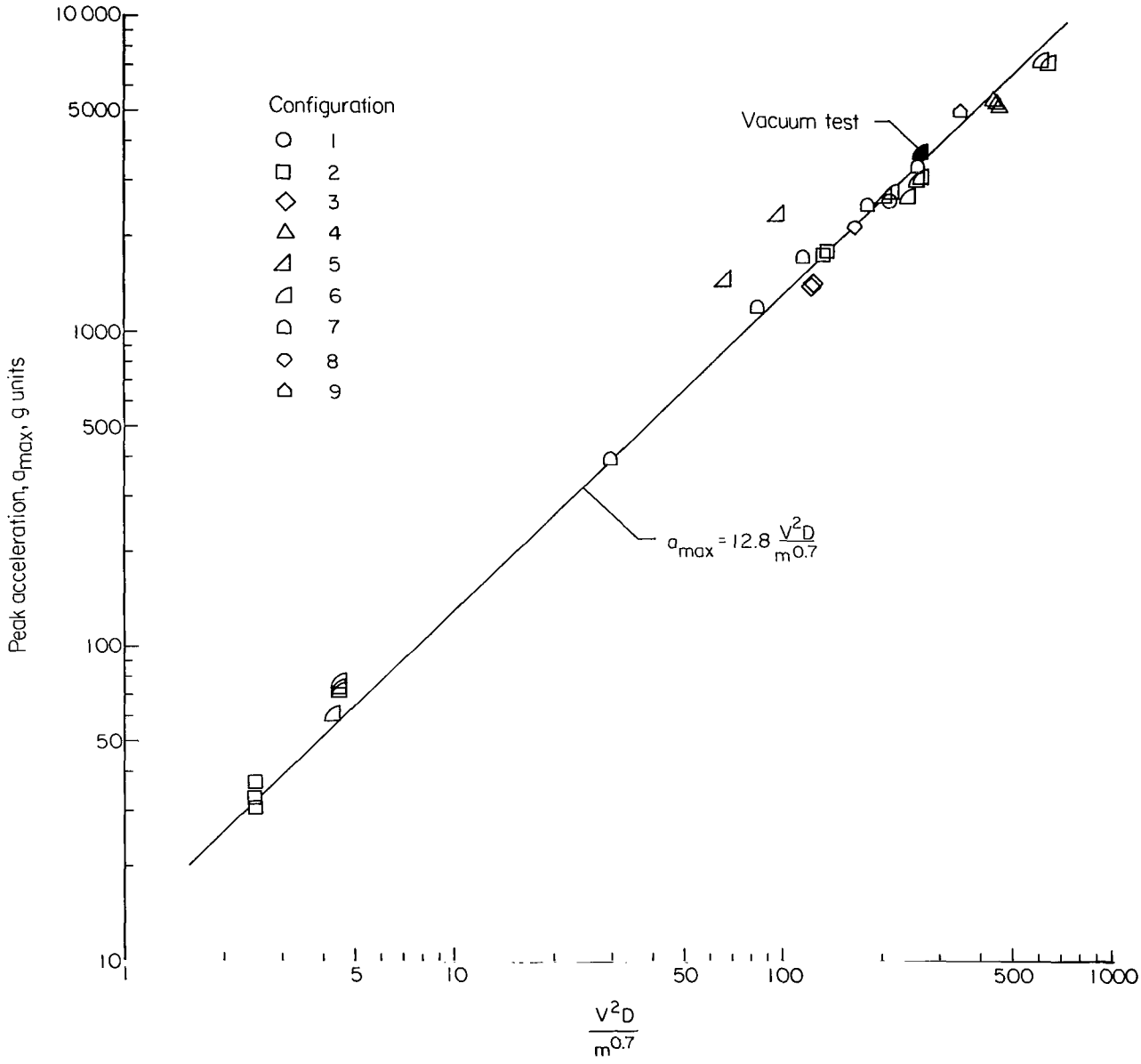

(c) Nevada 120 sand, lightly packed.

Figure 10.- Continued.

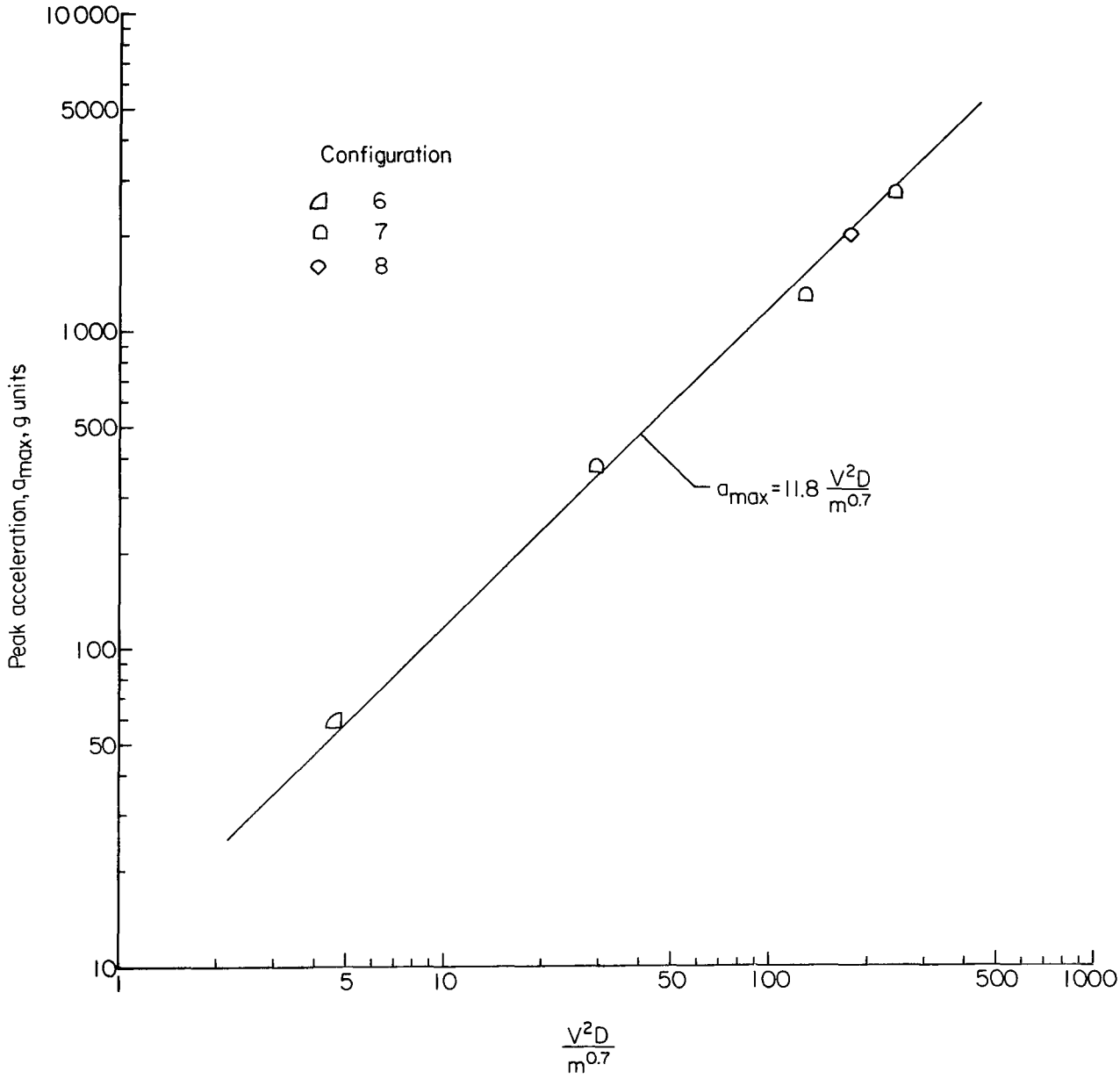

(d) Nevada 120 sand, loosely packed.

Figure 10.- Continued.

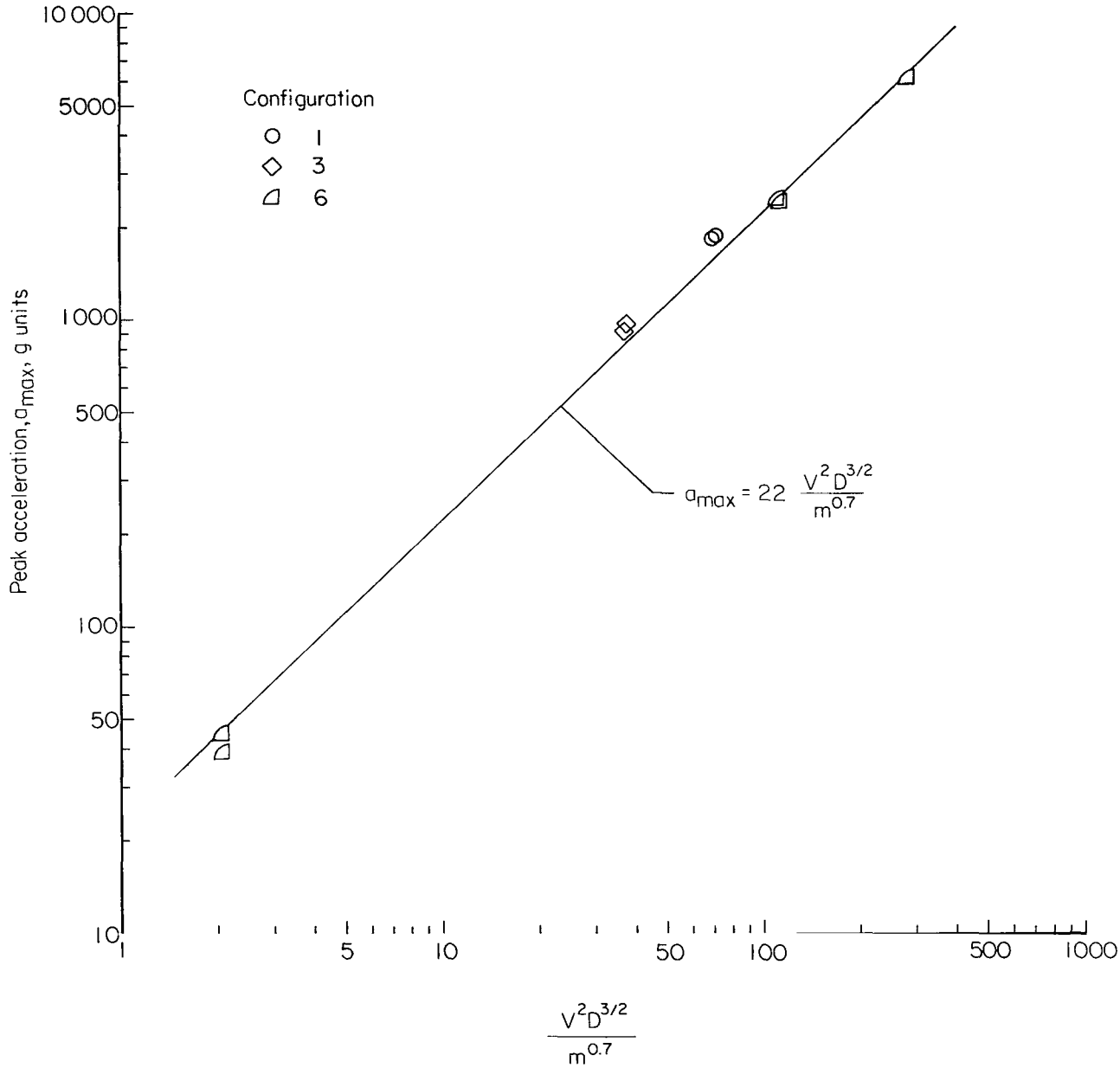

(e) Basalt sand.

Figure 10.- Continued.

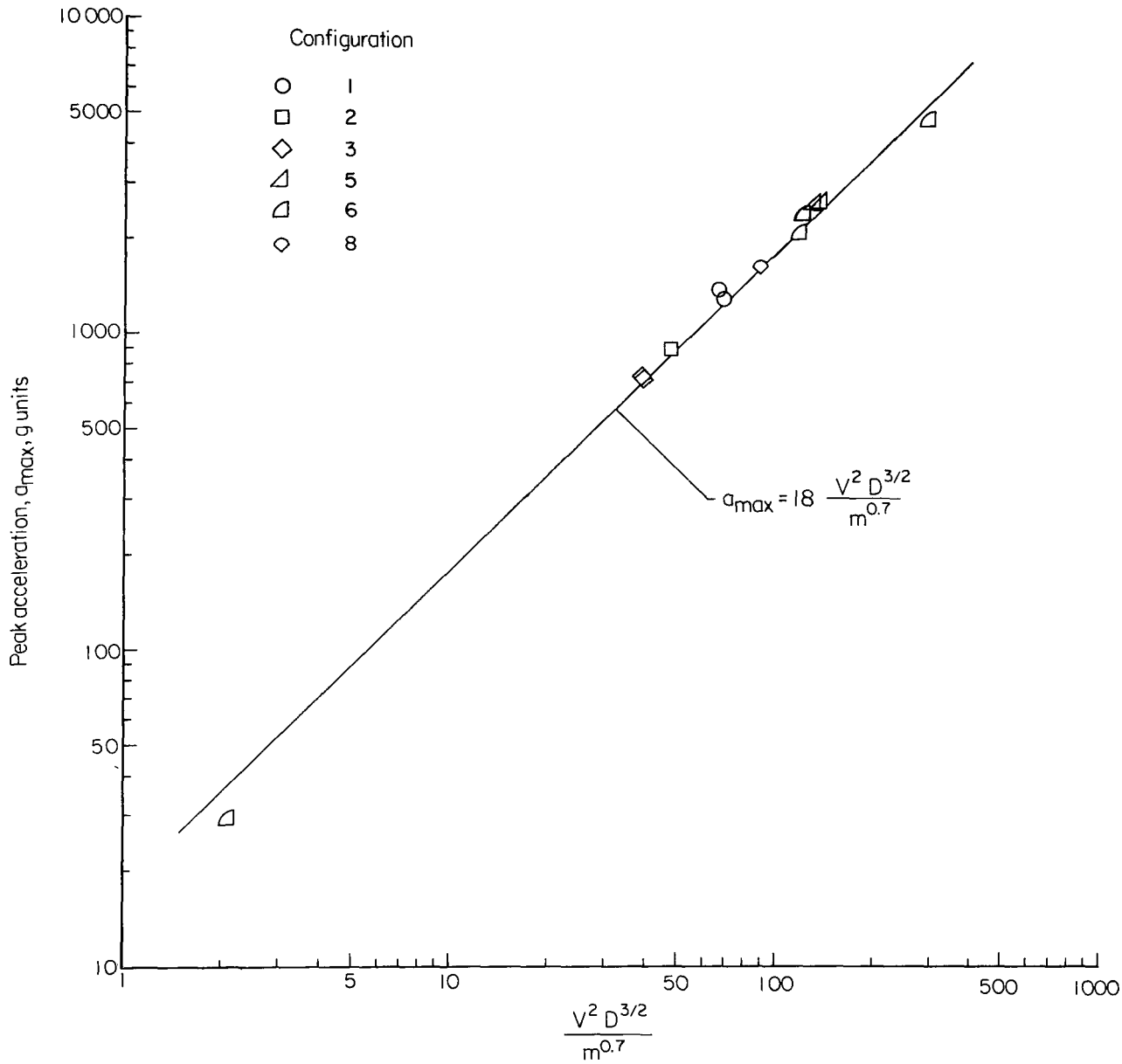

(f) Basalt silt.

Figure 10.- Continued.

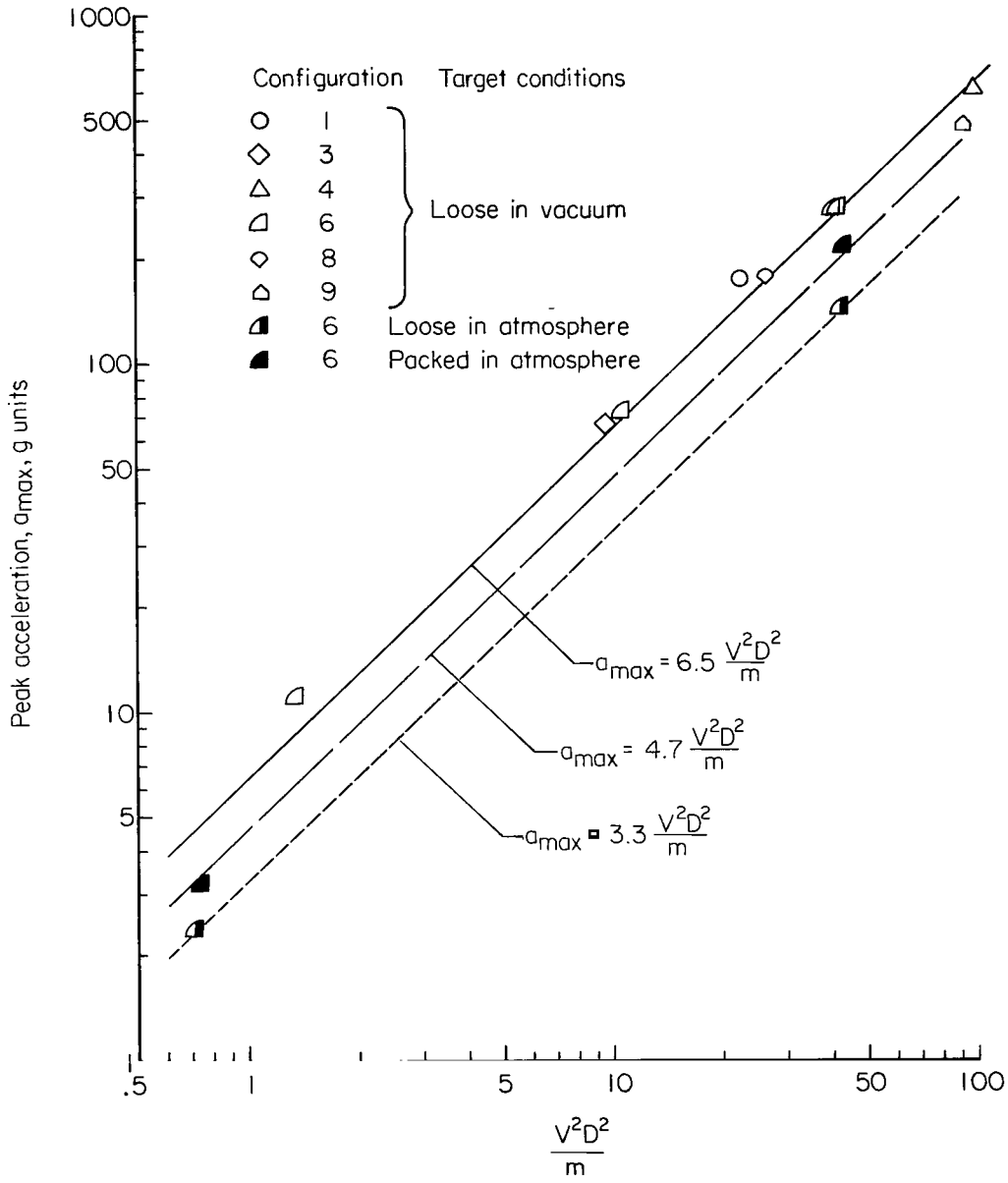

(g) Powdered silica.

Figure 10.- Concluded.

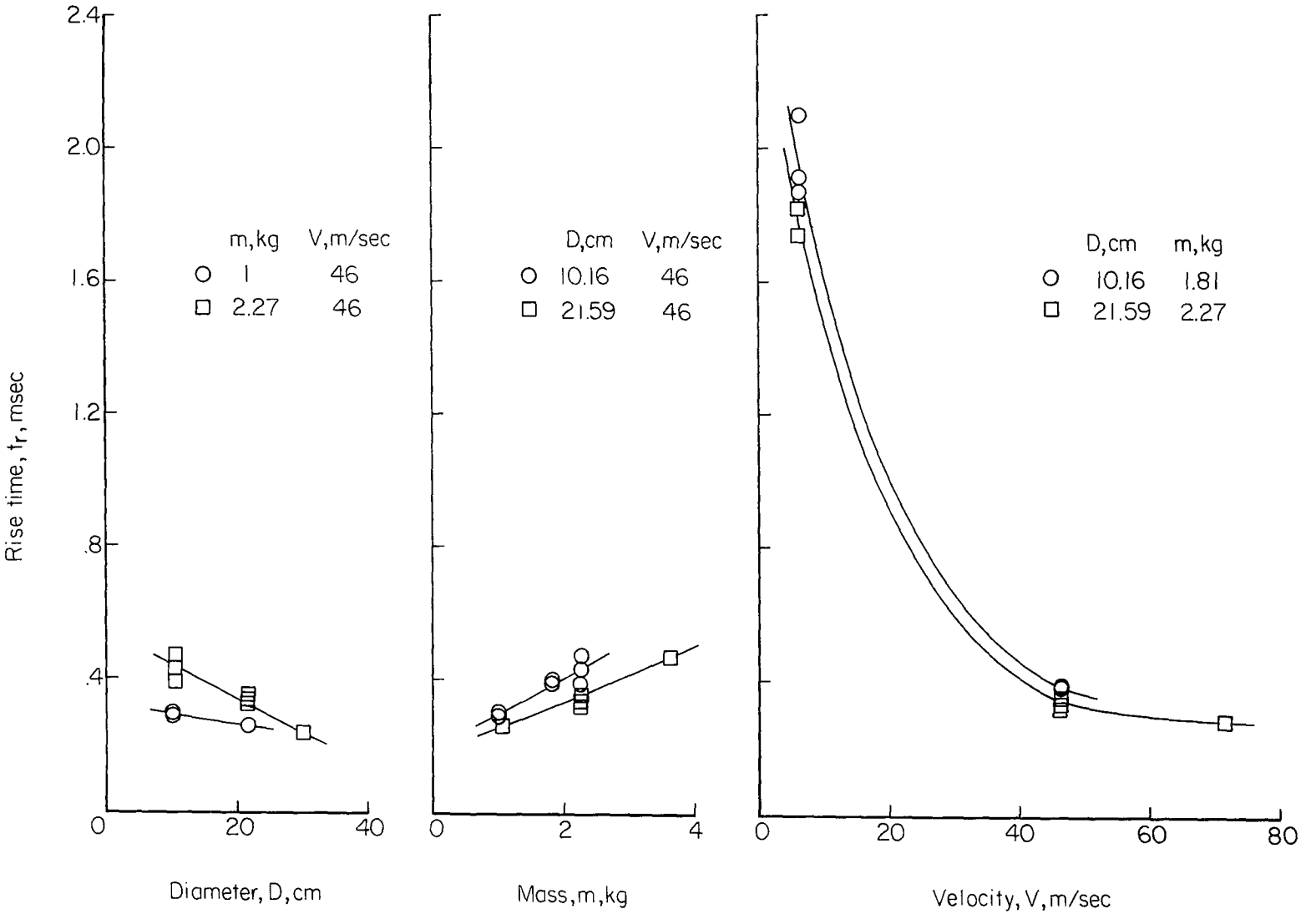

(a) Nevada 60 sand, loosely packed.

Figure 11.- Summary of rise time data from penetrometer impact tests.

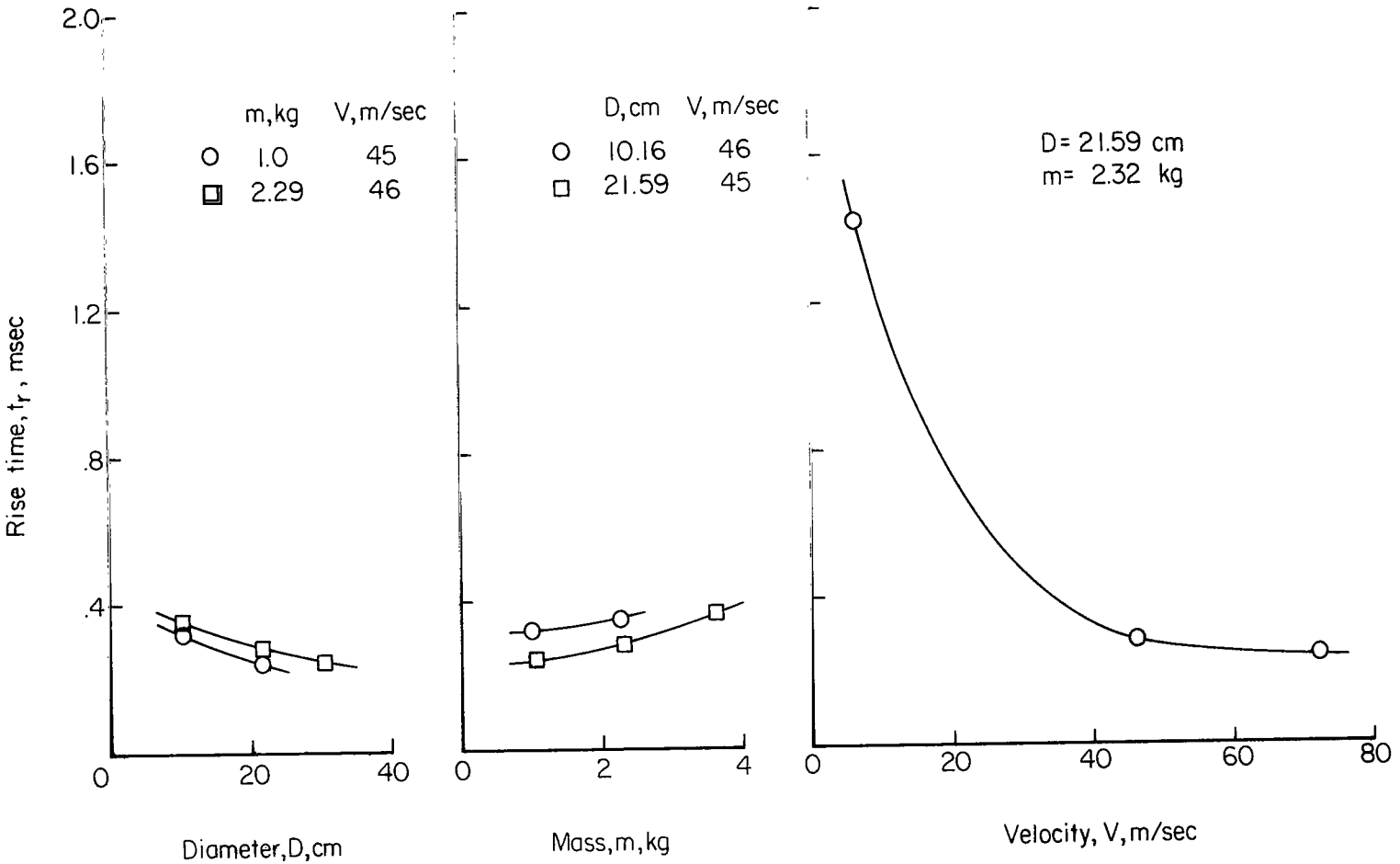

(b) Nevada 120 sand, densely packed.

Figure 11.- Continued.

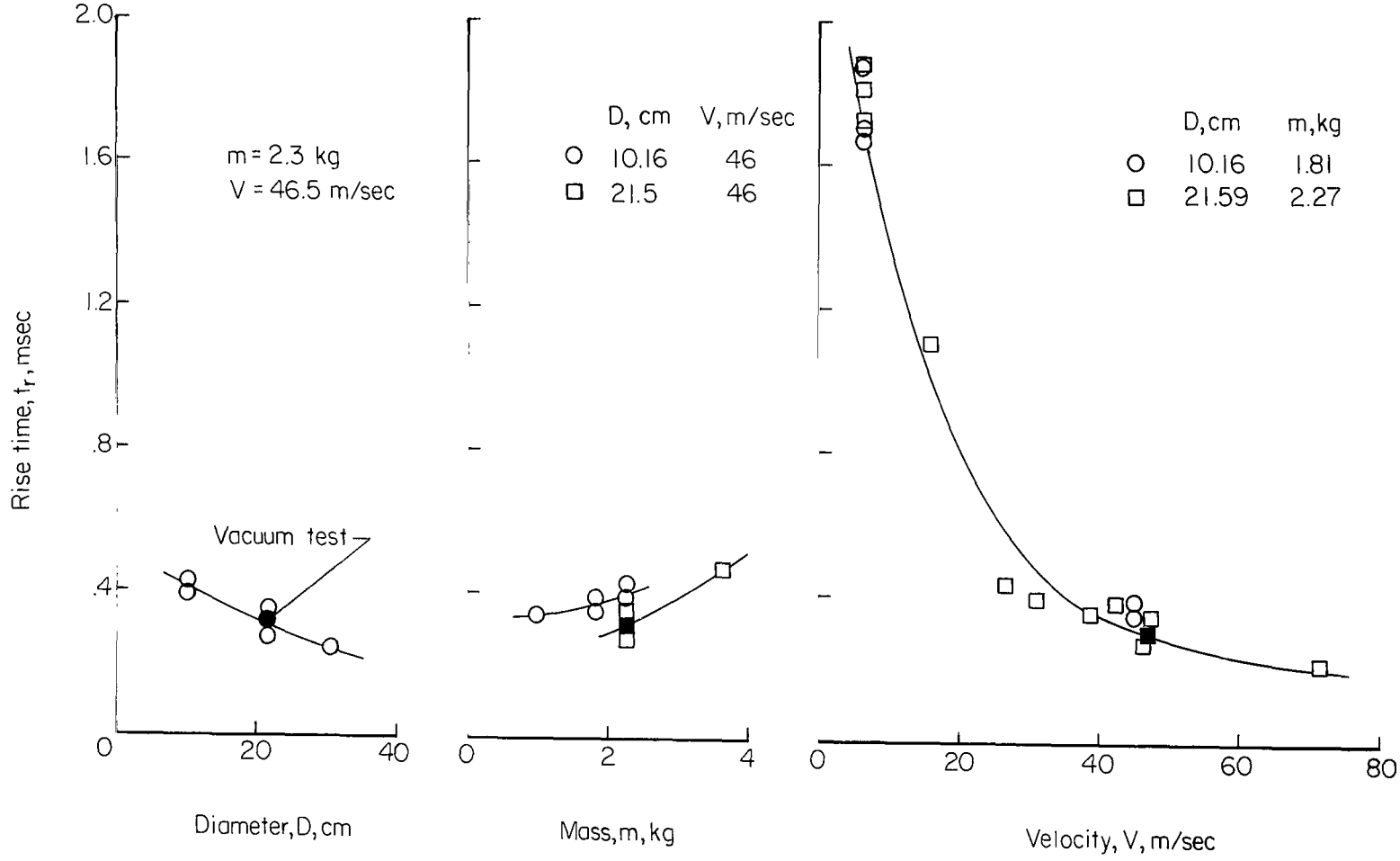

(c) Nevada 120 sand, lightly packed.

Figure 11.- Continued.

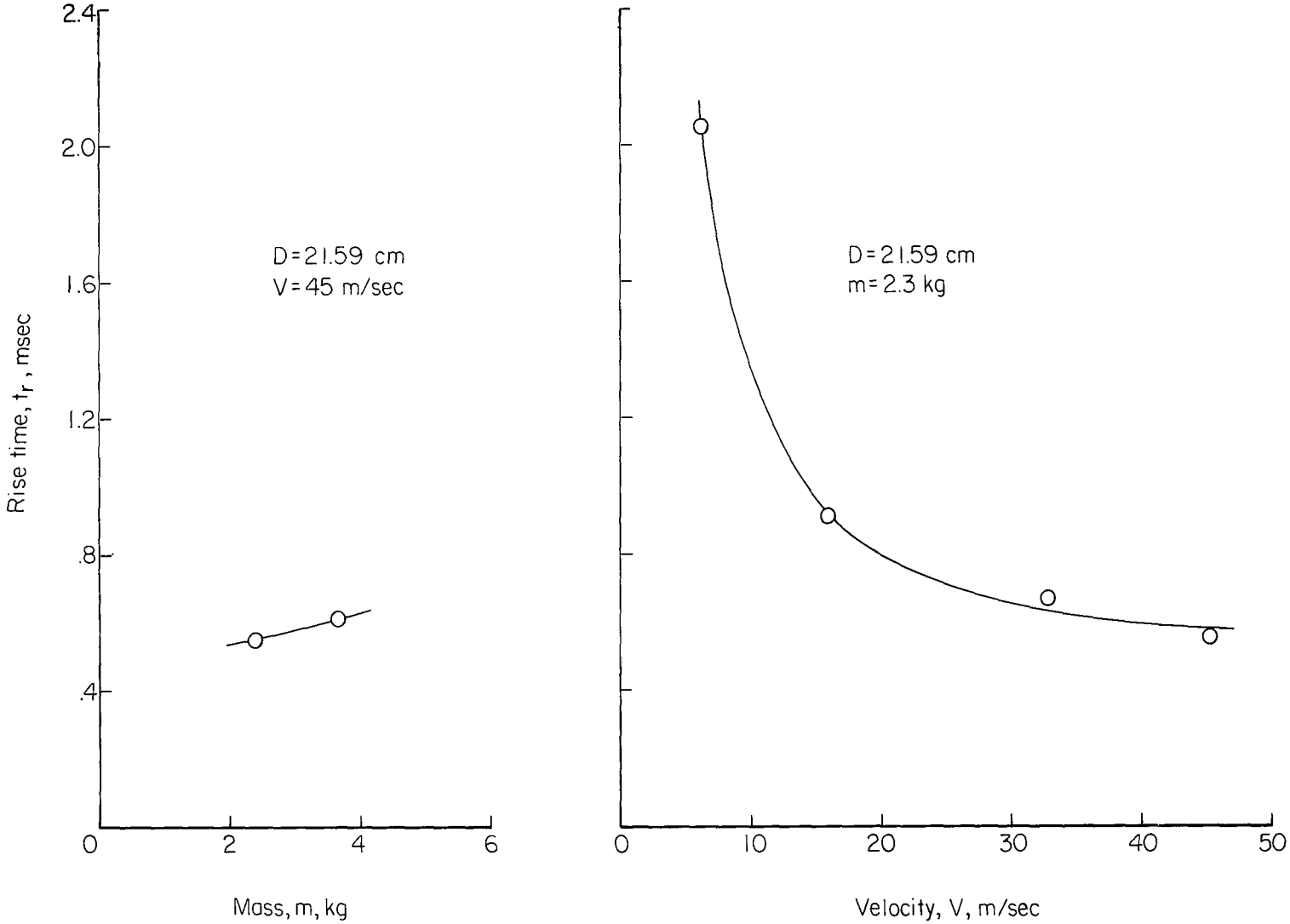

(d) Nevada 120 sand, loosely packed.

Figure 11.- Continued.

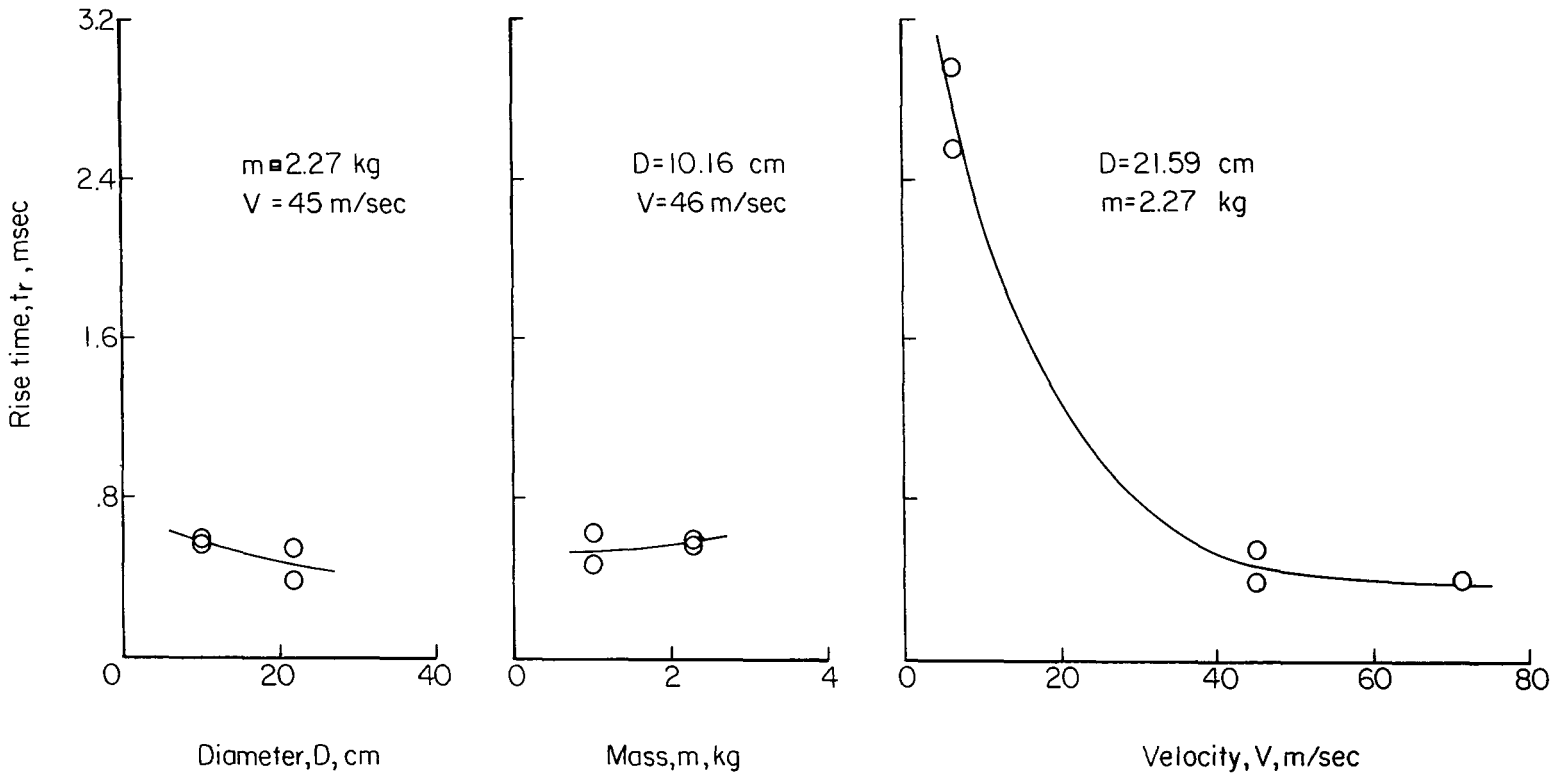

(e) Basalt sand.

Figure 11.- Continued.

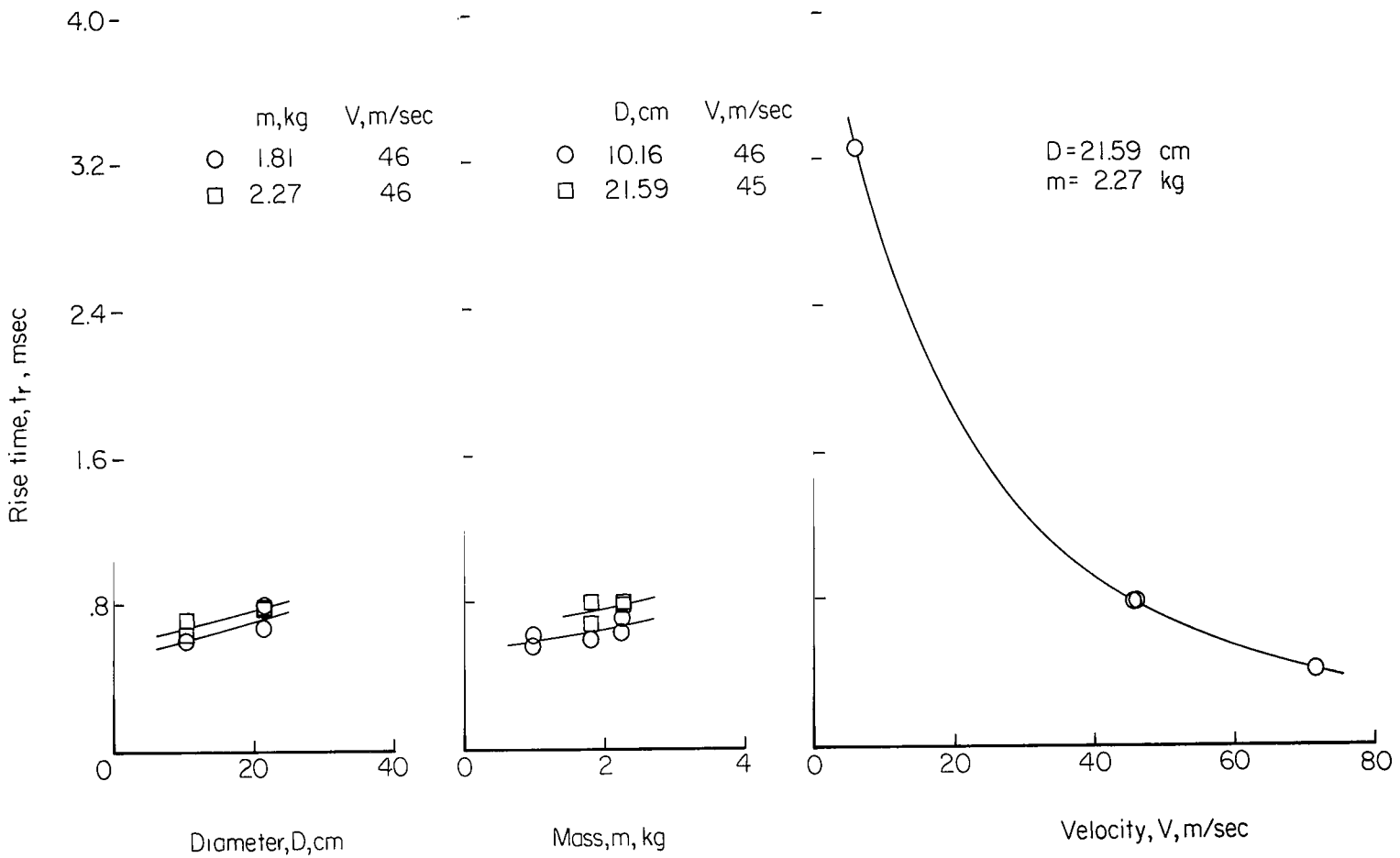

(f) Basalt silt.

Figure 11.- Continued.

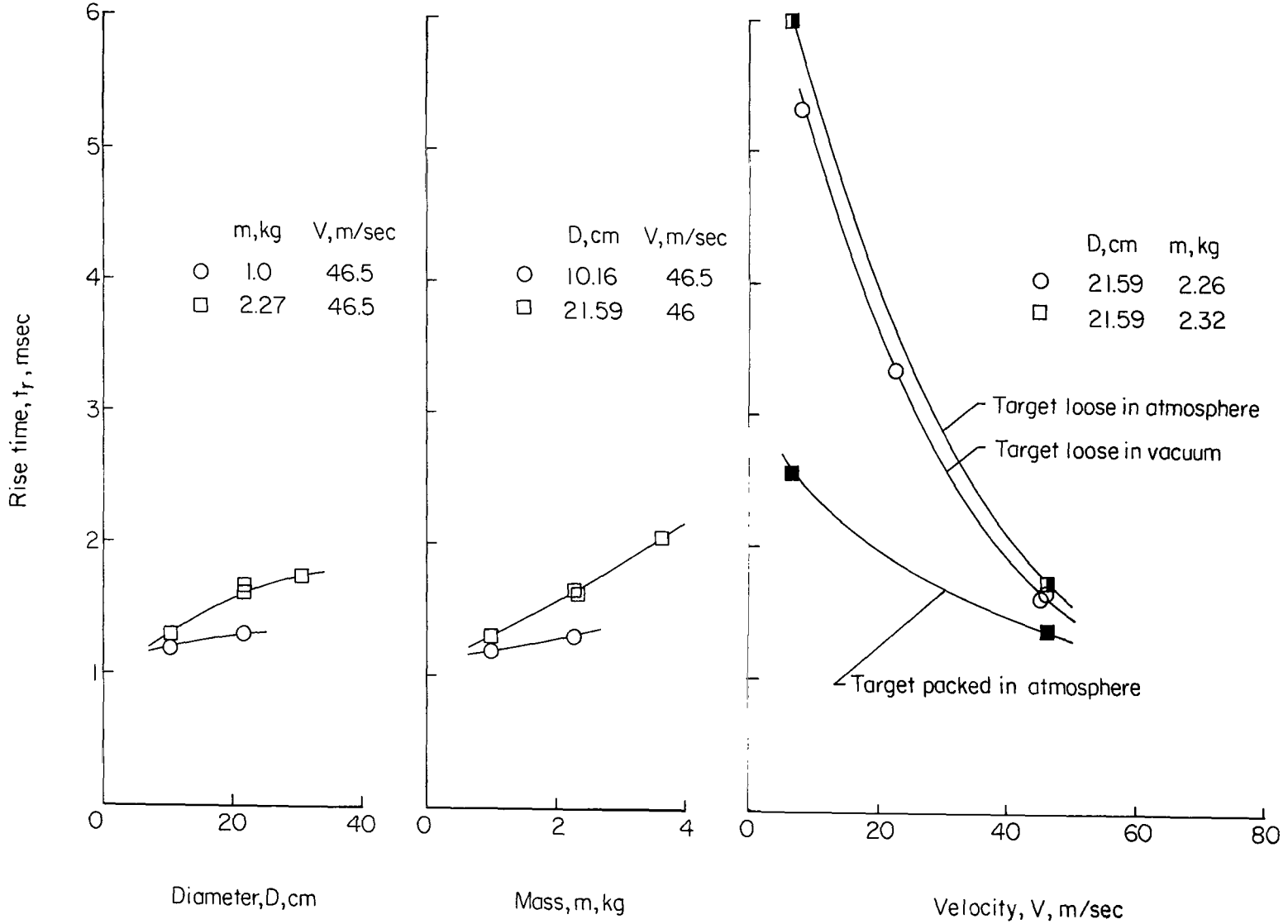

(g) Powdered silica.

Figure 11.- Concluded.

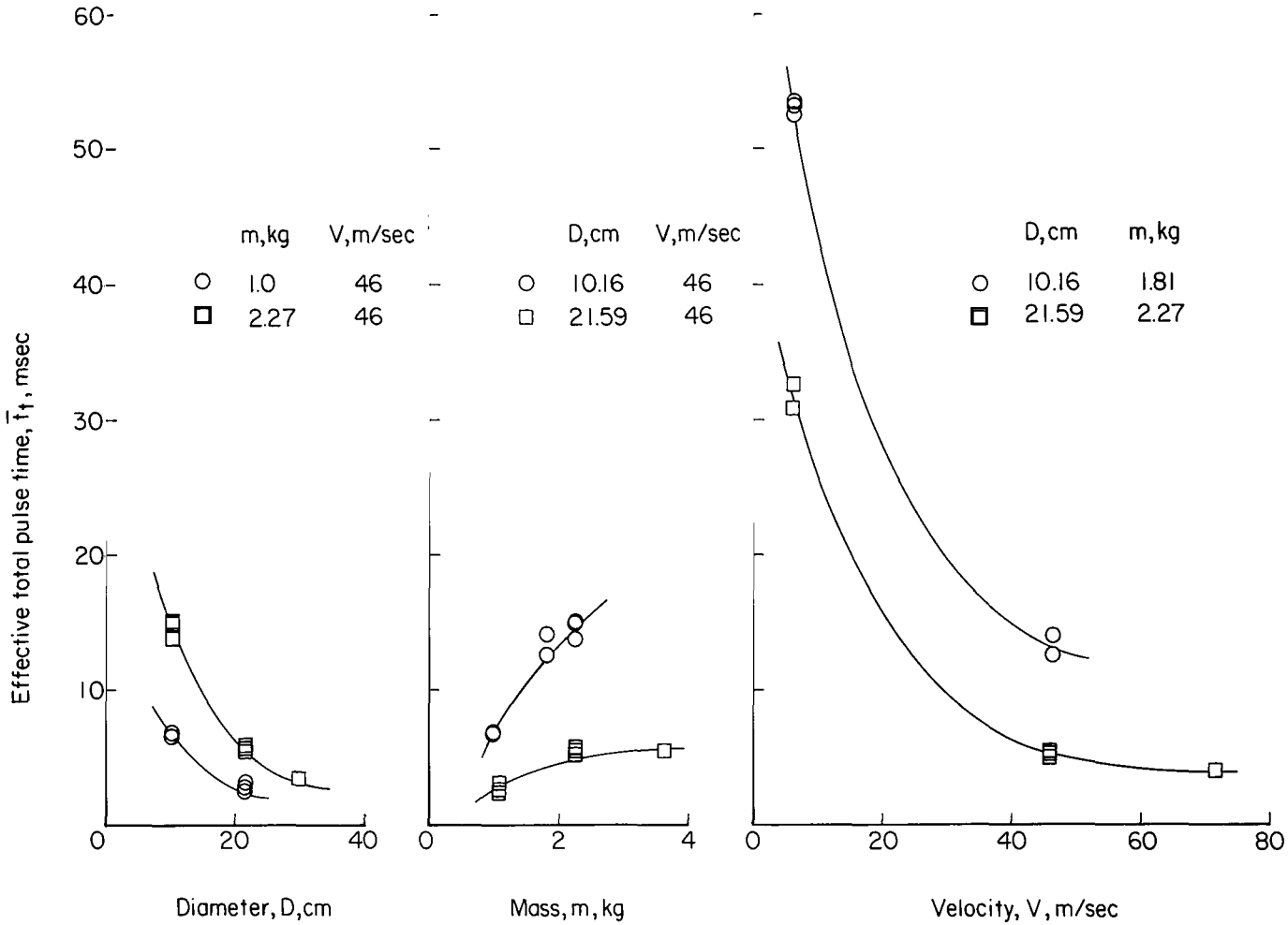

(a) Nevada 60 sand, loosely packed.

Figure 12.- Summary of effective total pulse time data from penetrometer impact tests.

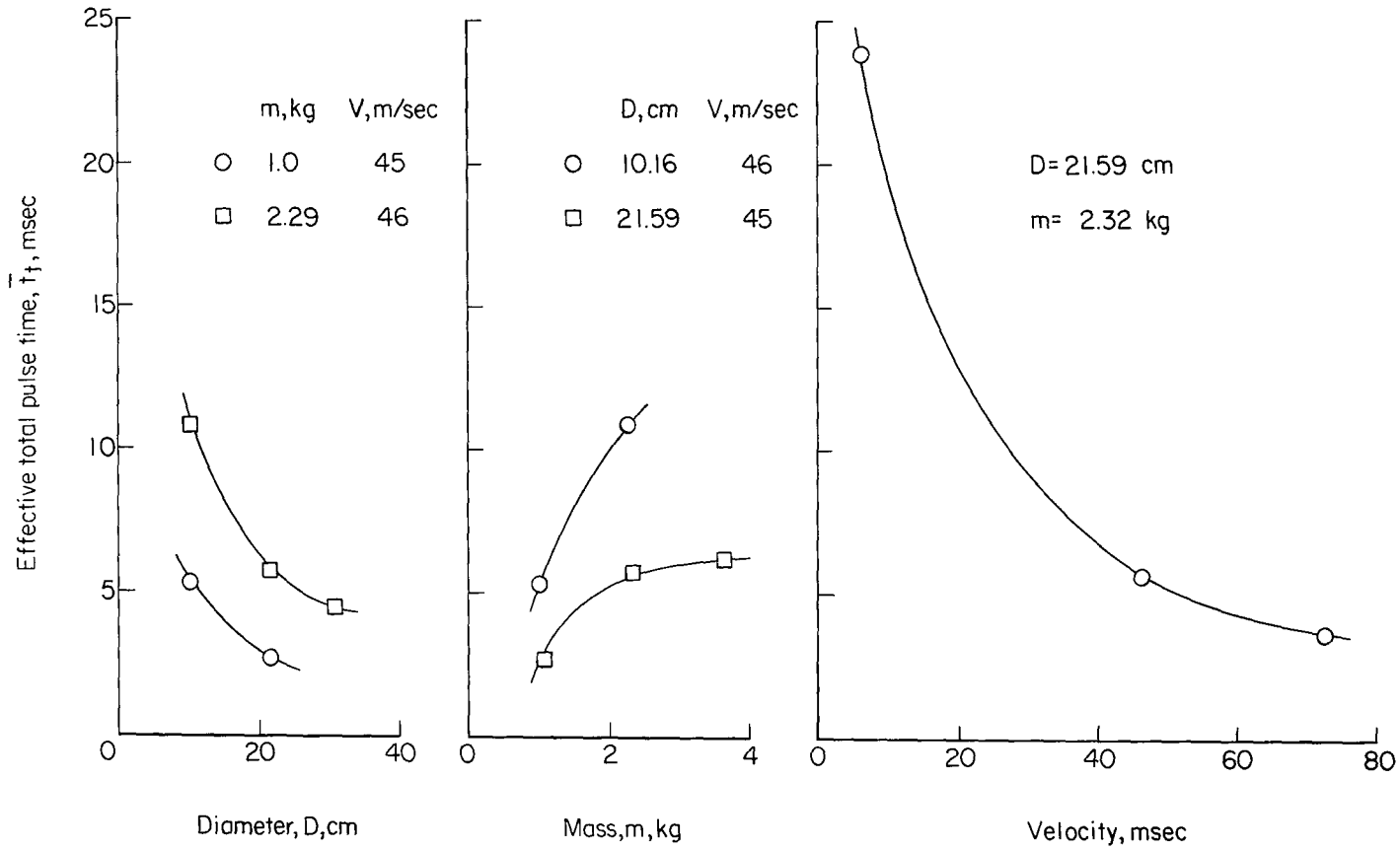

(b) Nevada 120 sand, densely packed.

Figure 12.- Continued.

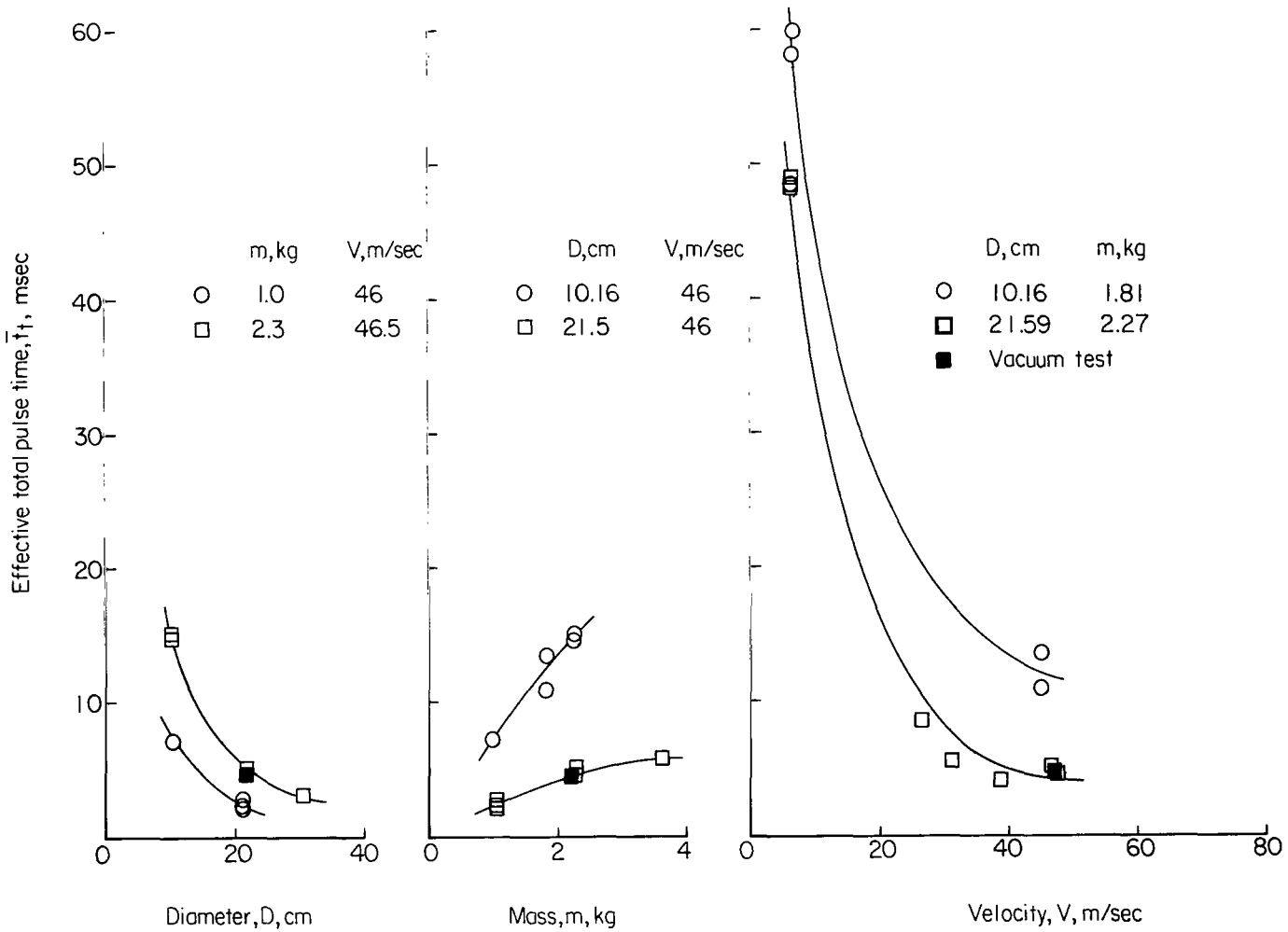

(c) Nevada 120 sand, lightly packed.

Figure 12.- Continued.

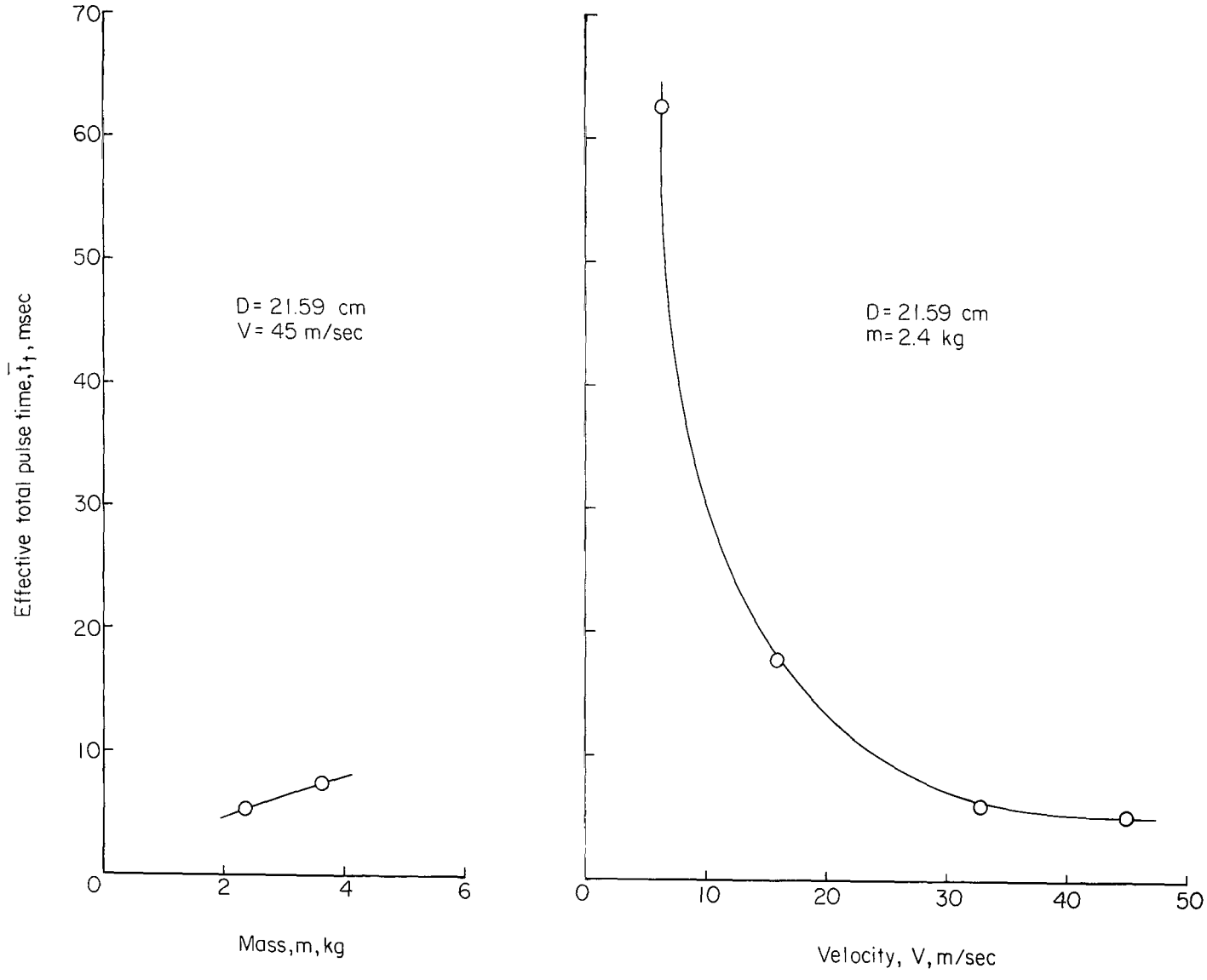

(d) Nevada 120 sand, loosely packed.

Figure 12.- Continued.

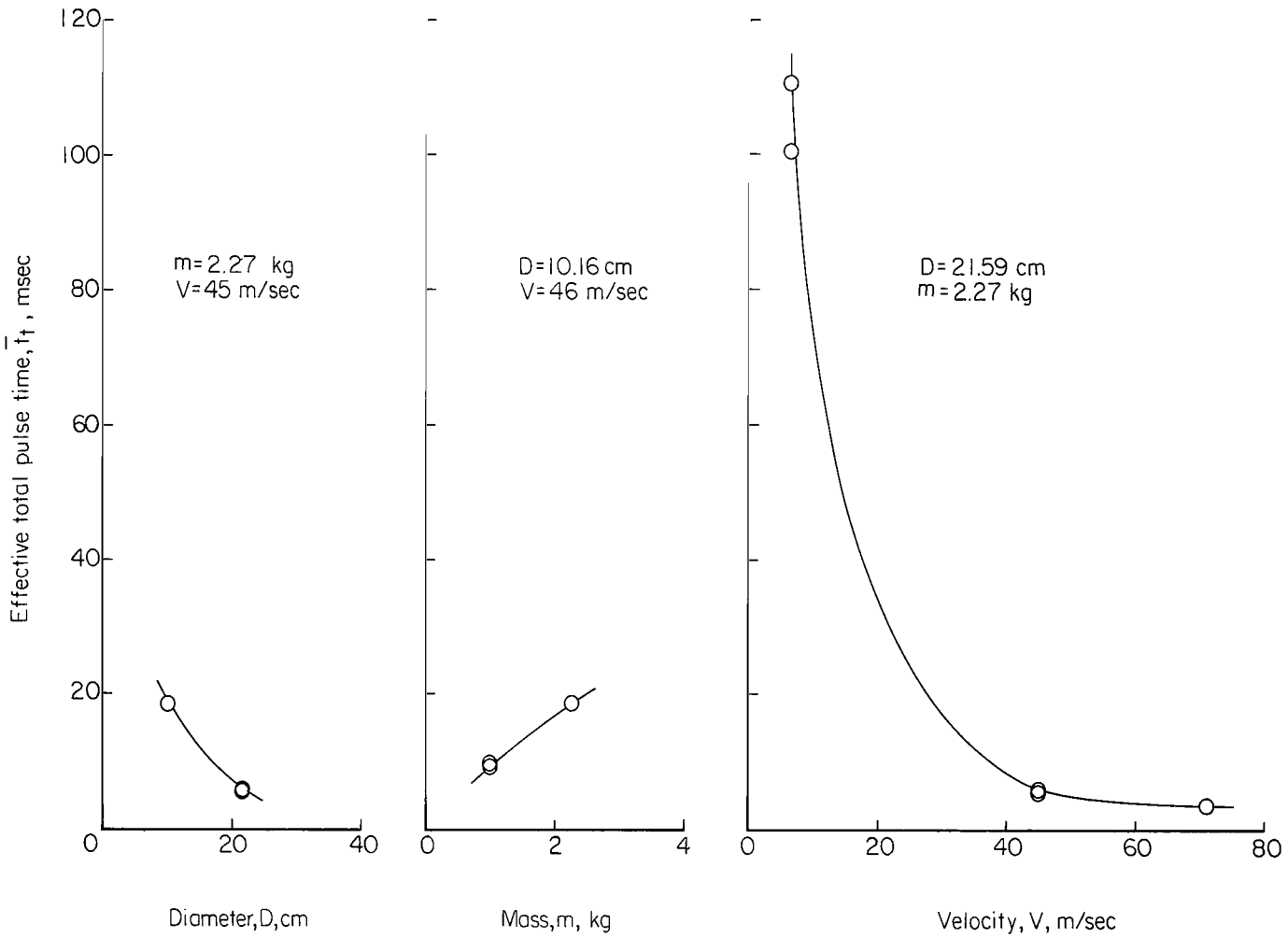

(e) Basalt sand.

Figure 12.- Continued.

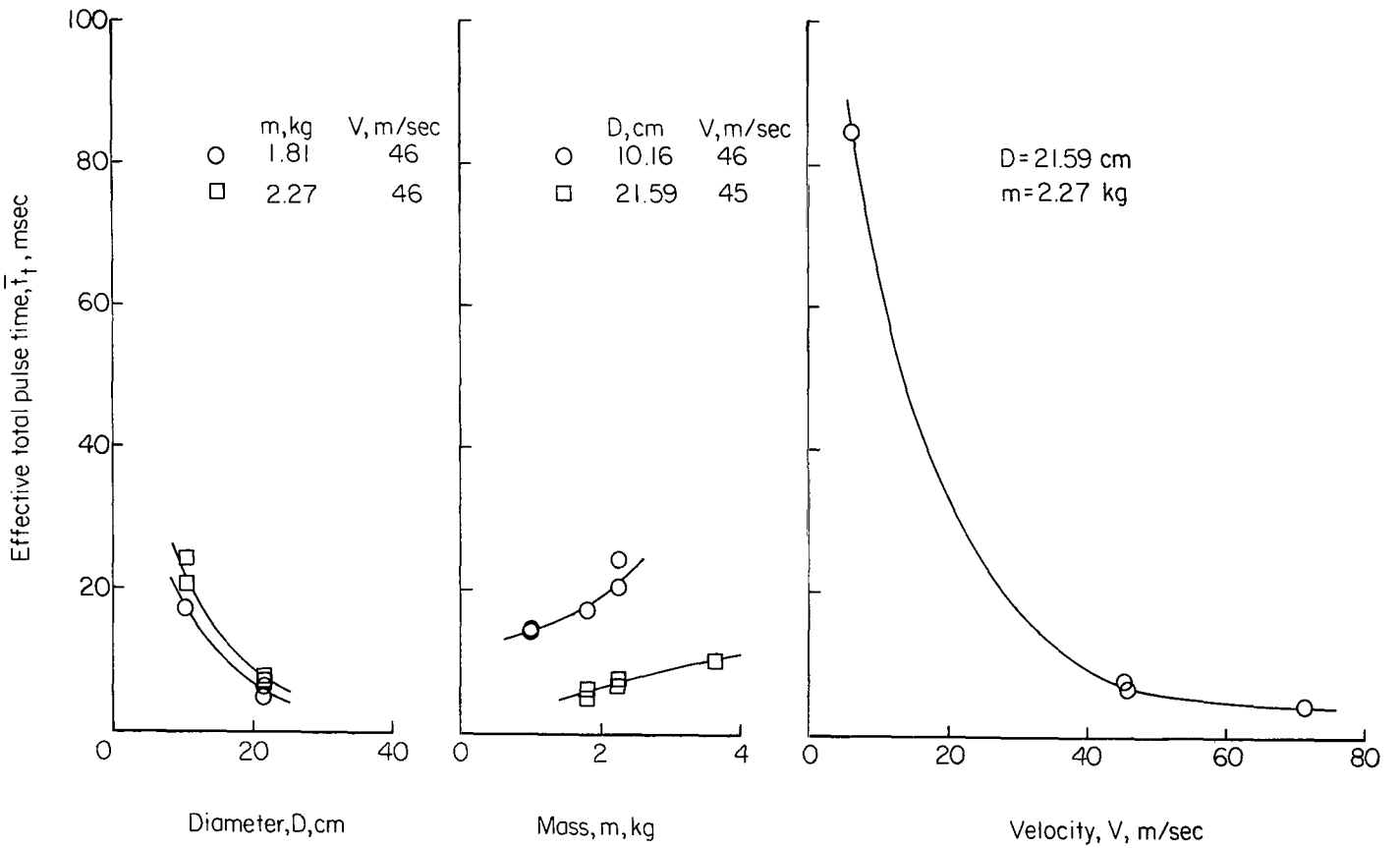

(f) Basalt silt.

Figure 12.- Concluded.

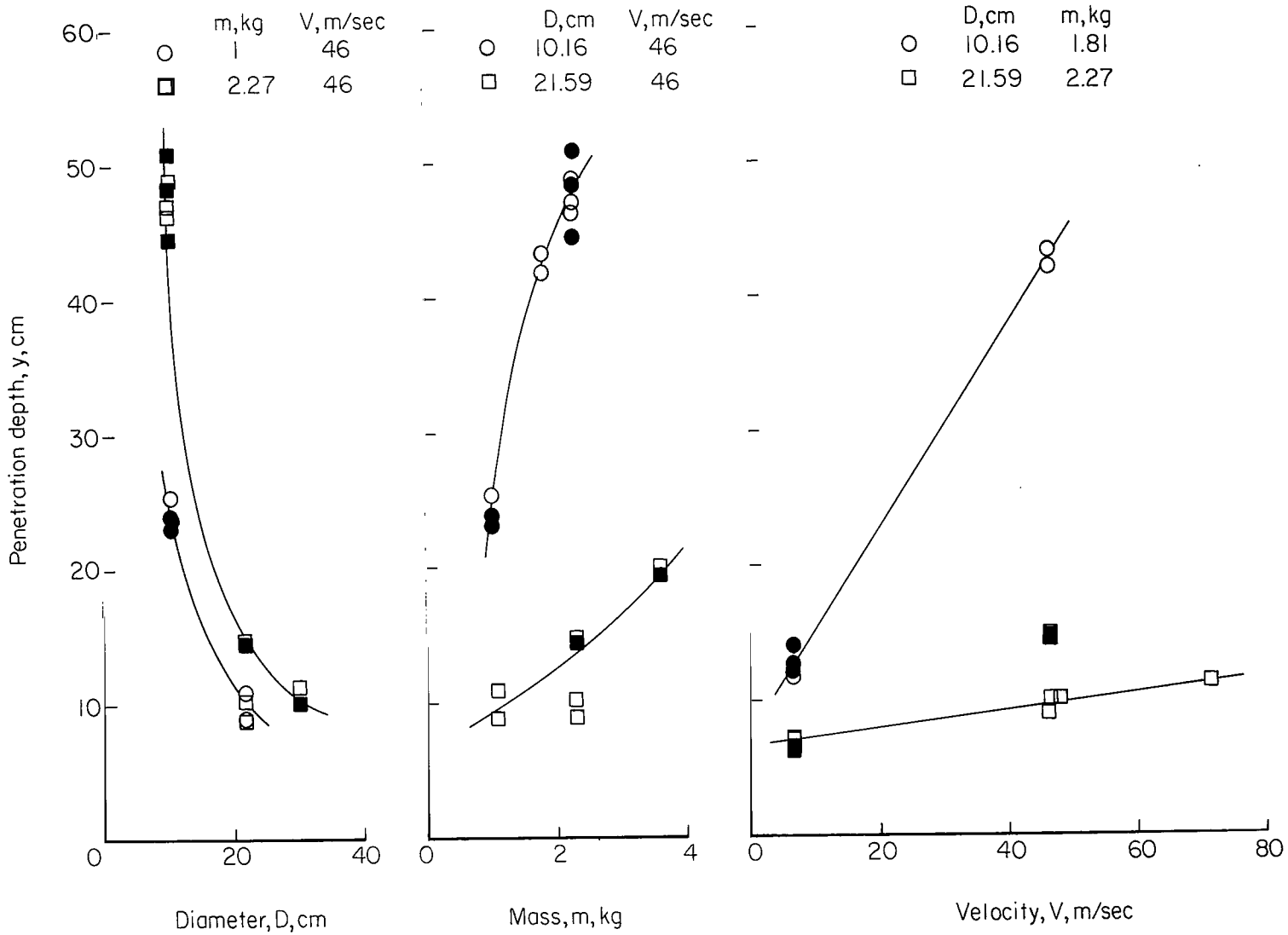

(a) Nevada 60 sand, loosely packed.

Figure 13.- Summary of penetration data from penetrometer impact tests. Open symbols refer to measured penetration depths; solid symbols refer to penetrations obtained through a double integration of the acceleration time histories.

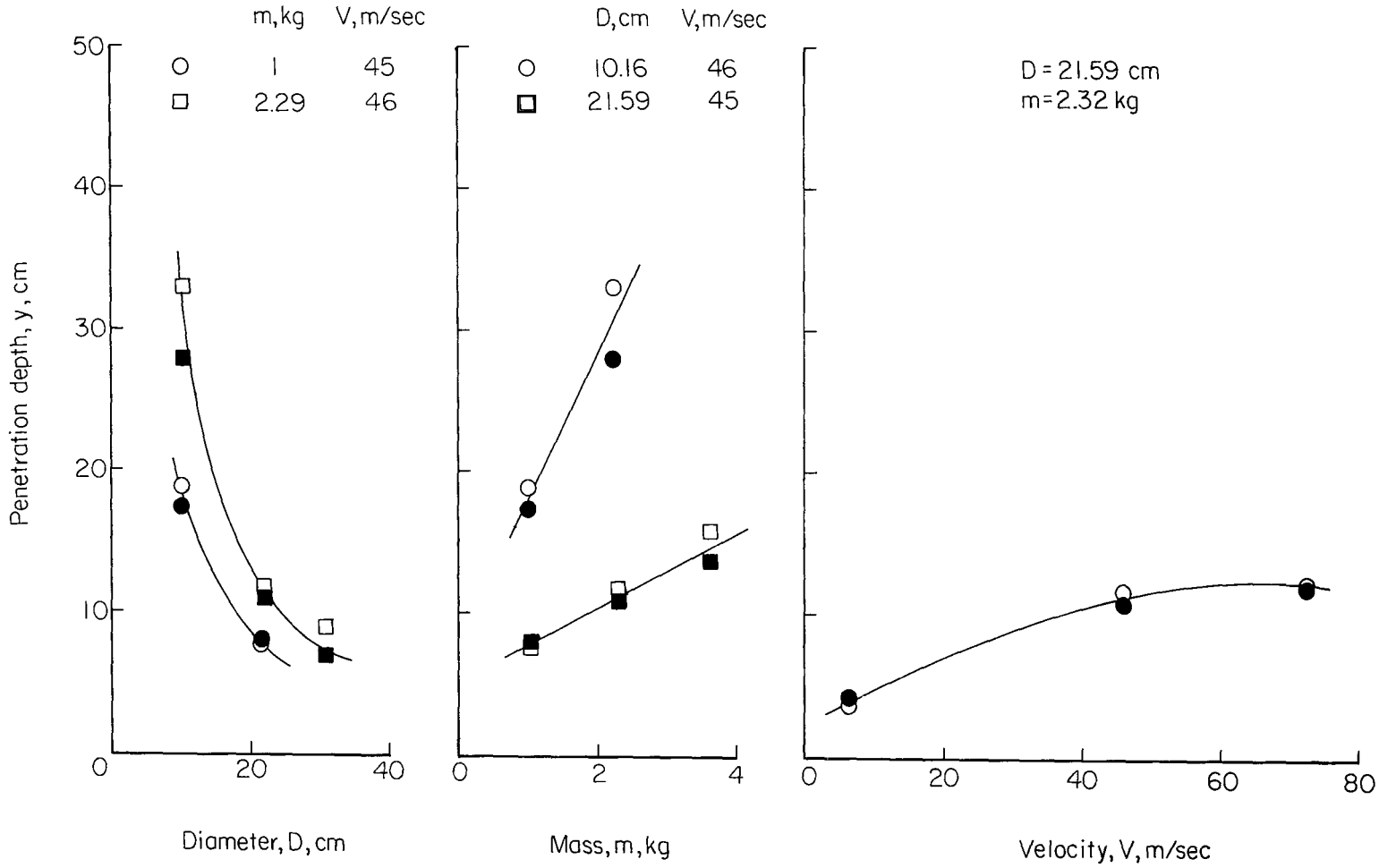

(b) Nevada 120 sand, densely packed.

Figure 13.- Continued.

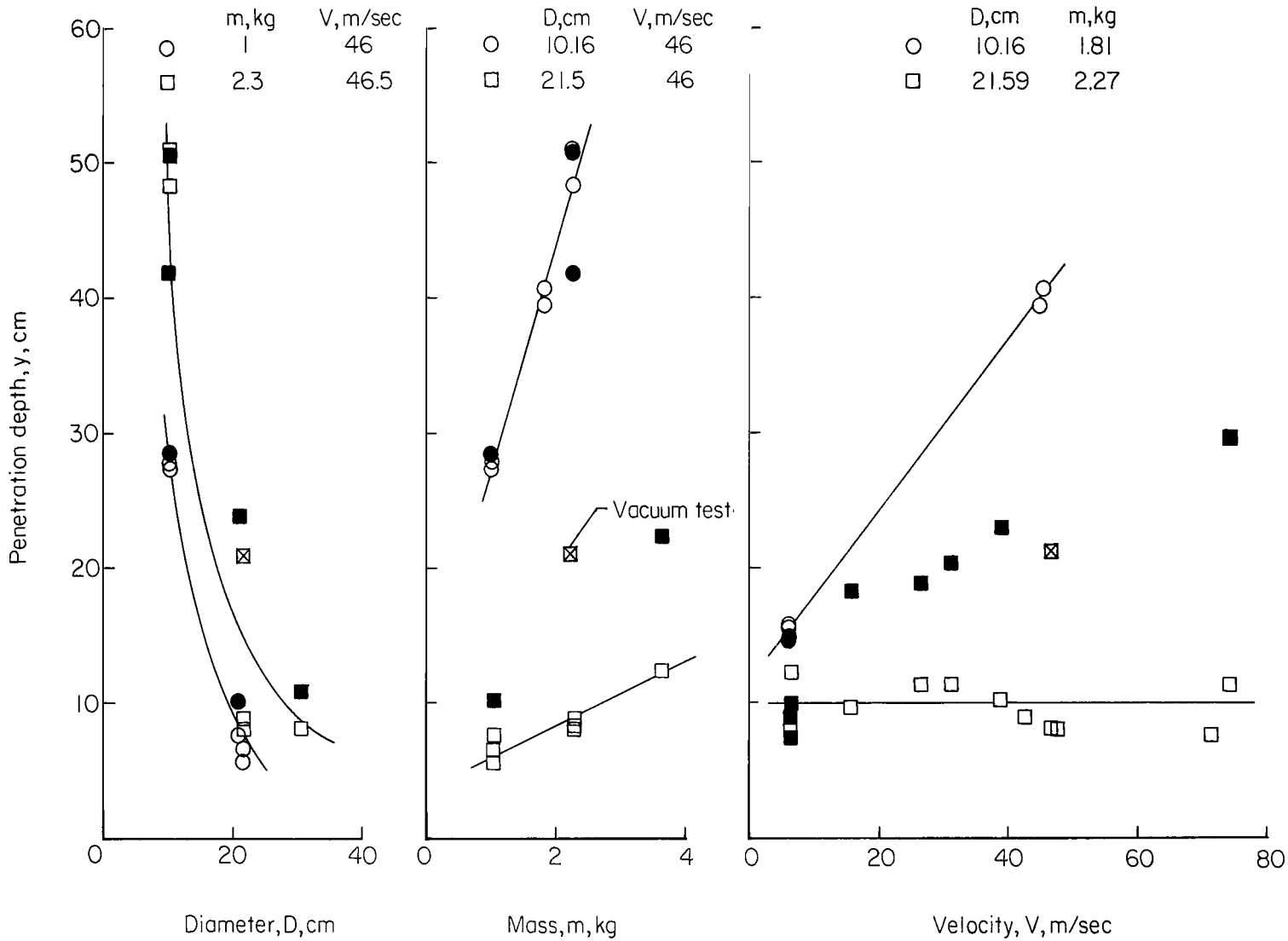

(c) Nevada 120 sand, lightly packed.

Figure 13.- Continued.

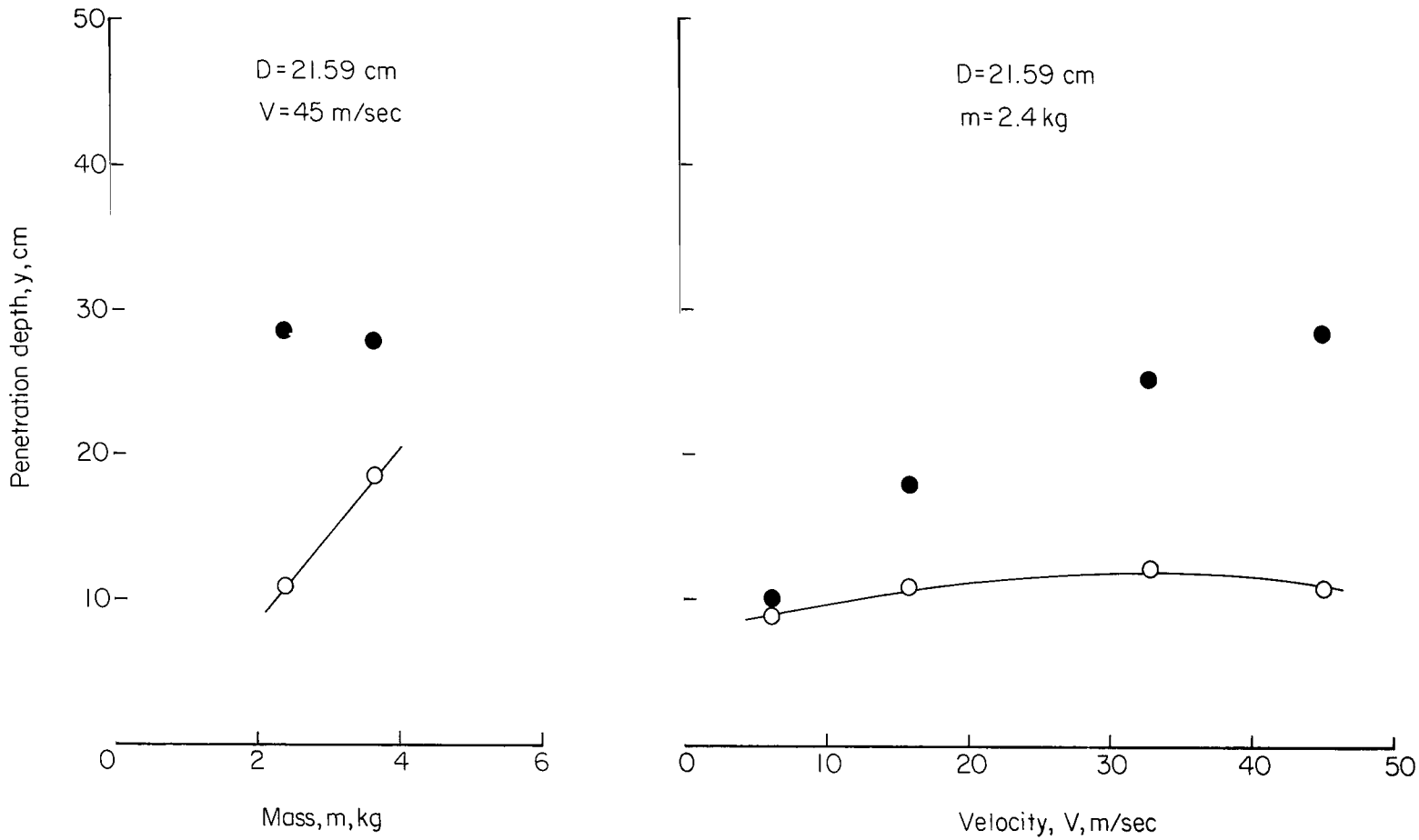

(d) Nevada 120 sand, loosely packed.

Figure 13.- Continued.

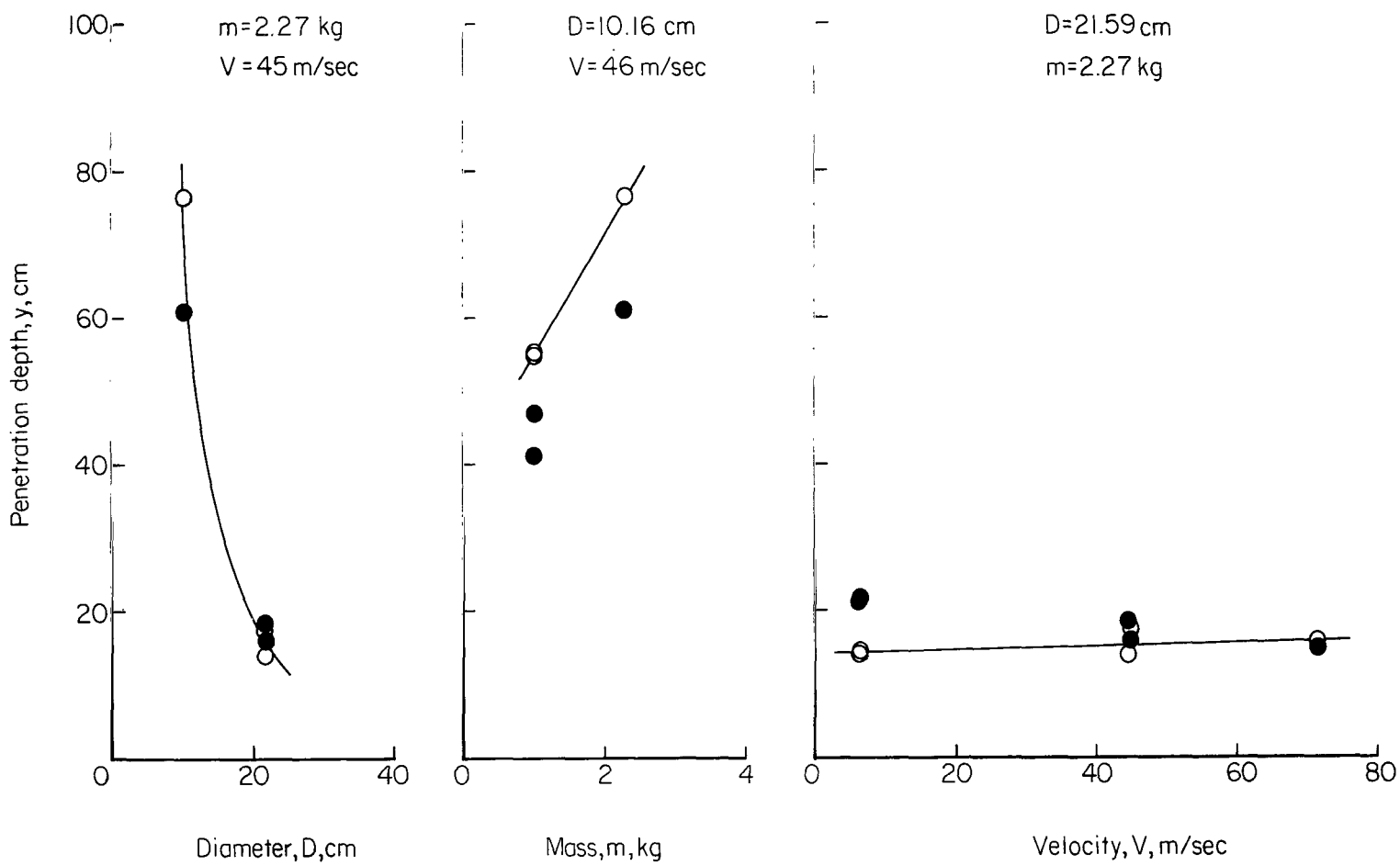

(e) Basalt sand.

Figure 13.- Continued.

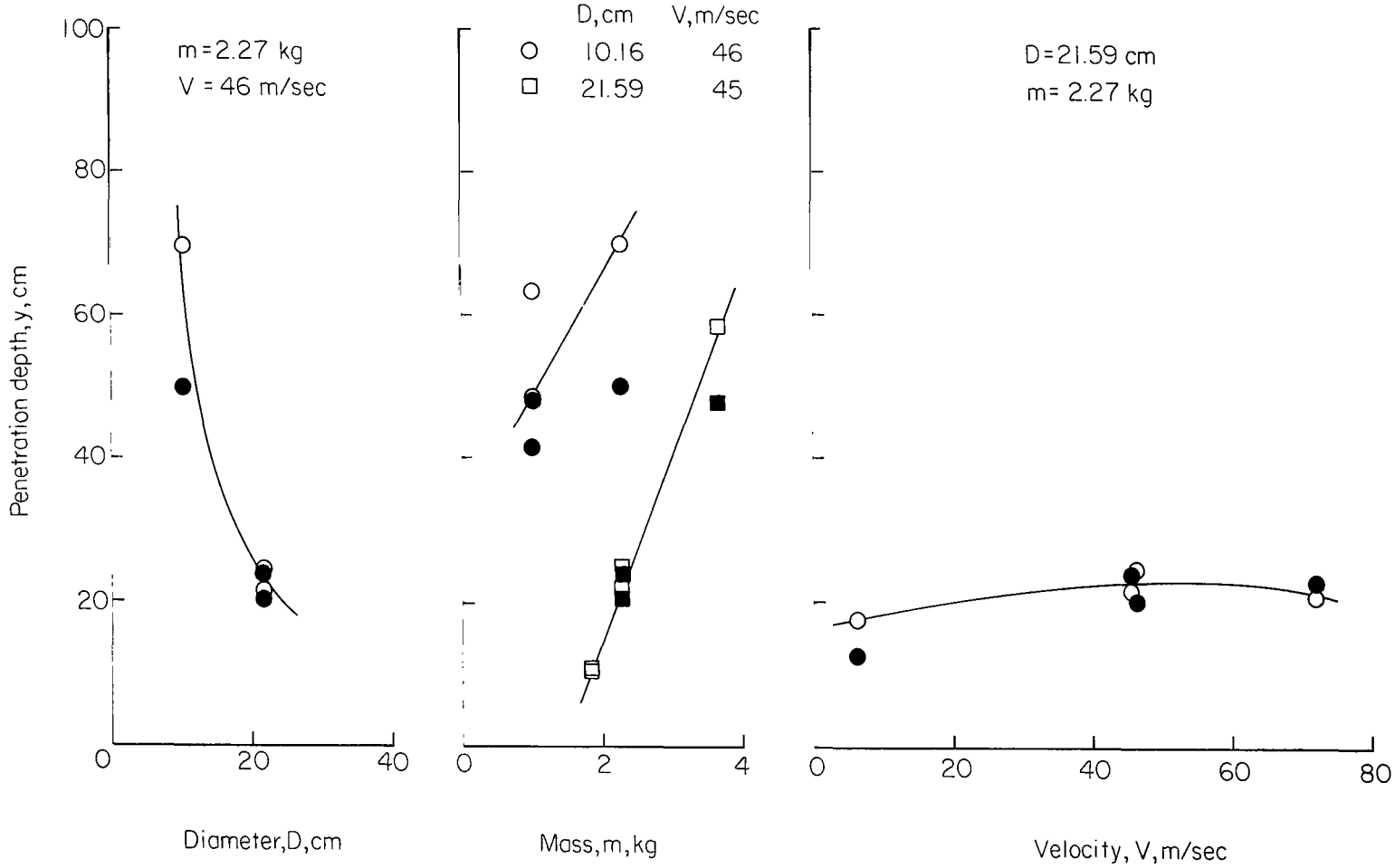

(f) Basalt silt.

Figure 13.- Concluded.

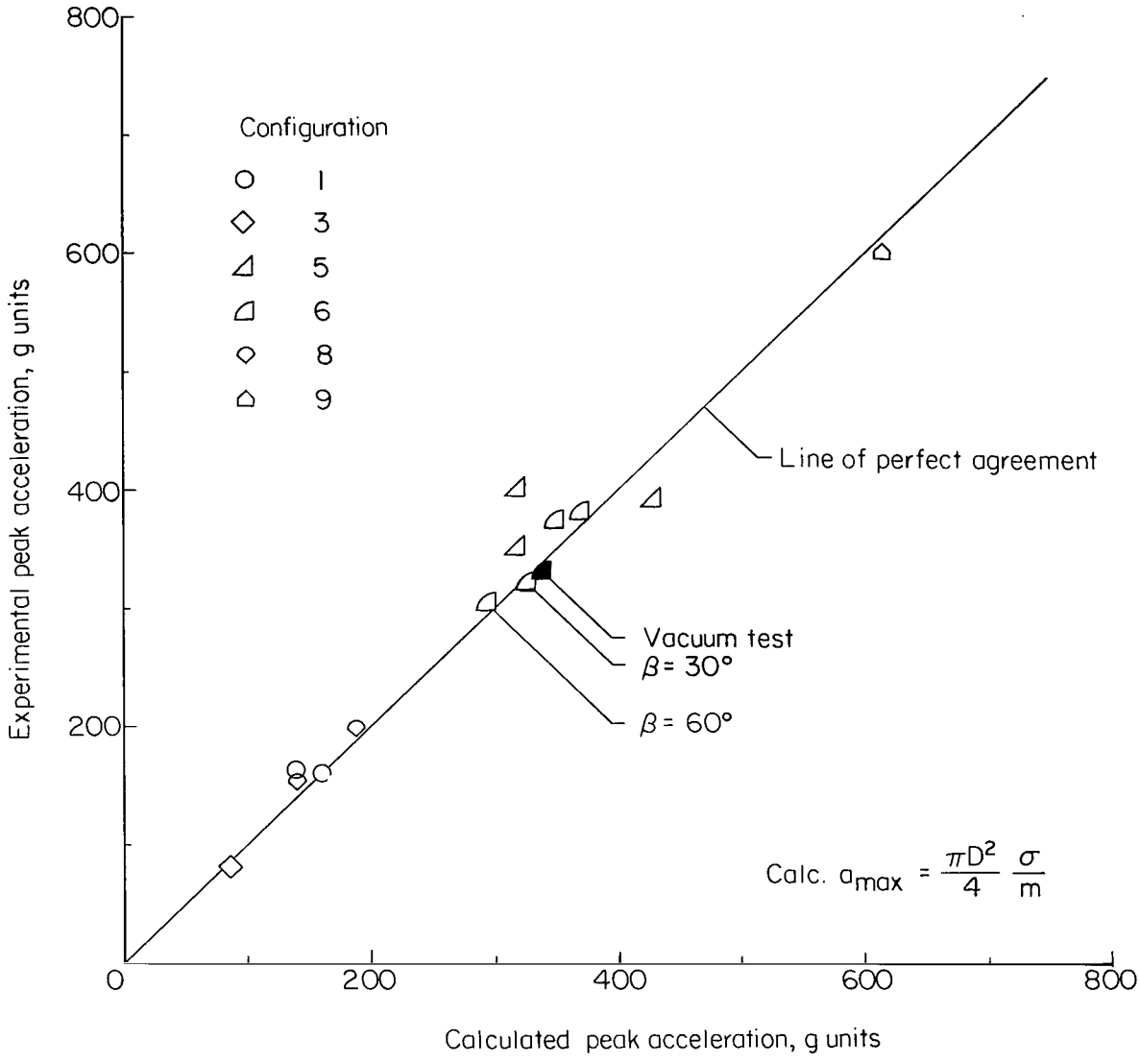

(a) Peak acceleration.

Figure 14.- Summary of impact data from penetrometer tests on urethane foam.

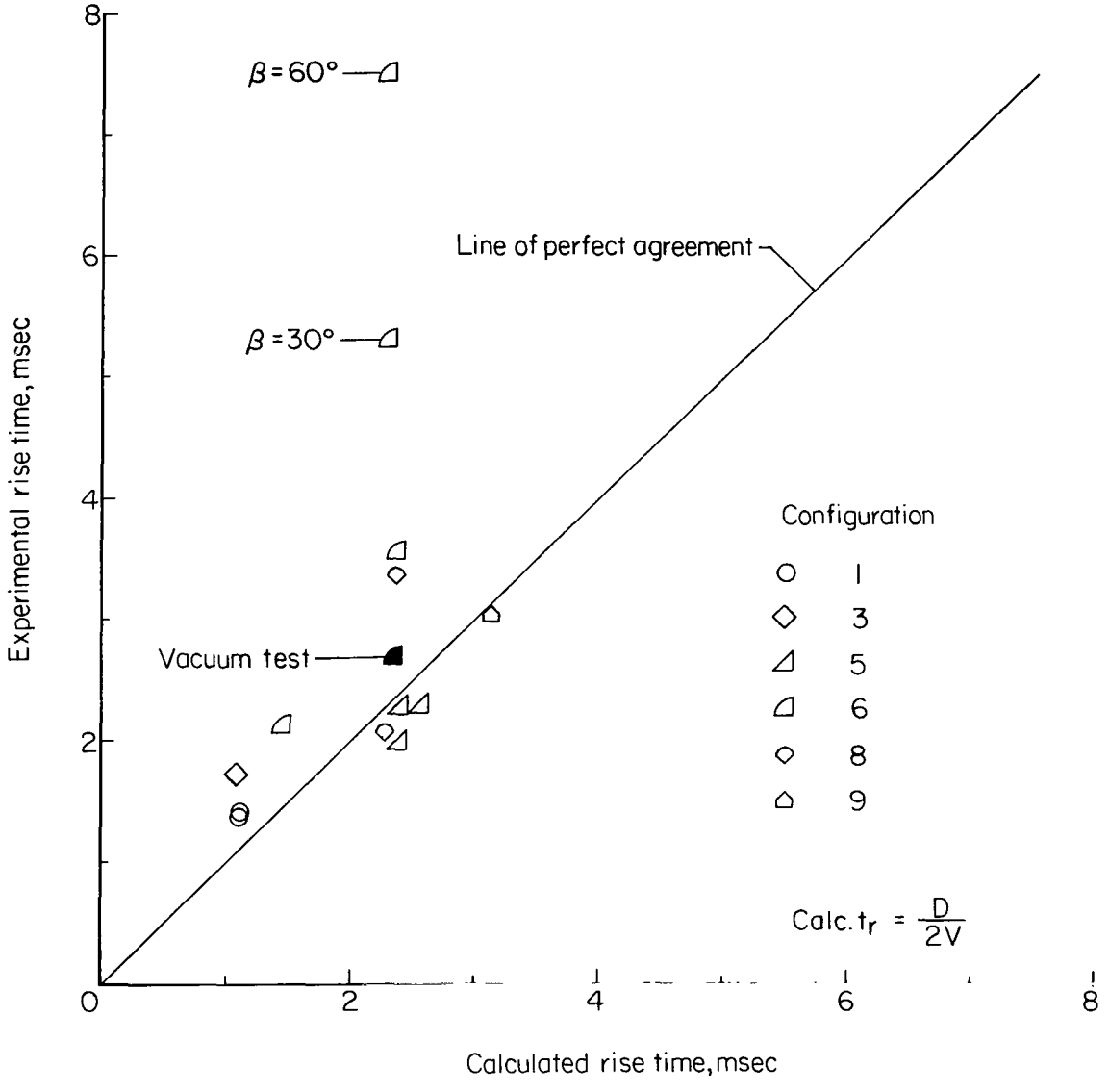

(b) Rise time.

Figure 14.- Continued.

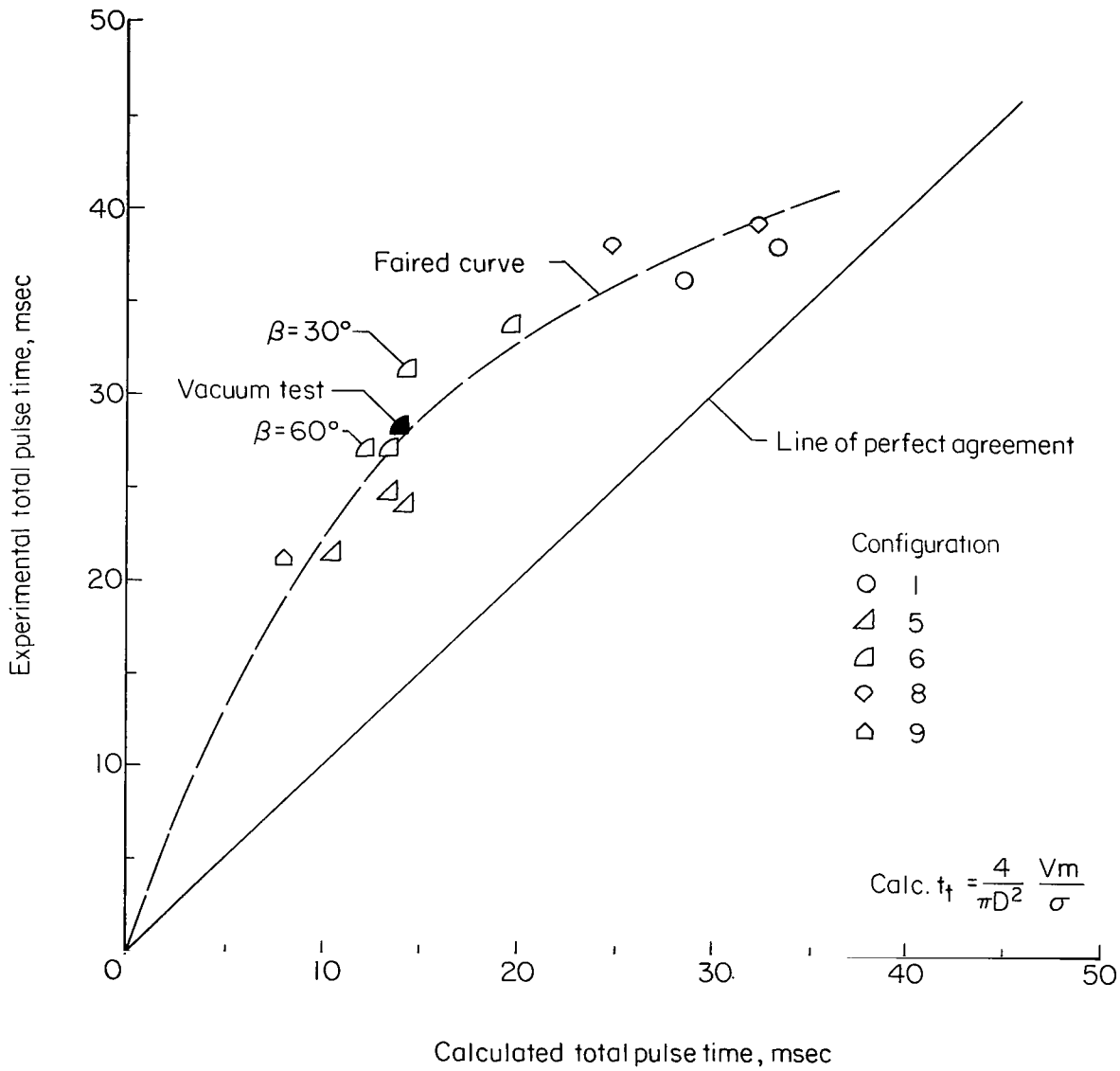

(c) Total pulse time.

Figure 14.- Continued.

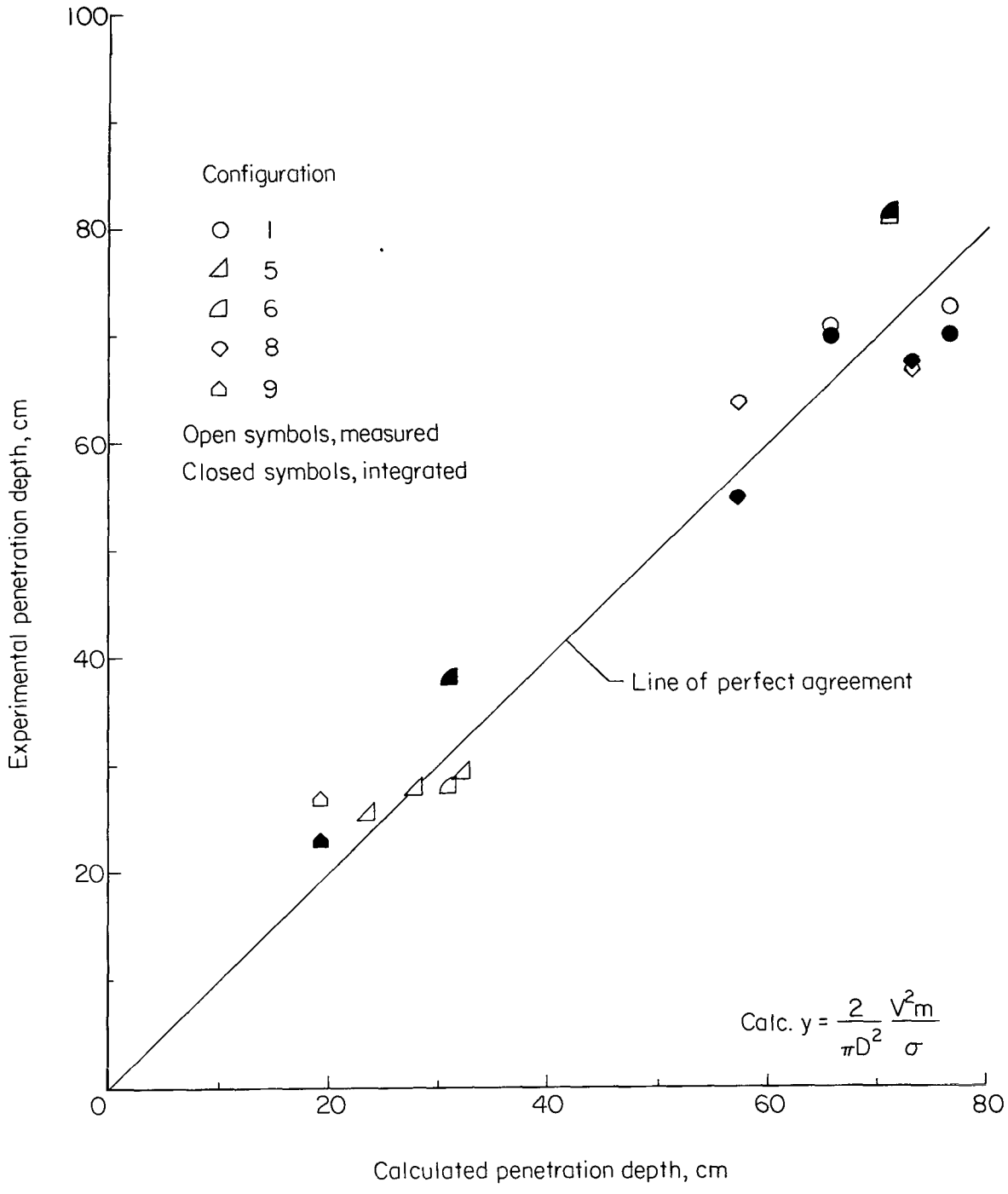

(d) Penetration depth.

Figure 14.- Concluded.

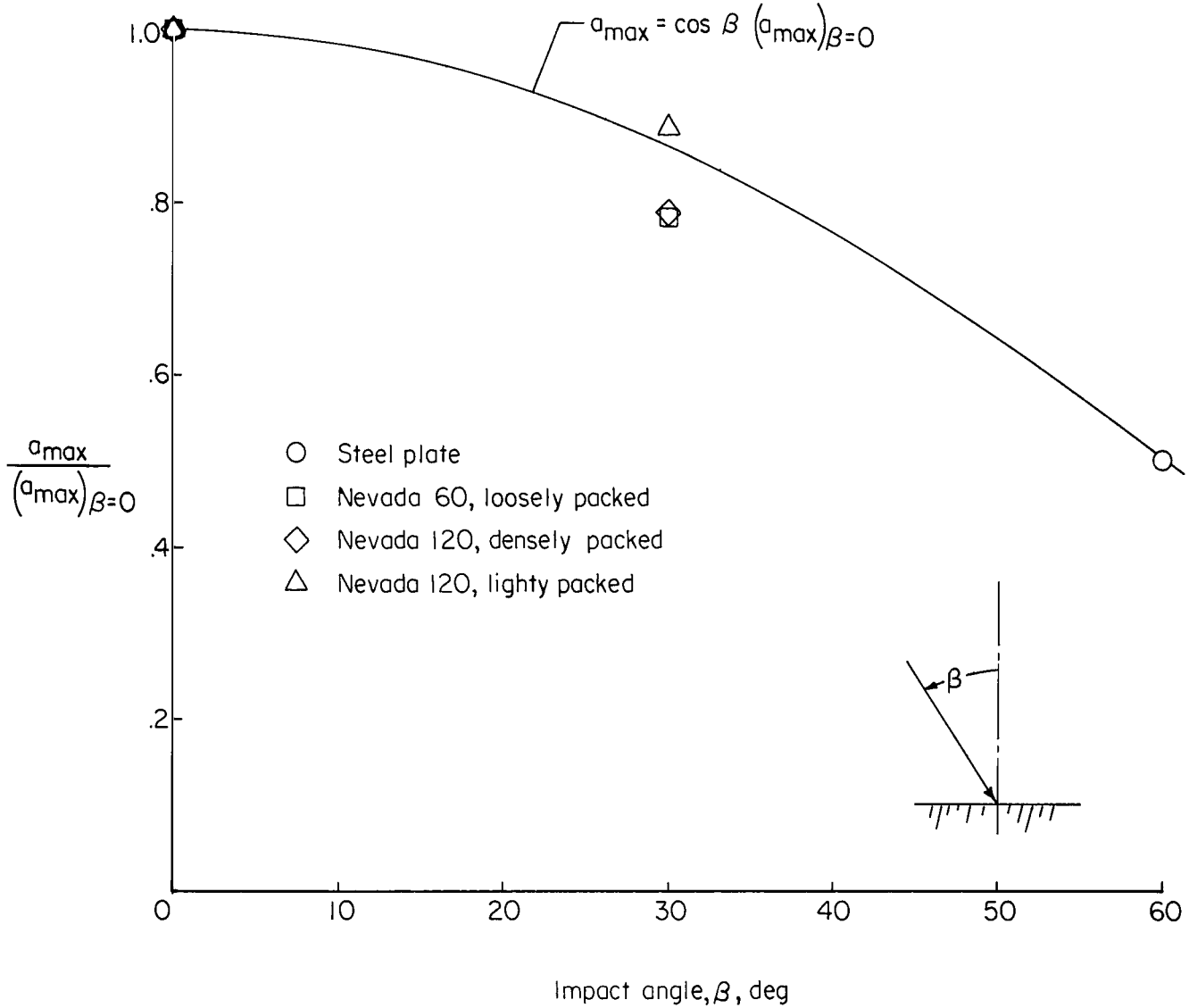

Figure 15.- Effect of penetrometer impact angle on peak acceleration.

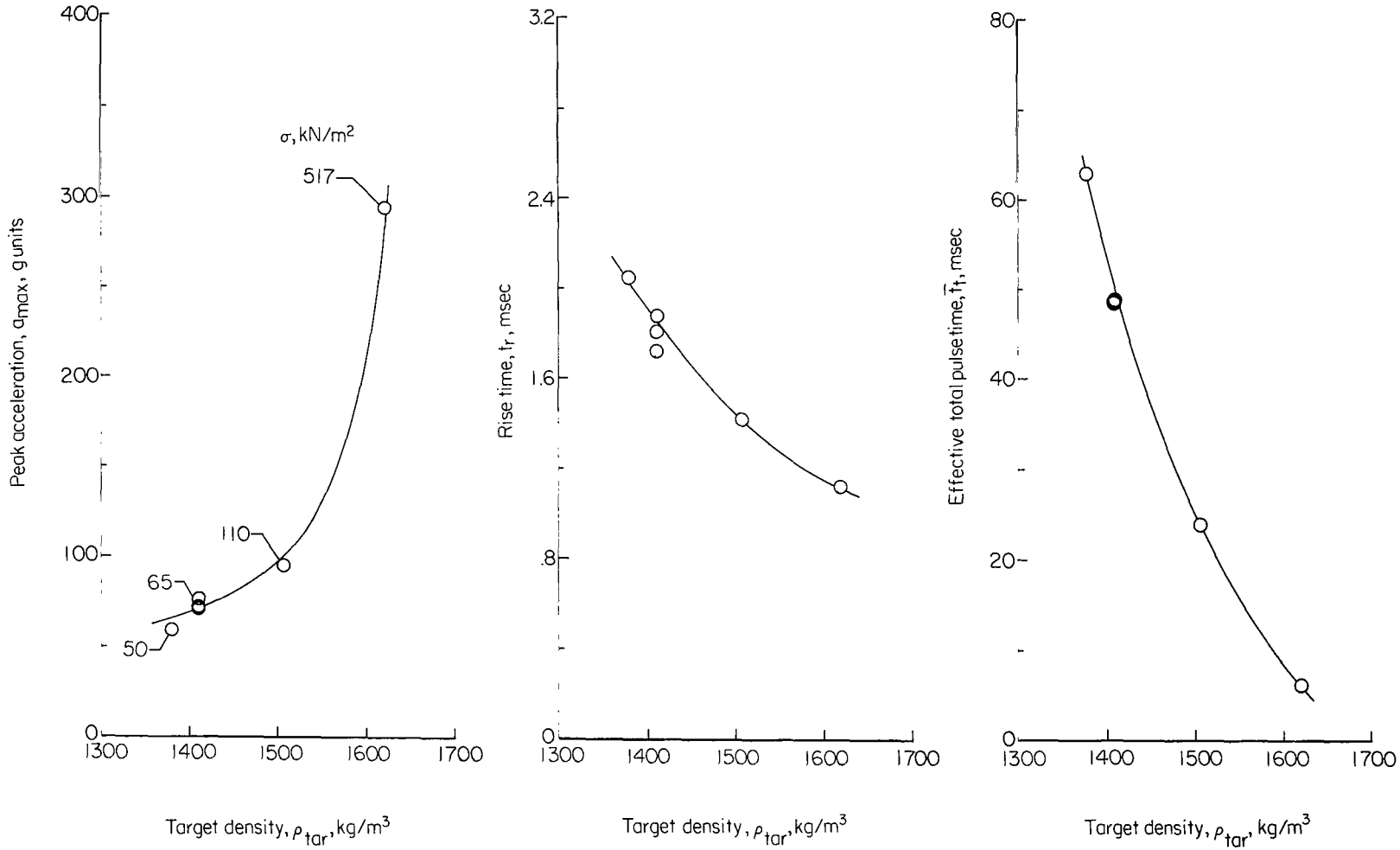

(a) Penetrometer configuration 6. V = 6.1 m/sec; Nevada 120 sand.

Figure 16.- Effect of target packing on characteristics of impact acceleration time histories.

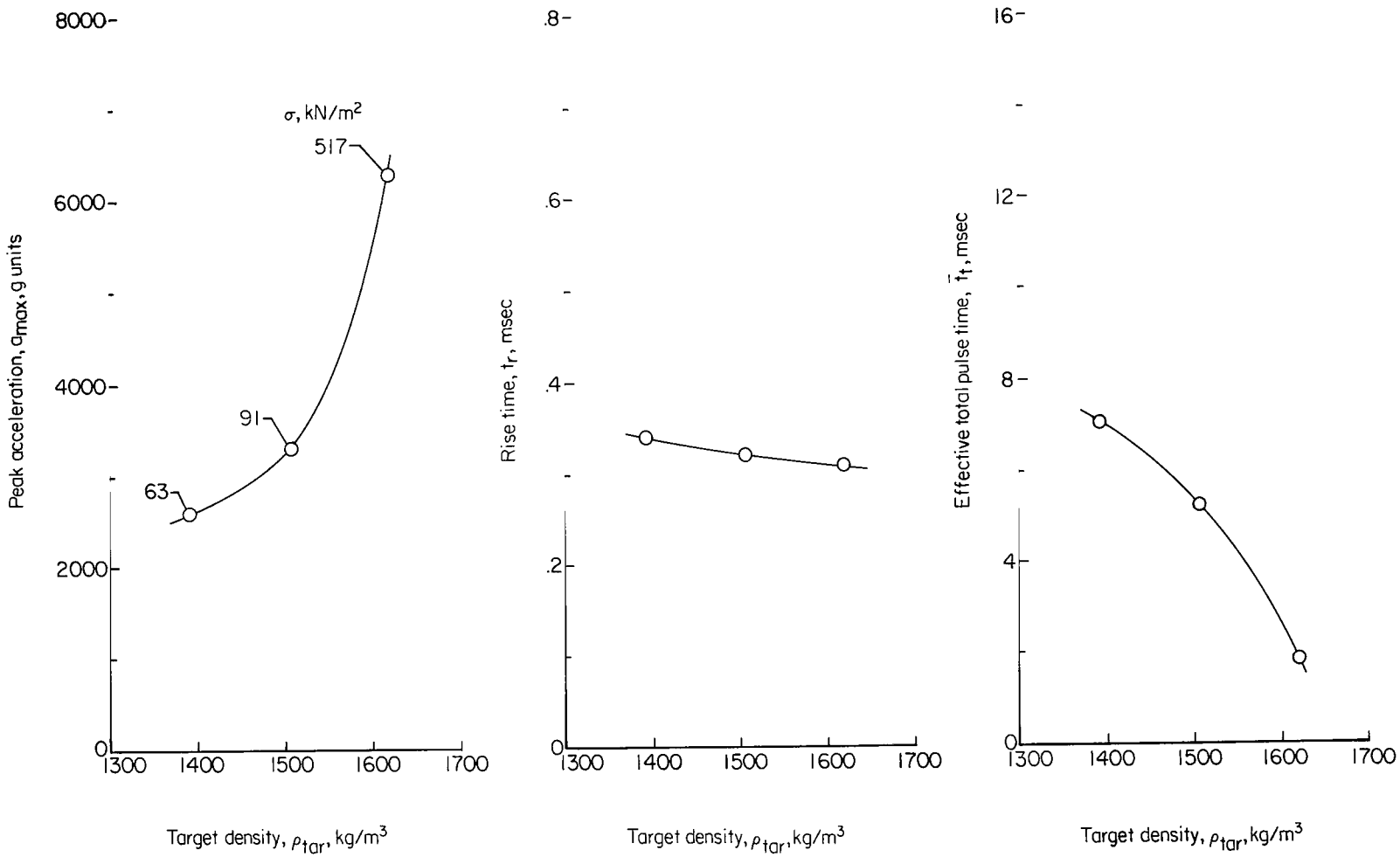

(b) Penetrometer configuration 1: V ≈ 46 m/sec; Nevada 120 sand.

Figure 16.- Concluded.

"The aeronautical and space activities of the United States shall be conducted so as to contribute . . . to the expansion of human knowledge of phenomena in the atmosphere and space. The Administration shall provide for the widest practicable and appropriate dissemination of information concerning its activities and the results thereof."

—NATIONAL AERONAUTICS AND SPACE ACT OF 1958

NASA SCIENTIFIC AND TECHNICAL PUBLICATIONS

TECHNICAL REPORTS: Scientific and technical information considered important, complete, and a lasting contribution to existing knowledge.

TECHNICAL NOTES: Information less broad in scope but nevertheless of importance as a contribution to existing knowledge.

TECHNICAL MEMORANDUMS: Information receiving limited distribution because of preliminary data, security classification, or other reasons.

CONTRACTOR REPORTS: Scientific and technical information generated under a NASA contract or grant and considered an important contribution to existing knowledge.

TECHNICAL TRANSLATIONS: Information published in a foreign language considered to merit NASA distribution in English.

SPECIAL PUBLICATIONS: Information derived from or of value to NASA activities. Publications include conference proceedings, monographs, data compilations, handbooks, sourcebooks, and special bibliographies.

TECHNOLOGY UTILIZATION PUBLICATIONS: Information on technology used by NASA that may be of particular interest in commercial and other non-aerospace applications. Publications include Tech Briefs, Technology Utilization Reports and Notes, and Technology Surveys.

Details on the availability of these publications may be obtained from:

SCIENTIFIC AND TECHNICAL INFORMATION DIVISION

NATIONAL AERONAUTICS AND SPACE ADMINISTRATION

Washington, D.C. 20546